To the Graduate Council:

I am submitting herewith a thesis written by Donald Matthew Walukas entitled "A Study of the Mechanical Properties and Oxidation Resistance of Nicalon®/SiC Composites with Sol-Gel-Derived Oxide Interfacial Coatings." I have examined the final copy of this thesis for form and content and recommend that it be accepted in partial fulfillment of the requirements for the degree of Master of Science, with a major in metallurgical engineering.

Charlie R. Brooks

Dr. Charles Brooks, Major Professor

We have read this thesis
and recommend its acceptance.

Thomas T. Meek

Accepted for the Council:

Associate Vice Chancellor
and Dean of The Graduate School

STATEMENT OF PERMISSION TO USE

In presenting this thesis in partial fulfillment of the requirements for a Master's degree at The University of Tennessee, Knoxville, I agree that the Library shall make it available to borrowers under the rules of the Library. Brief quotations from this thesis are allowable without special permission, provided that accurate acknowledgement of the source is made.

Permission for extensive quotation from or reproduction of this thesis may be granted by the major professor, or in his absence, by the Head of the Interlibrary Services when, in the opinion of either, the proposed use of the material is for scholarly purposes. Any copying of the material in this thesis for financial gain shall not be allowed without my written permission.

Signature J. Matt Wolak

Date 27 Apr 93

Requests for permission for extensive quotation from or reproduction of this thesis whole or in parts may be granted by the copyright holder.

A Study of the Mechanical Properties and Oxidation Resistance of Nicalon®/SiC Composites with Sol-Gel-Derived Oxide Interafacial Coatings

A Thesis

presented for the

Master of Sciences

Degree

The University of Tennessee

Donald Matthew Walukas

August, 1993

ACKNOWLEDGEMENTS

Research was sponsored by the U.S. Department of Energy, Office of Fossil Energy, Advanced Research and Technology Development Materials Program, under contract DE-AC05-84OR21400 with Martin Marietta Energy Systems, Inc. Special appreciation is extended to Jerry McLaughlin for his patience in answering a multitude of technical questions. A great debt of gratitude is due Karren L. More for her excellent and timely electron microscopy analysis. The author would also like to thank Jay Lane of Westinghouse Science and Technology Center for his invaluable service in the deposition of sol-gel oxide coatings.

The author would like to express many thanks to Theodore M. Besmann for his guidance of the project and his thorough review of the manuscript. The author also appreciates the comments and advice of Dr. Charles Brooks. Preparation of the final manuscript would not have been possible without the kindness of John and Sandra Haeussler. Special thanks are owed to Richard A. Lowden for all of his help and, more importantly, his belief that a free spirit can finally grow up.

The author expresses a very special thanks to Kristin L. Ploetz her patience, understanding and just enough subtle prodding to provide incentive to conclude this manuscript.

ABSTRACT

Previous studies of ceramic composites have revealed the fiber-matrix interface to greatly influence the mechanical properties of the composite. A weak interfacial bond is desired to allow for fiber pull-out, resulting in the toughening of the composite. Nicalon®-fiber/SiC-matrix composites have been fabricated with a carbon layer between fiber and matrix in order to provide the necessary weakening. Carbon, however, is susceptible to attack by oxygen, rendering it unsuitable as an interfacial material at high temperatures. Metal oxides were deposited on Nicalon fibers by sol-gel methods in an effort to find oxidation resistant coatings which may provide the necessary weakening of the interfacial bond.

Alumina, zirconia and titania were deposited on layers of Nicalon® cloth. A control sample with a pyrolytic carbon layer was fabricated as well. The cloth was placed in a holder and the composite densified by forced flow chemical vapor infiltration. The resulting composites were cut into bars and tested under four-point loading, both as-fabricated and after exposure to air at 1273 K for 1000 hours. Alumina and titania reacted with the fibers during processing to form mullite and TiC, respectively, as well as small amounts of graphite. These composite still displayed some weakening of the interfacial bond. Zirconia was stable, but bonded tightly to the matrix and fibers, resulting in weak and brittle

behavior. The control sample displayed abundant fiber pull-out in the as-fabricated condition.

Upon exposure to air at high temperature, the mullite layer was stable and the composite suffered no loss in strength or fracture toughness. The TiC layer and the control sample suffered some degradation and the composite lost significant strength and fracture toughness. SEM and TEM analysis revealed a strong correlation between debonding and interfacial smoothness.

TABLE OF CONTENTS

LIST OF TABLES

LIST OF FIGURES

1. INTRODUCTION

Recent improved designs in high velocity aircraft, aerospace vehicles and high temperature engines have created a demand for the development of high performance materials. Traditional metals and alloys possess neither the necessary mechanical properties at elevated temperatures, nor the thermal stability to meet design requirements. While many conventional ceramics and glass-ceramics demonstrate relatively high strength and stability at high temperatures, they lack stress relieving mechanisms and thus most ceramics are inherently brittle and sensitive to thermal shock. In an attempt to improve the fracture behavior of ceramic materials, platelets, particles, whiskers and fibers have been introduced to create barriers to crack propagation. It has been demonstrated that the introduction of these barriers leads to an increase in the work of fracture and toughness.[1-5]

Some of the most promising results in reinforcing ceramic matrices were found using continuous fibers.[6-8] Ideally, the fibers should possess high strength, low density and a high modulus of elasticity. In order to be useful at high temperatures the fiber should also be resistant to oxidation and be thermally stable. Most materials possessing this combination of attributes are ceramics, and therefore, inherently brittle. In combining two high strength, high modulus brittle materials, the role of the interface assumes

particular significance. The interfacial bond greatly affects the mode of failure or fracture behavior.[9-12] If the composite is strongly bonded at the fiber-matrix interface, a crack in the matrix will propagate undisturbed through the fibers, resulting in brittle failure. This gives no net gain vis-a-vis unreinforced ceramics. Therefore it is desired that the interfacial bond be relatively weak. In such composites the fracture process passes through several stages: debonding at the interface, matrix failure, fiber slip and pull-out and ultimately fiber failure.[13-14]

In recent years weakening of the interfacial bond has been achieved in ceramic composites through an interfacial layer. This layer must be composed of a substance which bonds weakly to the fiber and/or matrix. Previous studies of the interface in SiC-matrix composites reinforced with Nicalon®*, a SiC-based fiber produced from an organometallic precursor, have primarily employed pyrolytic graphite as an interlayer material.[15-18] The deposition of a thin (<0.5 μm) graphitic interlayer prior to the application of the SiC matrix was found to greatly improve the fracture behavior in room temperature flexure tests. However, the use of graphitic interlayers is limited by their poor oxidation resistance. Long-term exposure to air at high temperatures has been observed to greatly reduce the effectiveness of the

---

*Nippon Carbon Company, Tokyo, Japan.

composite.[19-20]

It is therefore necessary to find materials which will give the desired weakening of the interfacial bond, result in an increase in work of fracture, and possess the required thermal stability and oxidation resistance. These materials must be able to survive long term exposure to air at elevated temperatures and have thermal expansions compatible with matrix and fiber. Metal oxides are inherently stable to oxidation in air and possess thermal expansion coefficients relatively close to those of Nicalon® and SiC. Furthermore, sol-gel techniques developed at Westinghouse Science and Technology Center (STC) provide a simple and inexpensive method of depositing the coatings on the Nicalon® fibers.[21-23]

In this study the behavior of sol-gel derived oxide coatings on Nicalon® fibers was evaluated. The theoretical thermomechanical stresses, resulting from the cooling of the composite from processing temperatures, were calculated for each of six proposed oxides; alumina, cordierite, mullite, titania, zircon and zirconia. Based on this analysis alumina, titania and zirconia were chosen for further study. The thermochemical stability of the three oxides, was examined with respect to SiC matrix, Nicalon® fiber and the reactant gasses which are present during composite densification. Specimens of the resulting composites were fabricated using forced flow chemical vapor infiltration (FCVI) and were subjected to four-point flexure testing. The resulting

fracture surfaces were examined using a scanning electron microscope (SEM) and the fiber/matrix interfaces were analyzed using transmission electron microscopy (TEM).

2. BACKGROUND OF COMPOSITE MATERIALS

Composite materials are the product of two or more materials combined on the macroscopic level to form a useful product. Unlike alloys, which combine two or more materials on the microscopic level, composites are not macroscopically homogeneous. In composite materials both the reinforcing phase (platelets, whiskers, fibers, etc.) and matrix retain their physical and chemical identities. Composites are designed to exhibit the best properties of their constituents, and oftentimes some properties which neither constituent possesses. In traditional polymer- and metal-matrix composites, the fibers bear the load while the matrix keeps the fibers in the desired orientation and serves as a load transfer medium. The combination of matrix and fiber is chosen to improve strength, stiffness, weight and other factors depending upon the application. Fiber-reinforced resin composites, desired for their high strength-to-weight ratio are used in areas ranging from the aerospace industry to tennis rackets.

In order for a particular fiber-matrix combination to perform well as a composite, there are several compatibility requirements. The strengths and moduli of the materials must be such that the final composite material possesses the desired strength, toughness and ductility in accordance with the proposed application. In addition, when working with

ceramic matrix composites, the respective coefficients of thermal expansion, elastic moduli and Poisson's ratios must be considered. Most ceramic matrix composites require high processing temperatures. If the fibers and matrix are thermally incompatible, the material can be severely damaged by stresses induced by thermal cycling. Likewise, residual stresses inherent in the material after the post-processing cool-down have been shown to affect composite performance.

2.1. Mechanical Properties

Prediction of mechanical properties and behavior is a difficult task. Composite materials consist of two or more phases, each with differing chemical, mechanical and physical properties. The properties of the composite are derived from the properties of, and interactions between, the constituents. Seeking to make the calculations predicting mechanical behavior manageable, several assumptions must be made.[24-26]

1. The fibers are aligned perfectly parallel to the tensile axis and are surrounded by matrix.

2. The fibers, matrix and the composite elongate equally and in accordance with Hooke's Law.

3. The fibers are uniform in strength, size and shape.

4. The stress on the components is dependent on the modulus and the strain.

5. There are no internal stresses in the composite.

From these assumptions, linear expressions for the modulus and strength of a composite can be derived. Due to the broad assumptions on which they are based, these expressions are inherently inaccurate. They are, however, useful for exploring general trends regarding mechanical properties of a composite, such as elastic modulus and composite strength.

The contribution of fiber and matrix to the mechanical properties of the composite is proportional to their respective volume fractions.[25] In the region of linear stress-strain behavior, the stress in the composite can be expressed as

$$\sigma_c = V_f\sigma_f + V_m\sigma_m \ , \qquad (1)$$

where σ_f and σ_m are the stresses on the fibers and matrix, respectively, and V_f and V_m are the respective volume fractions. From assumption 2, the strains of the composite, matrix and fiber (ϵ_c, ϵ_m and ϵ_f) are equal in the linear-elastic region. Expressing the stress-strain relationship of the composite as

$$\sigma_c = E_c\epsilon_c \ , \qquad (2)$$

the modulus of the composite (E_c) follows the rule of

mixtures:

$$E_c = V_f E_f + V_m E_m \ , \qquad (3)$$

where E_f and E_m are moduli of the fiber and matrix, respectively. In the case of traditional metal-matrix and polymer-matrix composites, the matrix failure strain (ϵ_{mu}) generally exceeds the fiber failure strain (ϵ_{fu}). Maximum strength of the composite (σ_{cu}) is thus achieved when $\epsilon_c > \epsilon_{fu}$ and can be expressed by

$$\sigma_{cu} = V_f \sigma_{fu} + V_m \sigma'_m \ , \qquad (4)$$

where σ'_m is the matrix stress at the fiber failure. As the fibers fracture, the composite fails as in Figure 2.1a.

The mode of failure in ceramic composites differs significantly from the failure of traditional polymer- and metal-matrix composites. In this system of relatively brittle components, the failure strain of the fiber is usually greater than that of the matrix. Consequently, when the composite strain reaches ϵ_{mu}, matrix failure occurs while fiber failure occurs behind the matrix crack tip (Fig 2.1b.). From $\sigma_{mu}/E_m = \epsilon_{mu}$ and equations (2) and (3), an expression for the stress at which matrix cracking occurs and load transfer to the fibers begins (σ_{mc}'), can be derived,[27]

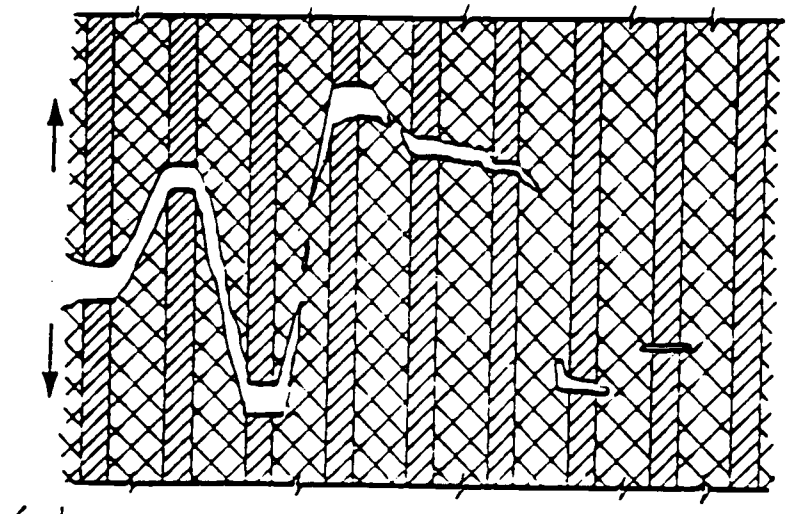

(a) $\epsilon_{mu} > \epsilon_{fu}$

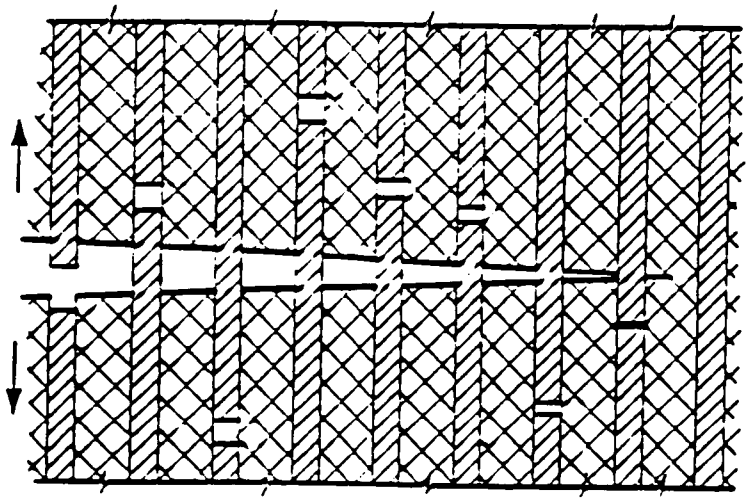

(b) $\epsilon_{mu} < \epsilon_{fu}$

Figure 2.1. The effect of failure strain mismatches on the mode of fracture in a fiber reinforced composite.

$$\sigma_{mc}' = [1+V_f(E_f/E_m - 1)]\sigma_{mu}. \qquad (5)$$

When matrix fracture is complete, the matrix is unable to bear any load. The ultimate strength of the composite (σ_{cu}) is

$$\sigma_{cu} = V_f\sigma_{fu} \ , \qquad (6)$$

provided that the fiber volume fraction is greater than the critical volume fraction (V_{fc}) necessary for transferring the load to the fibers and inducing multiple fracture.

Relationships establishing V_{fc} have been derived by Aveston.[13] The conditions for multiple fracture differ significantly between brittle-matrix and ductile-matrix systems. For the case $\epsilon_{fu} > \epsilon_{mu}$, as in most ceramic matrix composites, the critical fiber volume fraction can be expressed as:

$$V_{fc} = (\sigma_{mu}V_m + \sigma'_fV_f)/\sigma_{fu} \ , \qquad (7)$$

where σ'_f is the stress in the fiber at the onset of matrix cracking. The critical fiber volume fraction is dependent on the ultimate strengths, as well as the volume fraction, of the fiber and matrix. If $V_f < V_{fc}$, the composite will undergo single, catastrophical failure in accordance with Figure 2b. If $V_f > V_{fc}$, however, the fibers will be numerous enough to be able to support the load and bridge the crack. If ϵ_{fu} is

large enough, multiple cracks will form in the matrix until finally $\epsilon_c = \epsilon_{fu}$ and the fibers fail.

The above relationships assume the fibers to be uniformly distributed and aligned in the direction of the tensile stress. Expressions have been derived in which an allowance has been made for fibers not aligned with the stress field. The contribution of the fiber becomes less as it is rotated away from the axis of applied stress, thus, the actual fiber volume fraction can be much greater than the effective fiber volume fraction which is acting on the applied stress. In the above expressions V_{fa} should replace V_f, where $V_{fa} = \chi V_f$, χ being a correction factor and V_{fa} being the "effective" fiber volume fraction. For a composite in which the fibers are randomly distributed in a plane, χ will be approximately 0.38.[28]

2.2. Thermomechanical Compatibility

Due to the high processing temperatures of ceramic compounds, residual stresses often form upon cooling to ambient temperature if the composite constituents possess dissimilar coefficients of thermal expansion. It is necessary, therefore, to consider thermal expansion mismatches between fiber and matrix when searching for the proper combination of materials.[26,29-30] Large differences in thermal expansion coefficients can cause high stress levels leading to

severe damage upon thermal cycling, rendering many fiber/matrix combinations unsuitable for high temperature applications. Three cases should be considered when selecting a fiber/matrix combination: (1) the thermal expansion coefficient of the matrix is greater than that of the fibers ($\alpha_m > \alpha_f$), (2) the converse, where the fibers expand and contract more than the matrix ($\alpha_f > \alpha_m$), and (3) the coefficients are equal ($\alpha_f = \alpha_m$).

In the first case ($\alpha_m > \alpha_f$), the matrix will contract more than the fibers upon cooling from the processing temperature (Fig. 2.2a). The matrix will compress the fibers radially, increasing the frictional, and possibly the chemical, bonding at the fiber/matrix interface.[26] If the mismatch is very great, damage to the fibers may occur, lowering the strength of the composite. In the axial direction, upon cooling the matrix will again shrink more than the fibers, resulting in tensile stress on the matrix. If the thermal mismatch is large enough, the failure strain of the matrix may be exceeded, resulting in the development of cracks perpendicular to the fiber axis.

When the thermal expansion coefficient of the fibers exceeds that of the matrix ($\alpha_f > \alpha_m$), upon cooling the fiber will shrink away from the matrix in the radial direction (Fig. 2.2b). In the case of weak bonding, the fiber will debond from the matrix, resulting in a loss of frictional force at the interface. This may cause insufficient load transfer from

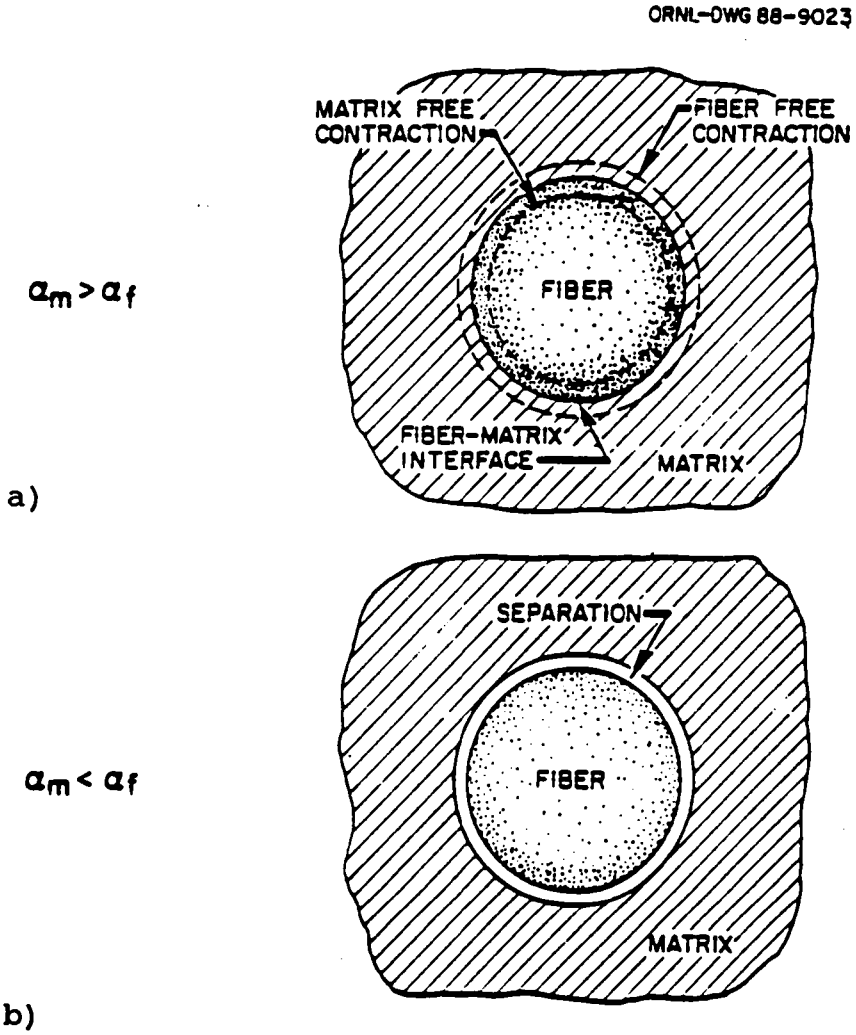

Figure 2.2. The effects of thermal expansion mismatch at the fiber-matrix interface.

the matrix to the fiber, such that the fibers provide little effective reinforcement. If the fiber-matrix bond and the fibers are sufficiently strong, a compressive stress in the matrix will result in the direction parallel to the axis of the fibers. By increasing the overall strain to initiate matrix failure, this compressive stress can result in a gain in strength for the composite. If the fibers lack the necessary strength, however, they will fracture. In the third case of $\alpha_f = \alpha_m$, there will be no thermally induced stresses from fiber/matrix interactions.

Mathematical expressions for thermally induced strains for a unidirectionally reinforced composite have been derived using a composite element model of one fiber in a tube of matrix.[26,29] Defining $\Delta\alpha = \alpha_m - \alpha_f$ and assuming perfect bonding between fiber and matrix, the strain in the matrix (ϵ'_{ma}) induced in the axial direction by cooling from the processing temperature can be expressed as

$$\epsilon'_{ma} = E_f V_f \Delta\alpha \Delta T / E_c \ , \qquad (10)$$

where ΔT is the temperature change from processing to ambient temperature. The axial strain induced in the fiber (ϵ'_{fa}) is

$$\epsilon'_{fa} = -E_m V_m \Delta\alpha \Delta T / E_c \ . \qquad (11)$$

Therefore, the stress at which matrix cracking begins (σ_{mc})

may now be written as

$$\sigma_{mc} = E_c \ (\epsilon_{mu} - \epsilon'_{ma}) \ , \qquad (12)$$

provided that the rule of mixtures is obeyed.

These relationships suggest that $\Delta\alpha$ should be kept to a value slightly > 0 in order to ensure some interfacial friction between fiber and matrix. If $\Delta\alpha < 0$, the fibers could be completely debonded from the matrix, causing a loss of reinforcement. If $\Delta\alpha$ is too large, it can induce cracking of the matrix. This phenomenon has been observed in carbon/epoxy composites with a moderately low residual stress giving a good combination of strength and toughness.[28] A high friction coefficient results in higher modulus and strength, but lower failure strain. In addition, these relationships help highlight the need to control frictional and chemical bonding at the interface.

2.3. The Fiber-Matrix Interface in Ceramic Matrix Composites

The fiber-matrix interface serves to transfer load from matrix to fiber in composite systems. In the case of ceramic matrix composites (CMC's), mechanical properties are greatly dependent on the properties of the interface. Addition of fibers to a ceramic matrix has been demonstrated to increase the matrix failure strain.[13-14] This increase is governed by

the interfacial shear stress. In addition, interfacial debonding and fiber pull-out are widely recognized to be the key contributors to the toughening of CMC's.[9-11,31] Both chemical and mechanical bonding are present to some degree at every interface. The presence of an intermediate layer between the fiber and matrix has been found to control the bonding to a large extent.[6,8,32-35]

2.3.1. The role of the Interface in Mechanical Properties

As a composite is progressively loaded, the stress-strain relationship is governed initially according to the rule of mixtures. This corresponds to the linear elastic region of the theoretical stress-strain curve in Figure 2.3. Deviation from linearity occurs upon matrix cracking as described previously. The Aveston-Cooper-Kelly, or ACK, model uses an energy balance to predict the onset of matrix fracture as the composite is loaded. This model accounts for additional energy absorbed by the fibers as well as the work done in debonding the fibers and pulling the fibers from the matrix.[13] The failure strain of the matrix (ϵ_{muc}) is thus

$$\epsilon_{muc} = [(24\tau\gamma_m E_f V_f^2)/(E_c E_m^2 r V_m)]^{1/3} , \qquad (13)$$

where r is the fiber radius, γ_m is the fracture energy of the matrix and τ is the interfacial shear stress. If τ is high

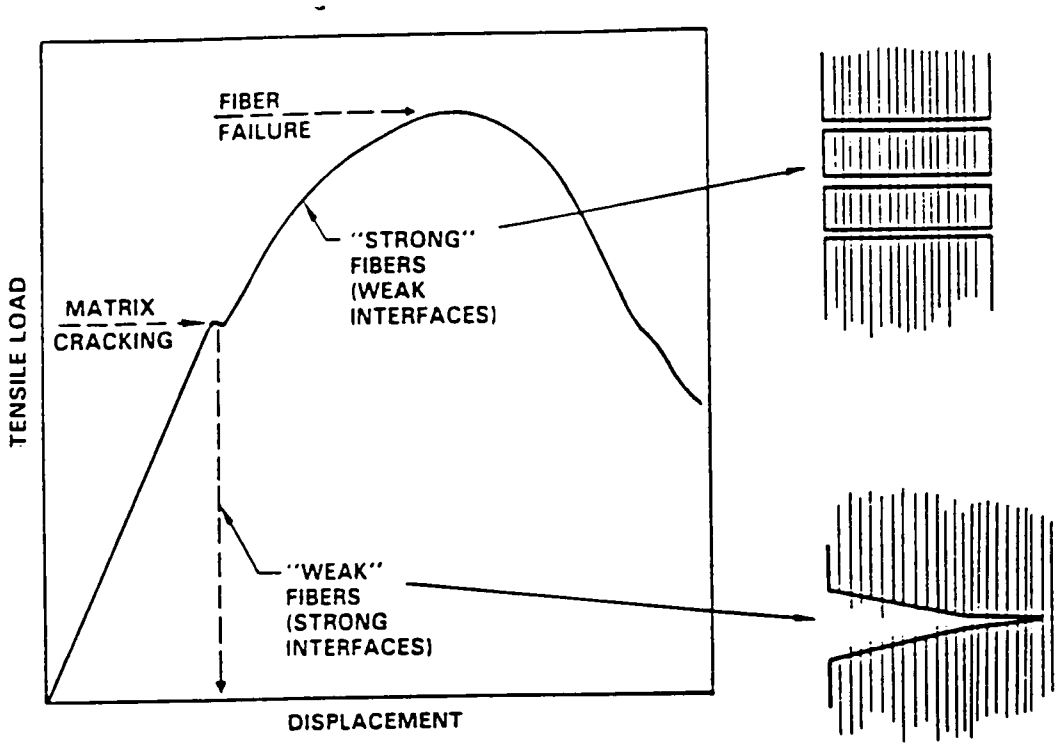

Figure 2.3. Theoretical stress-strain curve for a brittle matrix composite with strong and weak interfacial bonding according to Evans.[11]

enough, the presence of high-strength fibers will suppress cracking, extending the linear portion of the stress-strain curve. Conversely, weak interfacial bonding will lower the strain tolerance of the matrix.

When a CMC with strong interfacial bonding reaches the point of matrix fracture, a crack propagating in the matrix will cause fiber fracture at the crack tip. The composite will then fail catastrophically, very much like the failure of an unreinforced ceramic material (Fig. 2.3). On the other hand, when the interface is weak, fracture begins in the matrix and proceeds with debonding between fiber and matrix, matrix failure, fiber slip, and finally, fiber failure and pull-out[9-11,13]. By these mechanisms, energy is absorbed and fracture toughness improved. Depending on the desired properties, therefore, the fiber-matrix interfacial bond should be engineered to the appropriate level of adhesion.

As a crack propagates in the matrix of a composite with weak interfacial bonding, the fibers will debond from the matrix and bridge the crack. This mechanism governs the stress-strain relationship after matrix cracking. Load is transferred to the fibers according to the sliding resistance of the debonded fibers. A large sliding resistance results in a high transfer of load to the fibers. Consequently, if sliding resistance is large, the fibers will fail in locations near the crack plane, thus diminishing the failure strain of the composite and removing the contribution of fiber pull-out

from the toughening mechanism.[12] A high sliding resistance gives a composite with high stiffness, but lower fracture toughness. If the interface is exceedingly strong or the fibers too weak to bear the load, the composite will fail catastrophically upon matrix cracking. Conversely, a lower value of τ will produce a composite with lower stiffness and higher fracture toughness. In this case, the fibers fail in locations away from the crack plane, well behind the crack tip.[12,28] As previously mentioned, this effect has been similarly observed in carbon/epoxy composites.

As a ceramic-ceramic composite is loaded past the point where matrix cracking begins, stiffness is reduced as only the fibers are bearing the load (Fig. 2.3). The composite reaches its ultimate strength when the fibers fracture.[11] The sliding resistance now governs the downward curve of the stress-strain diagram. A higher value of sliding resistance results in a gradual reduction in stress as the composite is strained. A low sliding resistance will not allow for much energy absorption and the fibers will be pulled out from the matrix under light loading. In this case the stress drops swiftly with increasing strain.

The effects of interfacial properties on composite behavior are wide-ranging and critical. Improvement in certain properties may be coupled with detrimental effects to other properties. A strongly bonded interface may result in strengthening of the material through the raising of the

matrix fracture strain. The same strong interfacial bond may, however, produce an undesirable reduction in fiber pull-out and, consequently, of fracture toughness. Clearly, improvements in techniques of controlling interfacial properties is highly desirable. Attempts to modify interfacial properties have focused on the manipulation of an intermediate layer between fiber and matrix.

2.3.2 Interfacial Layers

In the early 1980's the development and wide availability of Nicalon® led to a renewed interest in CMC's.[4,5,7] In many instances, both brittle failure and composite fracture behavior (e.g. fiber pull-out) were observed in Nicalon®/LAS (lithium aluminosilicate) composites fabricated under seemingly identical conditions. Analysis of the fractured specimens revealed a correlation between the characteristics of fiber/matrix interface and the fracture process. In the composites which exhibited ductile, composite failure, a carbon rich layer was observed between fiber and matrix, whereas in those specimens demonstrating brittle fracture, such a layer was not observed.[35] It was theorized that the presence of a distinct interfacial layer between fiber and matrix weakens the bond and allows for fiber slip and pull-out. The presence of an interfacial layer may prevent reactions between fiber and matrix and thereby lower adhesion

and the strength of the fiber-matrix bond.[36]

The origin of this layer lies in the partial decomposition of the fibers during processing at high temperatures. Nicalon® fibers are fabricated from a polycarbosilane precursor and have been characterized as SiC grains in an amorphous silica or SiC_xO_y matrix with small amounts of free carbon.[37-39] When Nicalon® fibers are incorporated into a glass-ceramic matrix, it has been suggested that the silica diffuses into the matrix, while the free carbon present in the fiber diffuses to the interface.[40] The in-situ formation of this carbon layer, and the subsequent improvement in fracture behavior, has been noticed on numerous occasions.[11,32-34]

The apparent improved mechanical behavior has led to attempts to control the interface through the intentional deposition of an intermediate layer. Controlled deposition of an intermediate coating may give greater control over mechanical properties. Post-fabrication residual stresses may be more precisely engineered through choice of a fiber coating and coating thickness. In addition, fiber coatings may prevent degradation,during composite fabrication, of fibers such as Nicalon®.[41]

The presence of a distinct interfacial layer, however, complicates the analysis of post-fabrication residual stresses. Relationships derived by Hsueh[42] show the clamping stresses at the interface to be a function of modulus,

Poisson's ratio and coefficient of thermal expansion of the fiber, the matrix and the interfacial material (Appendix 1). These expressions were used to calculate post processing residual stresses in Nicalon®/SiC composites with a graphitic interlayer (Fig. 2.4).[20] Theoretically, coating thickness also has a major influence on the clamping stresses.

Several substances, including elemental silicon, boron, pyrolytic carbon, molybdenum and boron nitride, have been deposited on Nicalon® fibers as interface coatings via chemical vapor deposition (CVD). The coated fibers were then incorporated into a SiC matrix using the forced flow chemical vapor infiltration (FCVI) process.[15-16] Coatings of elemental silicon, boron and molybdenum failed to enhance the mechanical properties of the composite. Likewise, a composite with a boron nitride interlayer deposited from B_2H_6 and NH_3 was weak with little fiber pull-out.

The deposition of a thin (<0.5 μm) graphitic interlayer prior to the application of the SiC matrix was found to greatly improve the fracture behavior in room temperature flexure tests.[15-18] Improvements in toughness were both pronounced and reproducible, demonstrating an effective degree of control of the interface. Further investigations were conducted to explore the effect of varying the thickness of the coating. Fracture toughness and, to a lesser degree, composite strength, were shown to be dependent on the thickness of the coating (Fig. 2.5). In the Nicalon®/SiC

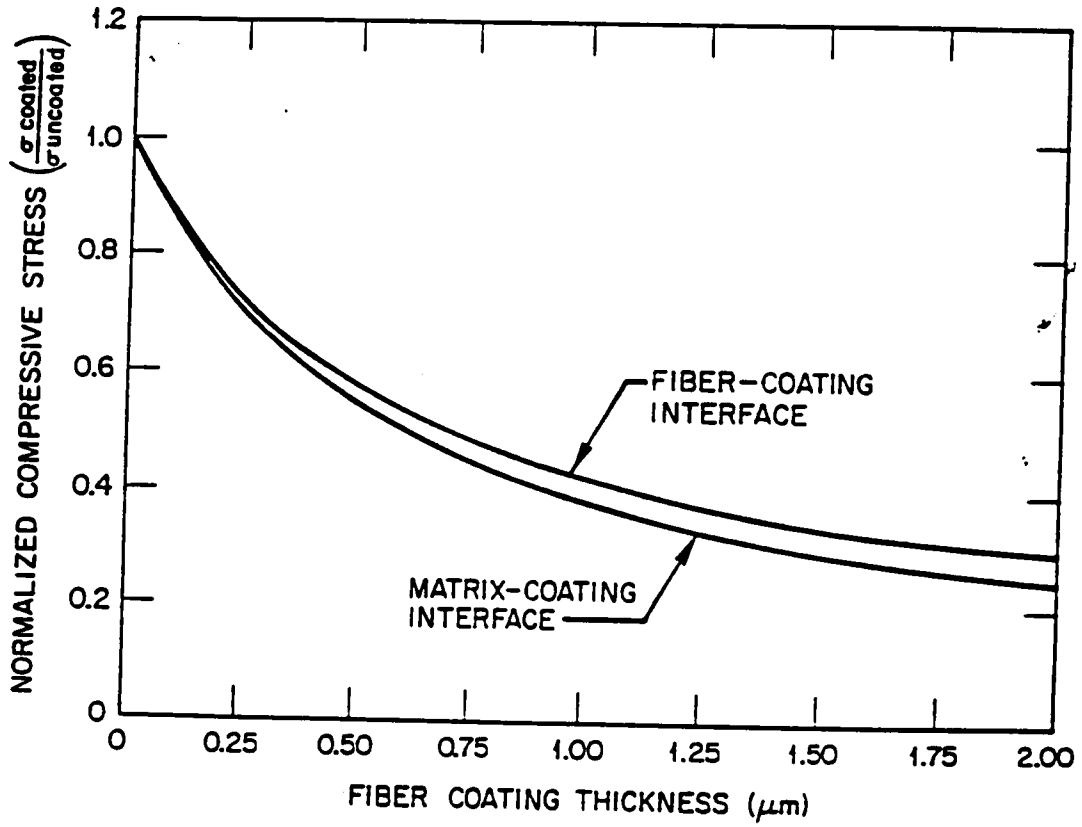

Figure 2.4. Reduction of residual interfacial stress with varying thickness of carbon interlayer in Nicalon®/SiC composites according to the theories of Hsueh.[42] (Figure taken from Lowden.[20])

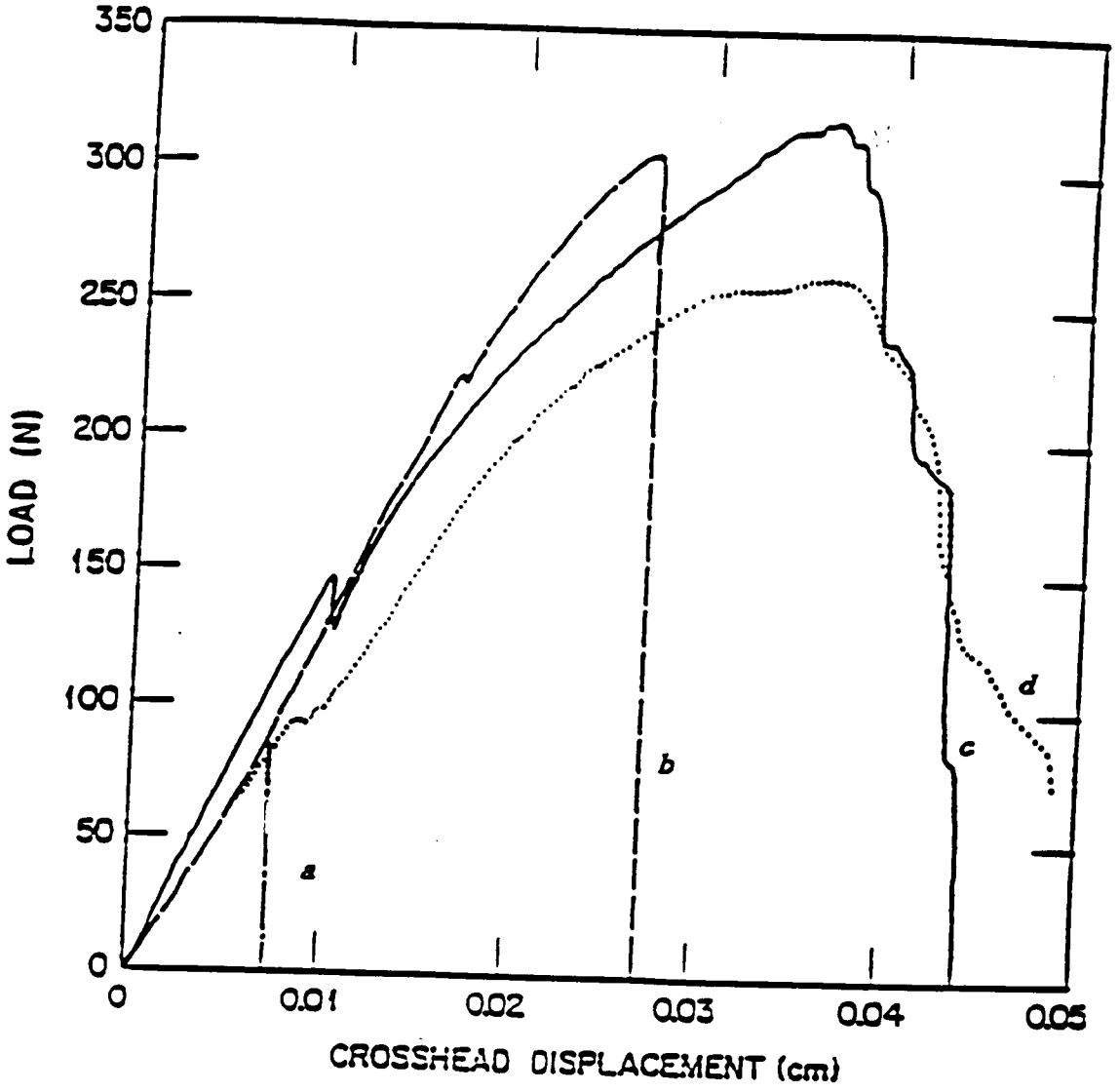

Figure 2.5. The effect of varying thickness of carbon interlayer on the fracture of Nicalon®/SiC composite samples: (a) uncoated, (b) 0.10 μm, (c) 0.17 μm, (d) 0.28 μm (Lowden).[16]

system, a combination of high toughness and high strength was found when a coating of carbon, approximately 0.2-0.3 μm thick was applied to the fibers prior to deposition of the matrix.[16] An interfacial layer of carbon was also found to improve properties of composites composed of boron monofilaments in a borosilicate matrix.[43]

The use of graphitic interlayers is limited, however, by the poor oxidation resistance of graphite. Samples with coatings formed in situ[11], as well as carbon coatings deposited by design[19-20], have proven very susceptible to oxidation. The oxidation of the carbon layer allows the higher oxygen diffusion into the composite. The oxygen reacts with Nicalon®, leading to the formation of a silica layer which replaces the carbon and tightly bonds fiber and matrix (Fig. 2.6). Nicalon®/SiC composites containing a graphitic interlayer were exposed to air at 1000°C for varying amounts of time. As exposure time was increased, fracture toughness and strength progressively degraded until the composite failed in a weak and brittle manner (Fig. 2.7). Deposition of a protective layer of SiC onto the outer surface of the composite prevents oxidation and allows retention of composite behavior in various corrosive environments. This is, however, not a practical solution to the problem of poor oxidation behavior, since flaws in the coating are possible and cracks will likely occur under loading. Thus, oxidation resistant interfacial coatings which can reduce fiber-matrix bonding

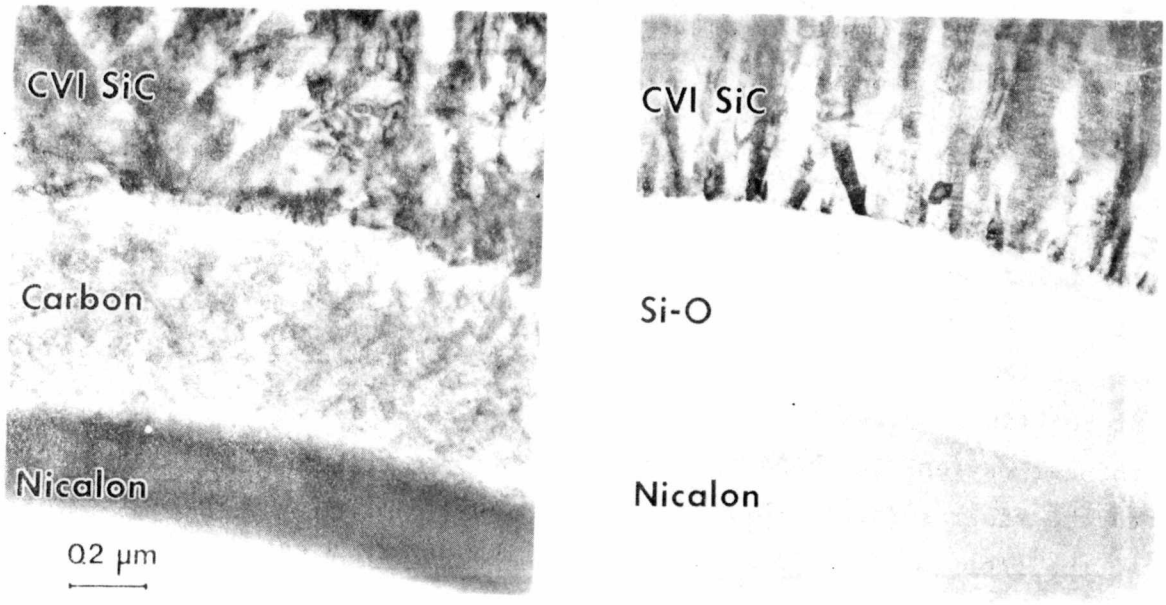

Figure 2.6. TEM micrographs of the interface region of Nicalon®/SiC composites (a) before and (b) after exposure to air at 1000 °C for 1000 hours.[20]

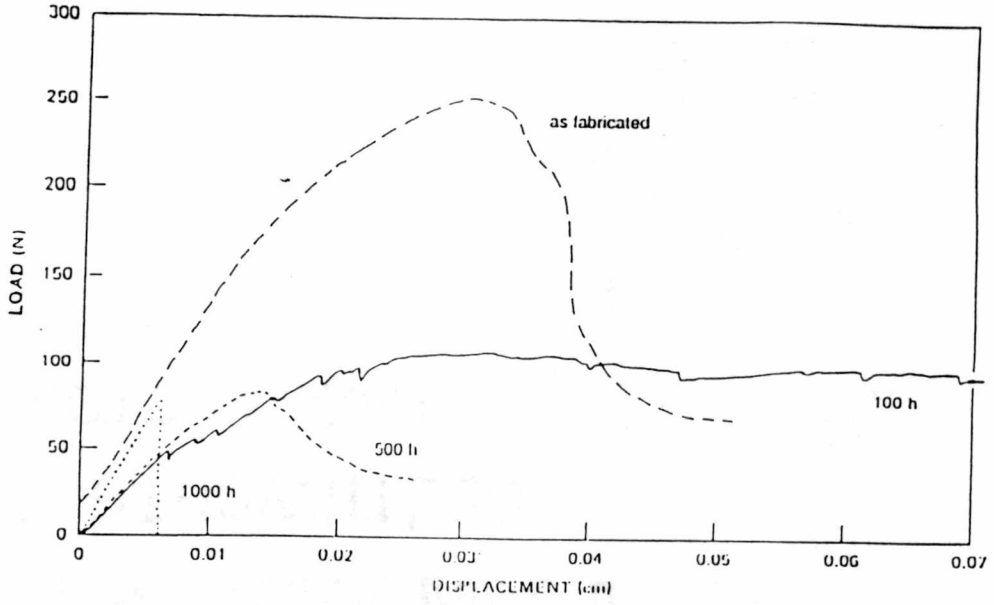

Figure 2.7. The progressive effects of exposure to air at 1000 °C on the flexure behavior of Nicalon®/SiC composites with carbon interlayer.[20]

must be found.

Boron nitride is among the possible interfacial coatings with greater oxidation resistance currently being investigated. Compared with uncoated fibers, deposition of boron nitride on SiC based fibers has resulted in improved room temperature mechanical properties in several matrices including zircon[44], silica, zirconia and mullite[34], as well as SiC.[45-46] The SiC composite, however, still possessed a continuous carbon layer between the fiber and the boron nitride after processing. It is theorized that this carbon layer is a product of the decomposition of the Nicalon® fibers.[46] The behavior of these composites under oxidation conditions is not known.

3. THERMOMECHANICAL COMPATIBILITY

The oxide coatings proposed for precoating Nicalon® fibers prior to densification include alumina, cordierite, mullite, titania, zircon and zirconia. Post-processing residual stresses were calculated for each of the aforementioned interfacial materials based on the relationships derived by Hsueh.[42] Ignoring fiber/fiber interactions, Hsueh derived a mathematical model for stresses on a coated fiber in an infinite matrix (Appendix A). Stresses result at the fiber-coating and coating-matrix interfaces when the composite cools from fabrication temperature to room temperature and components differentially shrink. Hsueh's model expresses these stresses as functions of coefficients of thermal expansion (CTE), Poisson's ratios and elastic moduli of the coating, fiber and matrix. The values of these constants for all materials of interest for this study appear in Table 3.1.

The results of these calculations are shown graphically in Figure 3.1. In a Nicalon®/SiC composite with no interfacial layer and assuming a temperature drop from 1473 K to 298 K, the calculated theoretical compressive stress at the fiber-matrix interface is ~312 MPa. The abscissa in Figure 3.1 is a normalized stress, obtained by dividing the values computed at various coating thicknesses by the stress value calculated for the case of no coating (~312 MPa). The graphs

Table 3.1. Thermomechanical properties of materials of interest.[47-48]

MATERIAL	CTE (10^{-6} K^{-1})	Poisson's ratio	Elastic Modulus (GPa)
Nicalon®	2.5	0.17	110
SiC	5.0	0.17	295
Alumina	8.0	0.22	386
Titania	8.8	0.28	283
Zirconia	8.0	0.32	241
Mullite	5.0	0.24	144
Zircon	5.6	0.27	206
Cordierite	3.7	0.21	117

therefore depict the relative compressive stress at the interface which remains compared to a composite with no interfacial layer.

A reduction in the compressive stress at the interface should lower local frictional forces and facilitate debonding, improving the fracture toughness of the composite. By this criterion, alumina, titania and zirconia are theoretically the coatings most likely to facilitate debonding at the coating-matrix interface and were thus selected for further consideration. Due to the low thermal expansion of Nicalon®, however, none of the six materials significantly lowers the compressive stress at the fiber-coating interface until coatings > 0.3 μm are used.

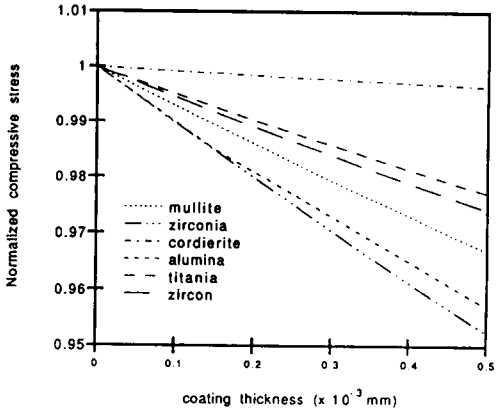

(a)

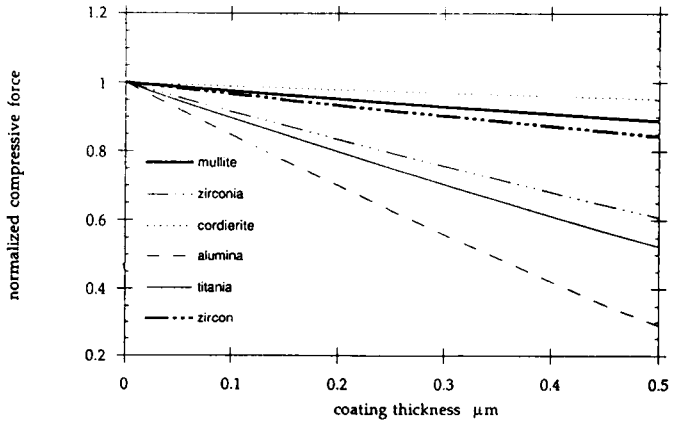

(b)

Figure 3.1. Calculated normalized compressive stresses at the (a) fiber-coating and (b) coating-matrix interfaces as a function of coating thickness. Calculations performed in accordance with Hsueh[42].

4. THERMOCHEMICAL ANALYSIS

Selection of the components of a composite system is based initially on the physical and mechanical properties of the individual components. However, chemical reactions at the fiber matrix interface have been shown to exert a strong influence on the mechanical behavior of a composite as well.[5,15-18,32] As noted earlier, exposure of Nicalon®/SiC composites with graphite interfaces to air at high temperatures, even for relatively short periods of time, has resulted in embrittlement of the interface, and hence, catastrophic failure. In the search for an adequate interfacial material, consideration of chemical compatibility is imperative.

At moderately high temperatures chemical reactions proceed quite rapidly and equilibrium can be achieved in a relatively short time. Therefore, an analysis of thermochemical stability should give insight into the chemical behavior of the systems at high temperatures. Numerical analysis of thermodynamic equilibrium is often complicated and tedious when many possible reaction products exist. Fortunately, the advent of computers has greatly simplified the task. Computer programs have been developed to determine the composition of any given system through calculation of the minimum free energy. Many of these programs are based on SOLGAS, a program created to examine systems composed of

gaseous and pure condensed phases.[49] A variation of this program, SOLGASMIX-PV,[50] was used in this study to predict the chemical behavior of the systems under consideration. An improved version of the program, CHEMSAGE,[51] became available recently and was also employed in the calculations.

The programs, CHEMSAGE and SOLGASMIX-PV, contain fairly comprehensive databases. The data base for SOLGASMIX-PV is based on the 1977 JANAF[52] tables, while the more extensive database for CHEMSAGE is from the European SGTE[53] tables. Thermodynamic values were extracted from these databases when possible. In those cases where the necessary values were not available, the databases were supplemented with values from Barin.[54] A table of the species considered appears in Appendix B. Entropy and enthalpy values were not available in these tables for the compound Ti_3SiC_2, therefore the values of Touanen[55] were used.

4.1. Processing conditions

Densification of the composite is achieved through the decomposition of methyltrichlorosilane (MTS or CH_3SiCl_3) into silicon carbide (SiC) and hydrochloric acid (HCl). A more detailed description of the process is found in Sec. 5.3. In order to evaluate thermochemical behavior during densification of the composite, calculations were performed at 1473 K (maximum densification temperature) with varying MTS/oxide

ratios. During the deposition of SiC by the FCVI process, large amounts of HCl are formed via the dissociation of MTS. All six oxides studied were shown to be susceptible to attack by chloride species. Detailed calculations were performed for alumina, titania and zirconia, the three oxides selected for further evaluation in this study. Assuming a fixed amount of oxide, thermochemical equilibria calculations were performed for increasing amounts of MTS. All calculations for processing conditions were conducted for a total pressure of 0.101 MPa. Due to the nature of the algorithm used by SOLGASMIX-PV, it was necessary to add minor amounts (0.1 mol) of argon to the mixture in some cases in order to fix the pressure at 0.101 MPa. Based on weight gain during sol-gel deposition, the coatings were assumed to be very thin (< 0.03 μm-see Sec. 6.1) Initial amounts of metal (Al, Ti and Zr) and oxygen were input in molar quantities to simulate the amount of oxide on the fibers (0.005-0.009 mols). Based on an MTS flow rate of 0.388 g/min and hydrogen carrier gas flow rate of 630 cm^3/min, the flow rates used to densify the composites in this study, the amounts of Si, C, H_2 and Cl_2 were increased step-wise with the amounts added to correspond with the molar amount that each would flow in 1 min.

At low MTS/oxide ratios, all three oxides possessed limited survivability. The results indicated that significant amounts of $AlCl_3$, $TiCl_4$, $TiCl_3$ or $ZrCl_4$ would form at equilibrium depending on the oxide material. In the case of

the alumina coating, as the amount of MTS is increased the amount of alumina remaining decreases. Initially, mullite forms, but it rapidly disappears as $AlCl_3$ forms. Titania is transformed into TiC which is in turn attacked and chlorinated. Zirconia is initially transformed into zircon ($ZrSiO_4$) which then decomposes to form $ZrCl_4$. In all three cases, the metal in the oxide was chlorinated completely once the MTS/oxide ratio reached a certain value. For coatings of alumina, titania and zirconia these MTS/oxide ratios were approximately 4/1, 9/1 and 2.5/1, respectively. Based on the total amount of alumina coating in the preform, this ratio corresponds to the amount of MTS which would flow through the preform in 13 min. For coatings of titania and zirconia the corresponding times were 23 and 7 min, respectively. Given the thinness of the sol-gel coatings, the threat of chemical attack is very significant.

4.2. Thermochemical stability of the interface coatings with respect to the SiC matrix

Using SOLGASMIX-PV, phase diagrams were calculated for systems containing SiC with alumina and zirconia. CHEMSAGE was utilized for the calculation of the SiC/titania system. Calculations were performed for 0.101 MPa pressure and temperatures of 1273 K, 1373 K and 1473 K in order to encompass the range at which the composites will be fabricated

and tested for oxidation resistance. Beginning with 95 mols of SiC and 5 mols of oxide, the amount of SiC was reduced and the amount of oxide increased in increments of 5 mols. When using SOLGASMIX-PV, 0.1 mole of Argon was added to the system. This was repeated for each of the three aforementioned temperatures. When a phase transformation occurred, the calculations were repeated in increments of 1 mole to better define the phase boundary.

The alumina/SiC and zirconia/SiC systems were found to be stable at all temperatures and concentrations at which calculations were performed. The titania/SiC system, however, was not stable. An approximate calculated TiO_2/SiC phase diagram appears in Figure 4.1. Because the coating is extremely thin (< 0.1 μm) in relation to the SiC matrix, the high SiC regions are of most importance. In the region of high titania concentration (> 50 mole % TiO_2), all titanium is present in the form of TiC. These calculations suggest titania will react with the matrix to form TiC and SiO_2.

4.3. Thermochemical stability of the Interface Coating with respect to Nicalon® fiber

Assessment of thermochemical stability of the three oxides with respect to Nicalon® proved to be more difficult due to the complex composition of Nicalon®. Nicalon® NLM 102, used in fabricating the composites of this study, is amorphous in structure, consisting of 49 mole % SiC, 40 mole % C and 11

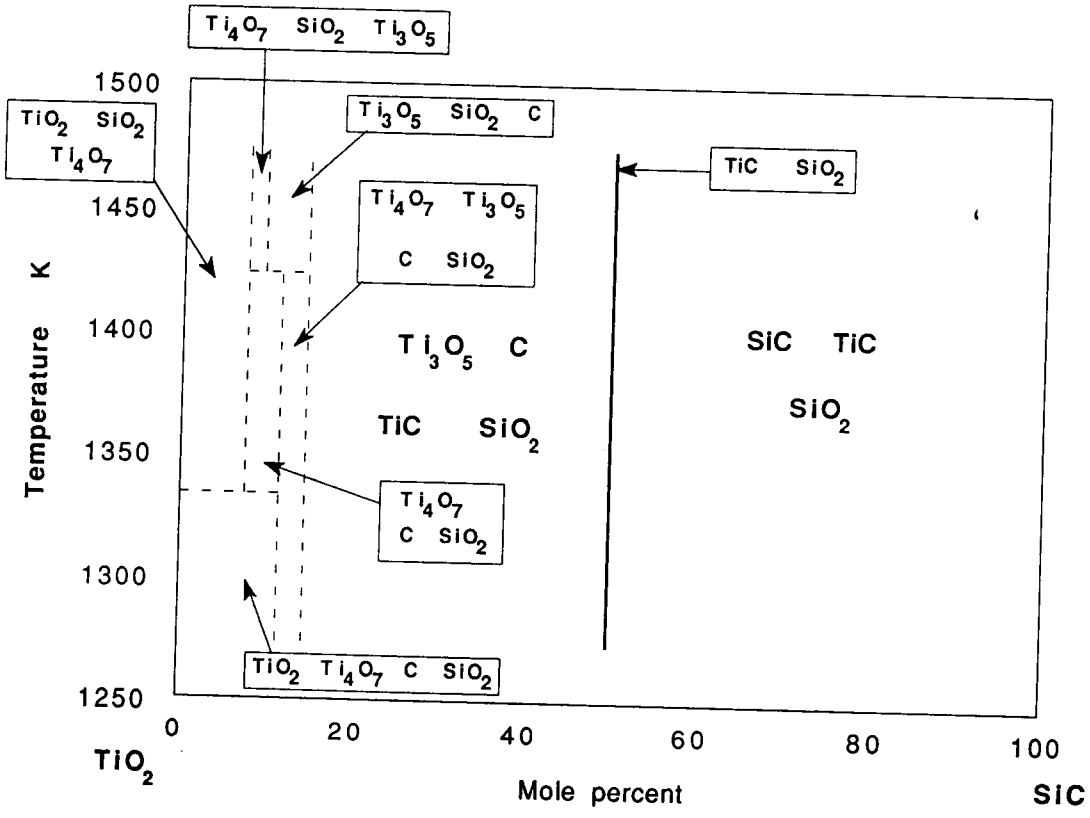

Figure 4.1. Calculated TiO_2/SiC phase diagram for the temperature range 1273-1473 K.

mole % SiO_2.[56] Thus for every mole of Si there are 1.48 moles of C and 0.36 moles of O. Pseudo-phase diagrams were calculated for each of the three oxides versus Nicalon® in a manner similar to the calculations of the oxide/SiC phase diagrams. Starting with 5 moles of oxide and 95 moles of Si with corresponding mole amounts of carbon and oxygen, the amounts were step-wise changed by 5 moles across the diagram. As seen in Figure 4.2. the Nicalon®/TiO_2 phase diagram is very similar to the SiC/TiO_2 phase diagram due to the high SiC content in Nicalon®. In the region of low titania concentration (< 43 mole % TiO_2), TiC is once again the only stable compound containing Ti.

The Nicalon®/Al_2O_3 and Nicalon®/ZrO_2 phase diagrams appear in Figures 4.3 and 4.4. It was found that for all alumina concentrations less than 26 mole %, alumina reacts completely with the silica in the Nicalon®fiber to form mullite ($Al_6Si_2O_{13}$). In similar fashion, for all zirconia concentrations less than 20 mole %, zirconia reacts with silica to form zircon ($ZrSiO_4$).

It should be noted that these diagrams are approximate and in places appear to violate the phase rule. For example, Figure 4.3 consists of two four-phase regions adjacent to one another. Due to the coarse, incremental nature of the calculations the three-phase region containing mullite, SiC and carbon never appeared in the calculations. This region must be narrow, lying between 26 and 27 mole % Al_2O_3.

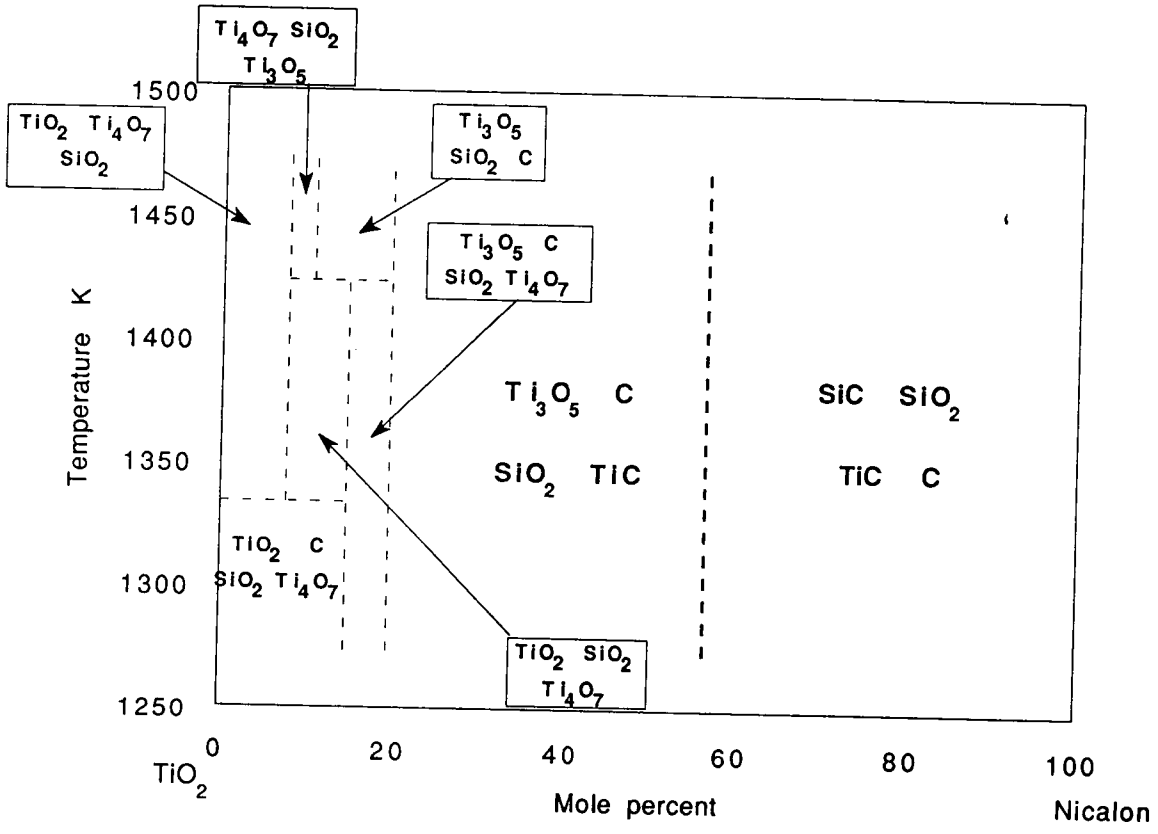

Figure 4.2. Calculated TiO_2/Nicalon® phase diagram for the temperature range 1273-1473 K.

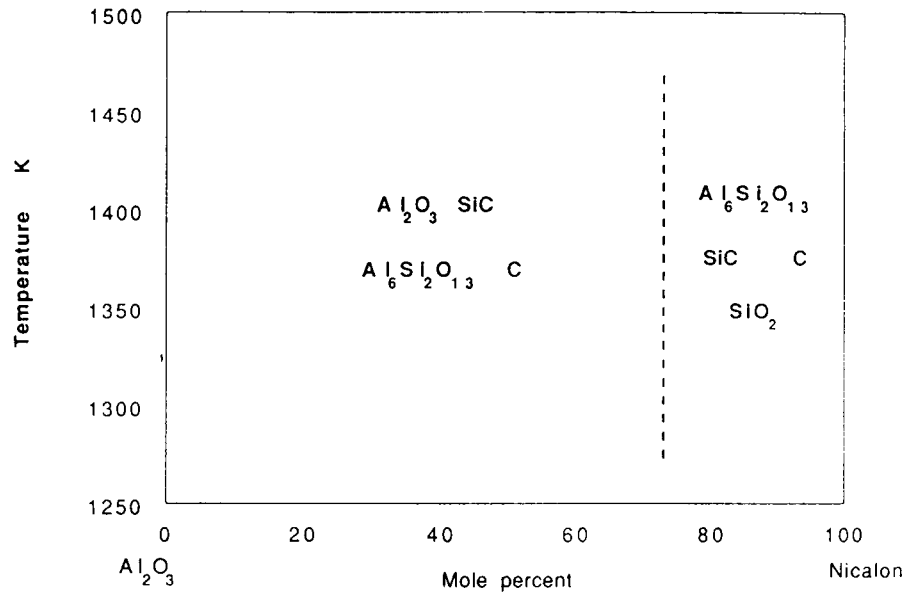

Figure 4.3. Calculated Al_2O_3/Nicalon® phase diagram for the temperature range 1273-1473 K.

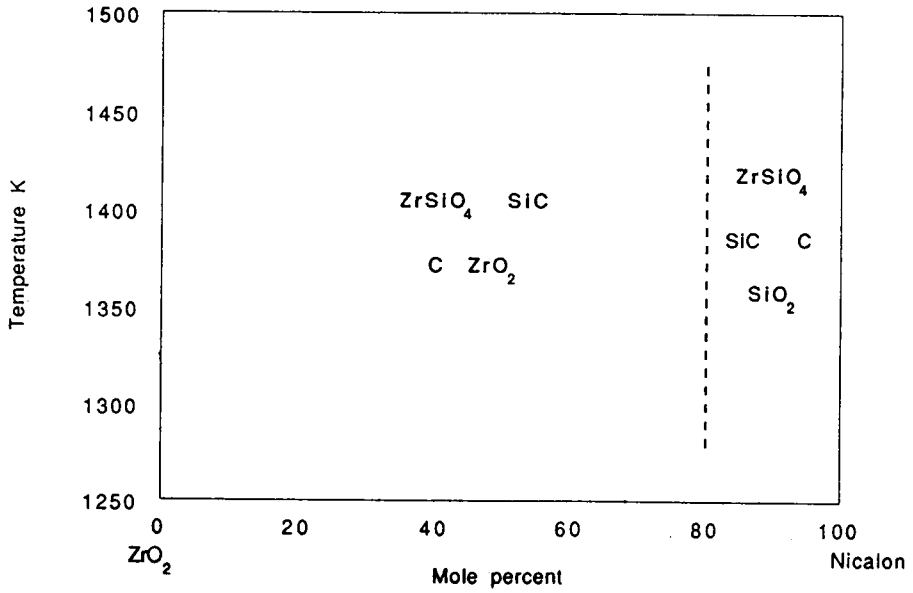

Figure 4.4. Calculated ZrO_2/Nicalon® phase diagram for the temperature range 1273-1473 K.

5. EXPERIMENTAL PROCEDURE

5.1. Materials

Composites were fabricated using Nicalon® NLM-102 ceramic grade, plain-weave cloth as the fiber reinforcement. The fibers were 15-20 μm in diameter, woven such that there are 500 fibers/bundle and 6.2 fiber bundles/cm. Carbon interlayers and SiC matrix were deposited from reactions using the following chemical substances: 99.97% pure methyltrichlorosilane (MTS)*, ultra high purity hydrogen gas (UN 1049)**, 99.997% pure Ar** and 99.96% pure propylene***.

5.2. Sol-Gel Coatings

Sol-gel oxide coatings were deposited on Nicalon® cloth at Westinghouse Science and Technology Center[21-23]. There are two different types of sol-gel processing. The first, known as the colloidal method, involves dispersing colloidal particles in a liquid, producing a sol. This is followed by the destabilization of the sol to produce the gel. The second method utilizes polymerization of organometallic compounds

---

* Eastman-Kodak Chemical Co., Rochester, New York.

** Liquid Air Co., Walnut Creek, CA.

*** Matheson Gas Products, Atlanta, GA.

such as alkoxides to produce a gel with a continuous bond network. Both the colloidal and the polymerization methods of gel formation may be applied to the deposition of ceramic thin films on Nicalon® cloth. Detailed descriptions are available in the literature for both colloidal[57] and polymeric methods[21,58].

The alumina sol was produced using the colloidal method. The precursor alkoxide, aluminum sec-butoxide or $Al(OC_4H_9)_3$, was hydrolyzed by introducing the alkoxide into excess double-distilled, deionized water at a water/alkoxide molar ratio of 100/1. The initial water temperature was approximately 80°C. The resulting slurry was briskly stirred for 15-20 minutes over a hot-plate. Following hydrolysis an acid must be introduced into the slurry to achieve the required peptization of the hydroxide. A wide range of acids, including nitric acid, acetic acid, sulfuric acid and hydrochloric acid, were found to be effective in the required peptization of the slurry.[22] In the application of oxide films on Nicalon® cloth, nitric acid was chosen as the acid least likely to introduce damaging impurities vis-a-vis the SiC matrix, Nicalon® fibers and alumina coating. Nitric acid was added to the slurry so that an acid/aluminum molar ratio of 7/100 was achieved. The slurry was then covered and placed in an oven at 80°C and left for approximately 12 hours.

Coatings of titania and zirconia were produced from a polymeric sol. The precursors, titania ethoxide and zirconia

n-propoxide, were dissolved in ethanol at room temperature to produce sols of 3 wt.% TiO_2 and 4 wt.% ZrO_2, respectively. Due to the hygroscopic nature of the precursors, creation of the solution must be carried out in a dry-box. The solutions were stirred with a magnetic rod until they were clear with no precipitates. At this point the sols were ready for deposition onto the substrate.

Nicalon® cloth was cut into strips approximately 26 x 8 cm. Nicalon® fibers are coated with a polyvinyl acetate sizing to protect the fibers during handling and weaving. The strips, therefore, were washed in acetone in order to remove the sizing. The strips were then dipped in the appropriate sol. In an attempt to vary coating thickness, the strips were withdrawn from solution at two different rates, 23 cm/min and 80 cm/min. Due to viscosity effects, a slower rate of withdrawal results in a thinner coating. The sol-coated strips were dried and heated in air to 450°C at a rate of 15°C/min. The strips were held at 450°C for 30 minutes.

5.3. Composite Fabrication

Densification was achieved employing a chemical vapor infiltration technique developed at Oak Ridge National Laboratory (ORNL).[6] The apparatus is shown in Figure 5.1 and is described in detail elsewhere.[16] The furnace was heated resistively with the hot-side temperature being regulated

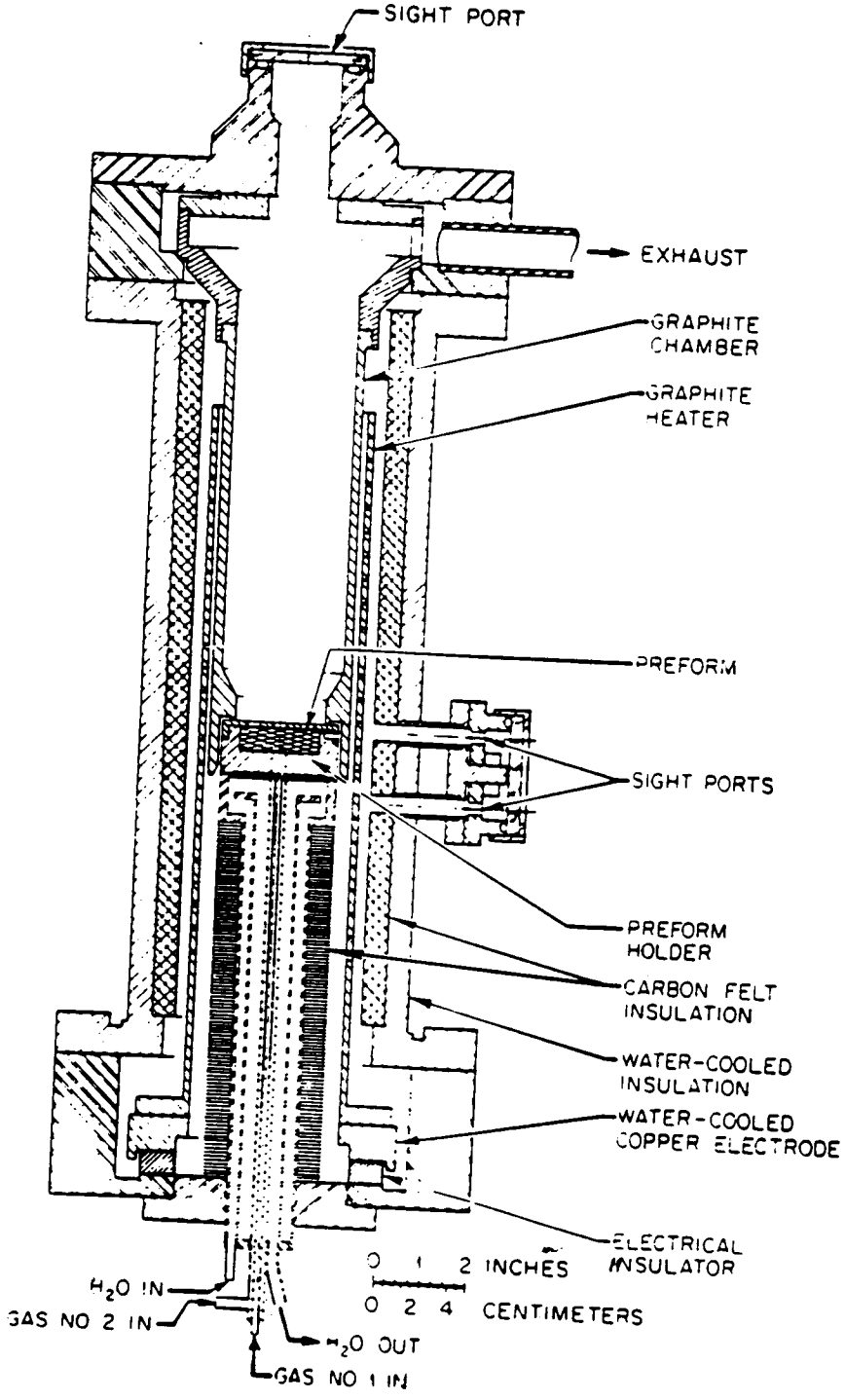

Figure 5.1. Schematic of the chemical-vapor-infiltration furnace used to densify fibrous preforms by FCVI.

through the use of an external Ircon® 2000 series optical pyrometer*. This pyrometer reads the temperature of the top of the graphite holder through the top sight port. The temperature readings were verified by a hand-held Leeds and Northrup® 8627** optical pyrometer which was calibrated to account for reading differences induced by the prism and sight glass. The pyrometer was verified at 650 nm against a gas transfer lamp which has been calibrated by the Instrumentation and Controls Division at ORNL against a standard lamp in accordance with NIST standards.[59] Calibration was performed by supplying a known current to the gas lamp, which illuminates the filament to a known brightness temperature. The reduction in the temperature readings due to loss in the sight glass and prism was measured using an automatic optical pyrometer at several temperatures. Measurements were repeated for statistical accuracy. Readings were taken with the pyrometer against the gas lamp with and without the prism and sight glass. The percent loss due to sight glass and prism was then recorded and accounted for during use.

The critical components of the infiltration system are the water-cooled injector and the graphite holder. The fibrous preform is placed atop the water-cooled injector, which is composed of several concentric stainless steel tubes.

---

* Ircon, Inc., Niles, IL.

** Leeds and Northrup, North Wales, PA.

These tubes are connected as to form separate gas and water passages through which the cooling water and the reactant gases enter the system. Contact with the water-cooled injector serves to cool the bottom and side surfaces of the preform (Fig. 5.2), thus creating a steep thermal gradient within the preform. The reactant gases, hydrogen and MTS, pass through the cool portion of the preform unreacted. The MTS then decomposes and deposits SiC in the hot portion in an overall reaction which can be written as:

$$CH_3SiCl_3 \xrightarrow{H_2} SiC + 3HCl$$

The hydrogen acts as both carrier gas and as reaction catalyst in a series of intermediate reactions.[60-61]

The flow rates of the necessary gases were controlled by MKS-1259c* mass flow controllers, which were calibrated against a wet test meter which, in turn, was calibrated by the Instrumentation and Controls Division at ORNL. Argon gas was passed through a drying column to eliminate moisture. Other gases, hydrogen and propylene, were used as received. MTS exists as a liquid at room temperature. Therefore, it was necessary to pass hydrogen gas through a reservoir of liquid MTS, in order to carry MTS vapor to the reaction chamber. The system is designed to allow control of not only the MTS vapor flow, but of the hydrogen/MTS flow ratio as well. This is

---

* MKS Instruments Inc., Andover, MA.

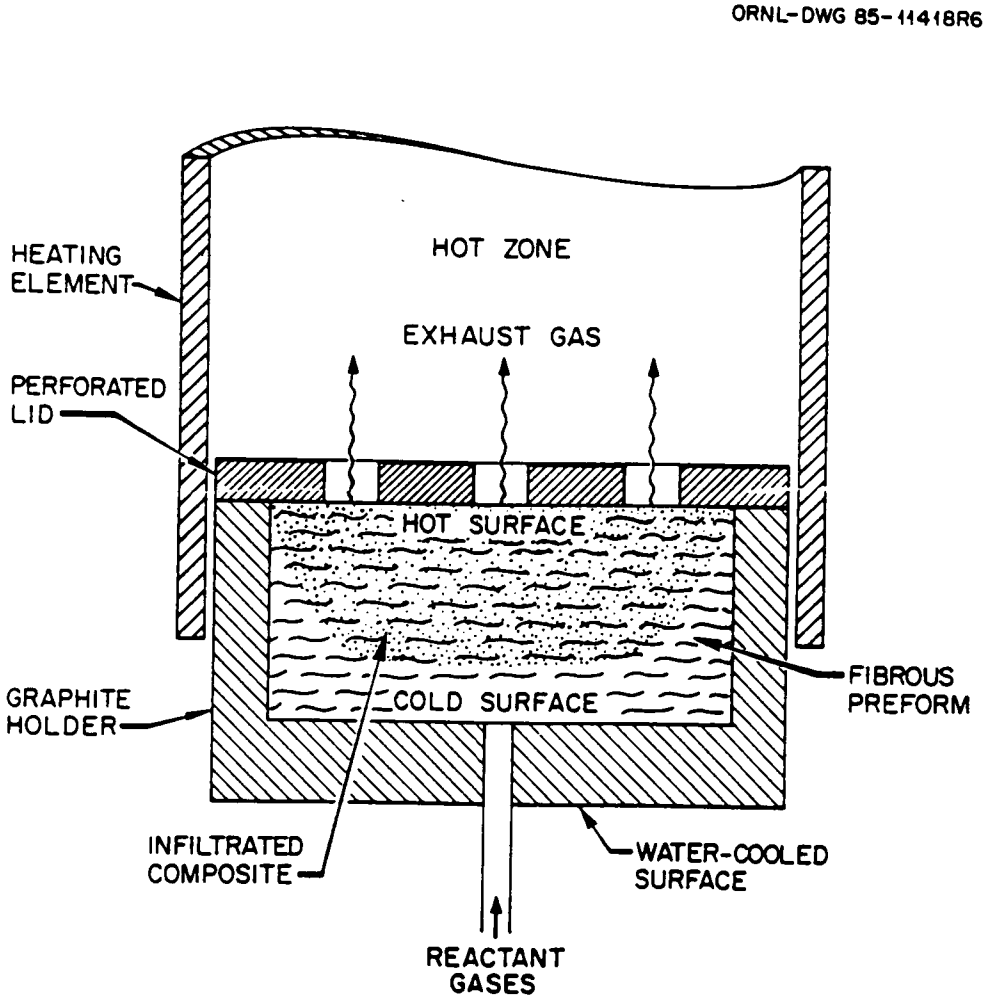

Figure 5.2. Schematic of the thermal-gradient FCVI process developed at ORNL.

accomplished through the use of a Tylan® source 5* mass flow controller in series with a vapor-source controller. This was calibrated by allowing MTS to flow through the system for a fixed period of time and weighing the MTS container to verify the amount which flowed through the unit. Weight loss was determined after each densification run in order to confirm the flow rate.

5.3.1. Preform Fabrication

Fibrous preforms were fabricated by stacking multiple layers of Nicalon® plain-weave cloth in a graphite holder, with the orientation of the fiber bundles rotated in a 0-30-60-90° sequence (Fig. 5.3). The layers were hand compressed to produce a preform with nominal fiber loading of 40 vol %. The cloth was held in place by a perforated graphite lid pinned to the holder. The nominal diameter and thickness of the preform were 75 mm and 15 mm, respectively. Preforms were fabricated for each of the three oxide coated cloth samples. Each preform was made of 62 cloth layers, 36 of which were oxide coated. The remaining 26 layers were composed of cloth as received from the manufacturer. From the top (hot-side) of the preform, the distribution of the fiber layers is as follows: 3 layers as received, 18 layers with thick

---

** Tylan, Inc., Torrance, Ca.

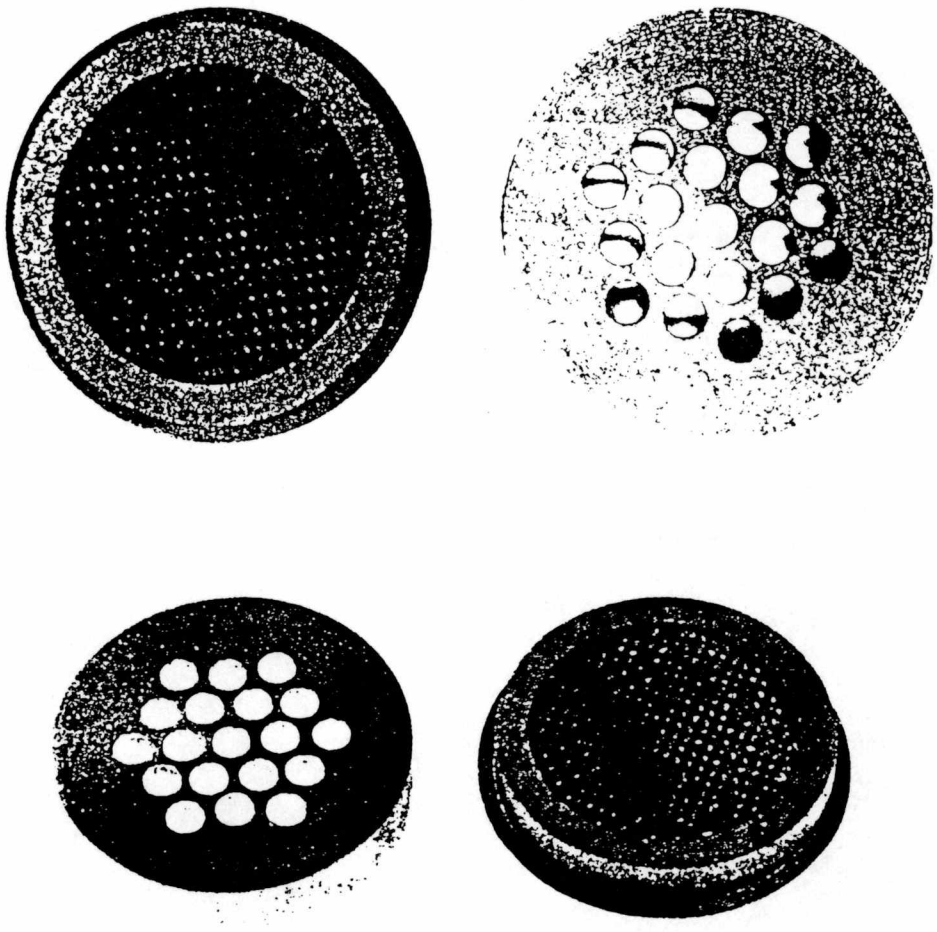

Figure 5.3. Graphite holder containing plain-weave Nicalon® cloth layers.

coating, 5 layers as received, 18 layers with thin coating, and 18 layers as received. One more preform was fabricated using only as-received fibers to serve as a control. It was necessary to remove the protective sizing on said layers. This was accomplished by placing the holder containing the fibers in an acetone bath for 10 minutes. The acetone was replaced and the procedure repeated twice.

5.3.2. Graphite coating

Protective precoats of < 0.01 μm graphitic carbon were deposited on the sol-gel coated and control fibers prior to densification. The coatings were prepared under isothermal conditions and reduced pressure within the FCVI furnace. In order to create isothermal conditions within the preform, the preform cannot be in contact with the water-cooled injector. A spacer, therefore, was placed between the water-cooled injector and the preform. The apparatus was evacuated to a pressure < 133 Pa. Argon was then allowed to flow through reactant supply lines and to the preform at a rate of 1400 cm^3/minute for several minutes. The lines were thereby flushed insuring minimum contamination. The system was then raised to a deposition temperature of 1373 K. Propylene (C_3H_6) was then allowed to flow through the preform at a rate of 40 cm^3/minute, establishing an operating pressure of 13.3 kPa. The furnace was held under these conditions for 10 min.

The propylene flow was then terminated and the furnace was allowed to cool to room temperature.

5.3.3. Densification

The coated preforms were densified using the FCVI process. The spacer was removed and the preform was placed in contact with the water-cooled injector, thereby creating the desired thermal gradient. The chamber was again evacuated to a pressure < 133 Pa. Hydrogen was allowed to flow through the gas lines and the argon purges opened to establish atmospheric pressure in the furnace. The furnace was heated to a deposition temperature of 1473 K, while the hydrogen flowed through the vaporizer by-pass. When the furnace temperature was stabilized at 1473 K, hydrogen flow was diverted through the evaporator. The flow rates of MTS and hydrogen were 0.388 g/minute and 630 cm^3/minute, respectively.

As the preform densifies, the permeability of the preform decreases, thereby raising the pressure of the entering reactant gases. The furnace was programmed to initiate a shut-down procedure when this pressure reached 170 kPa. Previous infiltrations have shown the preform to be 85-90% dense at this pressure.[7,16] At this point the hydrogen flow was diverted back to the vaporizer by-pass and the power to the heating element shut off. The furnace then cooled to room temperature and the samples were removed from the

furnace. The MTS reservoir was weighed after every run to verify reactant usage.

5.4. Mechanical Properties

5.4.1. Sample Preparation

The densified composites were weighed to evaluate the effectiveness of the densification procedure. All the samples were found to be > 80% theoretical density, therefore the composite samples were ready for mechanical testing. The graphite holders were cut and ground from the composite samples using carbide tipped tool bits. The samples were machined into bars ≈ 3 mm x 4 mm x 50 mm for flexure testing. All cutting and grinding was accomplished using a high-speed grinder/slicer with metal-bonded low-concentration diamond slicing blades and low-concentration resin-bonded diamond grinding wheels. The sample dimensions were measured and the bars machined so that each bar would contain approximately 12 layers of coated cloth. Approximately 13 bars were obtained for each different coating and thickness.

All bars were measured and weighed to determine densities. The test bars for each coating were divided into three groups of four bars each. The first group was tested as fabricated; the second group was placed in a 1273 K air environment for 1000 h; and the third group was seal-coated

with an external layer of SiC, deposited by chemical vapor deposition, and placed in the high temperature environment along with the second group.

The seal coating of the third group of bars was accomplished by placing them in a curved alumina dish so that contact between the bars and the holder would be minimal. The dish was fixed horizontally in a quartz tube. In previous coating runs of this type, SiC was deposited on the quartz tube. The tube was lined with graphoil® (graphite foil) to prevent SiC deposits from breaking the tube. The system was evacuated to a pressure < 133 Pa and was resistively heated to 1273 K. Temperature was controlled using an Ircon® 2000 series pyrometer and verified using a Leeds and Northrup 8627 hand-held optical pyrometer. Hydrogen gas and MTS were flowed in the same manner as in the densification procedure. The flow rates for hydrogen and MTS were 1000 cm^3/min and 0.1 g/min respectively. The furnace was held under these conditions for 6 hours.

Upon weighing the bars to check coating thickness, the bars placed furthest from the source of reactants, were found to have minimal weight gain. This phenomena is assumed to be due to the depletion of the reactants as they pass through the reaction chamber. The bars were placed again in the dish in an order opposite from the first run. In addition, they were rotated 180° so that the points of contact with the dish differed from the first run. These steps insured a relatively

even coating with minimal flaws.

5.4.2. High temperature treatment

Samples with and without the protective SiC layer were oxidized in static air at 1000°C for 1000 hours. The bars were placed in the cavity of an atmospheric box furnace and heated to temperature at a rate of ~300°/hr. When the furnace reached 1273 K, the temperature was verified using a hand held Leeds and Northrup 8627 optical pyrometer. The temperature was maintained at 1273 K with a thermocouple-controlled programmer. Upon completion of 1000 hours exposure, the furnace was shut off and allowed to cool to room temperature.

5.4.3. Flexure testing

The strengths of all samples were measured using a four-point bend test conducted at room-temperature. While the four-point flexure test does not yield a true measure of the tensile strength of a material, the test does give a qualitative estimate of strength. Furthermore, the test is rapid and easy and can be used to compare similar specimens exposed to different conditions. The fixture employed had top and bottom spans of 20 mm and 40 mm respectively. Displacement was measured as a function of time and crosshead speed. The crosshead speed was 0.051 cm/minute. The

specimens were loaded perpendicular to the layers of cloth. Load versus time curves were recorded to characterize fracture behavior.

Flexure strength was calculated using the method described in ASTM test method D790-81, according to the equation

$$\sigma_{uF} = 3\ [(b-u)/2][P/wt^2]\ ,$$

where P is the applied load, w is the specimen width, and t is the specimen thickness.[62] The parameters b and u are the lower and upper spans, respectively, of the four point fixture.

5.5. Microanalysis

Upon completion of flexure testing, the samples were washed in acetone for examination of the fracture surfaces. Specimens which did not completely fracture during flexure testing were broken by hand so that the fracture surfaces could be examined. The surfaces of the specimens were examined using a Hitachi S-800 scanning electron microscope (SEM) with energy dispersive X-ray (EDX) capability. In some cases it was necessary to sputter the fracture surfaces with a thin conductive gold coating to prevent charging.

The fiber-matrix interfaces were characterized using

transmission electron microscopy (TEM). Sections of fractured specimens, 200-300 μm in thickness, were cut for TEM analysis using a low-speed diamond saw such that the ends of several fiber bundles were visible. The samples were then ground with a 6-μm embedded diamond disc to a thickness of ~75 μm, polished and dimpled to a center thickness of ~20 μm. The samples were then ion milled to electron transparency using argon ions. Microstructural and microanalytical results were obtained at 200 kV in a JEOL 2000FX analytical electron microscope equipped with a Kevex "Quantum" ultra-thin window energy dispersive X-ray spectrometer (EDX). High resolution electron microscopy was performed in a JEOL 4000EX operated at 400 kV. Images were recorded using a 1 mrad convergence semi-angle at Scherzer defocus (~ 47 nm). Optical diffraction patterns from the high resolution images were used to calculate d-spacings and thereby identify the interfacial coating phases.

6. EXPERIMENTAL RESULTS

6.1. Fiber Coatings

A summary of the weight gain during deposition of the sol-gel derived oxide coatings appears in Table 6.1. Weight gain is reported in percentage, as related to the initial weight of the Nicalon® cloth. These values were subsequently used to calculate coating thickness, based on fiber surface area and density of the sol-gel oxide, and assuming uniform application. Density values for titania, zirconia and alumina were available in the literature.[47] These calculations suggested coating thicknesses in the range of 0.015-0.030 μm. SEM examination of the coated fiber showed that the attempt to

Table 6.1 Withdrawl rate, calculated coating thickness and average weight gain during deposition of sol-gel derived oxide coatings on Nicalon® fibers.

Coating	Withdrawal rate (cm/min)	Coating thickness (μm)	Percent weight gain
Alumina	23	0.028 ± 0.003	1.16 ± 0.11
Alumina	80	0.030 ± 0.004	1.20 ± 0.19
Titania	23	0.015 ± 0.002	0.68 ± 0.11
Titania	80	0.020 ± 0.003	0.74 ± 0.06
Zirconia	23	0.019 ± 0.001	1.21 ± 0.07
Zirconia	80	0.023 ± 0.001	1.38 ± 0.08

vary coating thickness by varying the withdrawal rate was only partially successful.

SEM photographs also revealed the thicker alumina coating to be uneven with nearly every fiber only partially coated (Fig. 6.1b). The coating often failed to penetrate between the fibers, presumably due to viscosity effects. The thin alumina coating, however, was much more uniform with most fibers fully covered by the sol-gel coating (Fig. 6.1a). The coatings of zirconia and titania, both thick and thin, were mostly uniform with similar appearance to the thin alumina coating (Fig.6.2). A thin carbon layer was deposited to protect the oxides from chloride attack during deposition of the SiC matrix. Weight gain measurements after deposition of the graphite layer in the samples containing indicate carbon layer thicknesses of 0.012 μm, 0.021μm, 0.019 μm for the samples containing fibers coated with sol-gel alumina, titania and zirconia, respectively. Weight gain measurements of the control sample indicated a carbon layer thickness of 0.035 μm.

6.2. Composite properties

The infiltrated composites had average densities ranging from 2.36 ± 0.13 g/cm^3 to 2.65 ± 0.02 g/cm^3, which is approximately 80-90 % of theoretical density. The theoretical density is defined as the sum of the volume fractions of the individual composite components times their respective

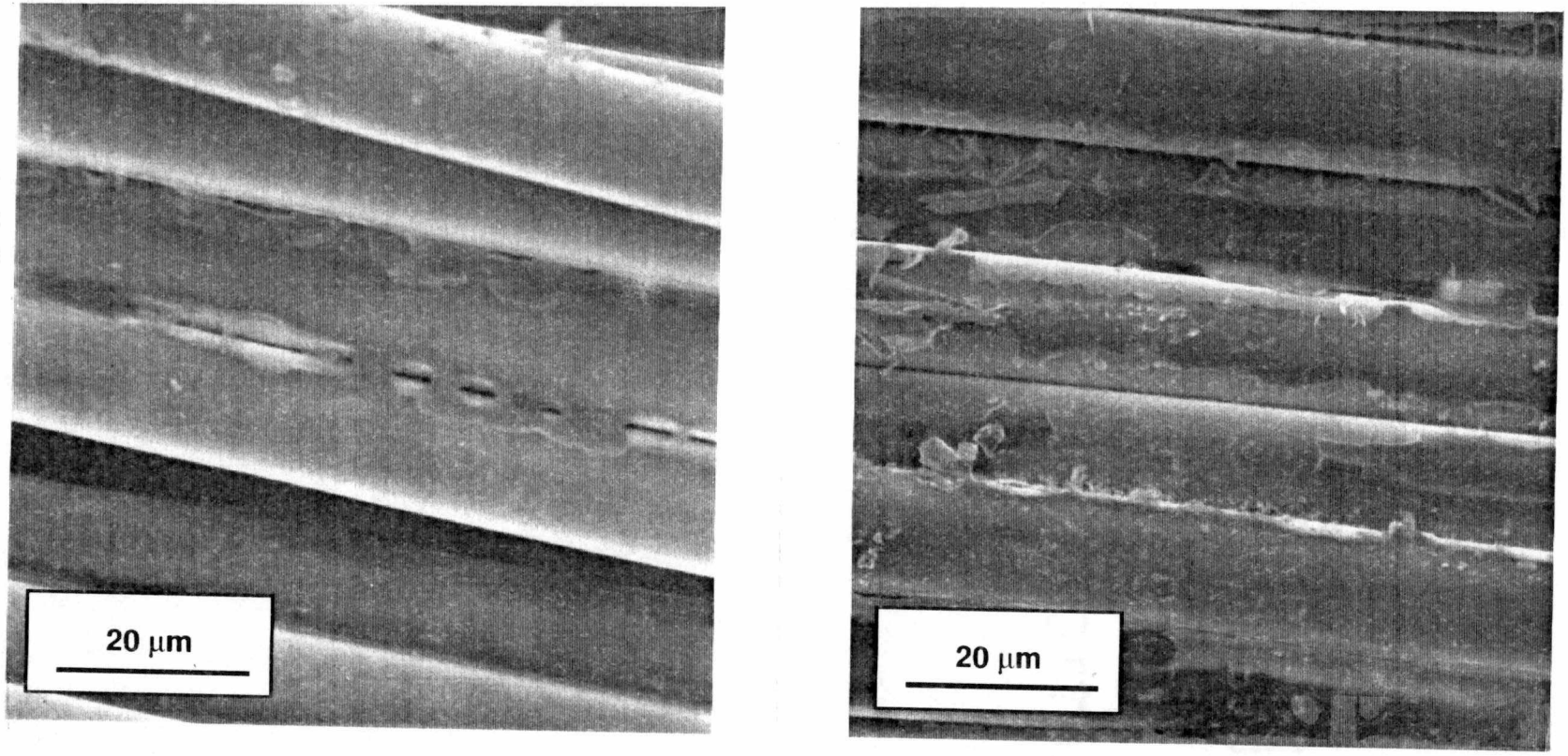

(a) (b)

Figure 6.1. SEM photographs of Nicalon® fibers with (a) thin and (b) thick alumina sol-gel derived coatings prior to carbon coating and densification.

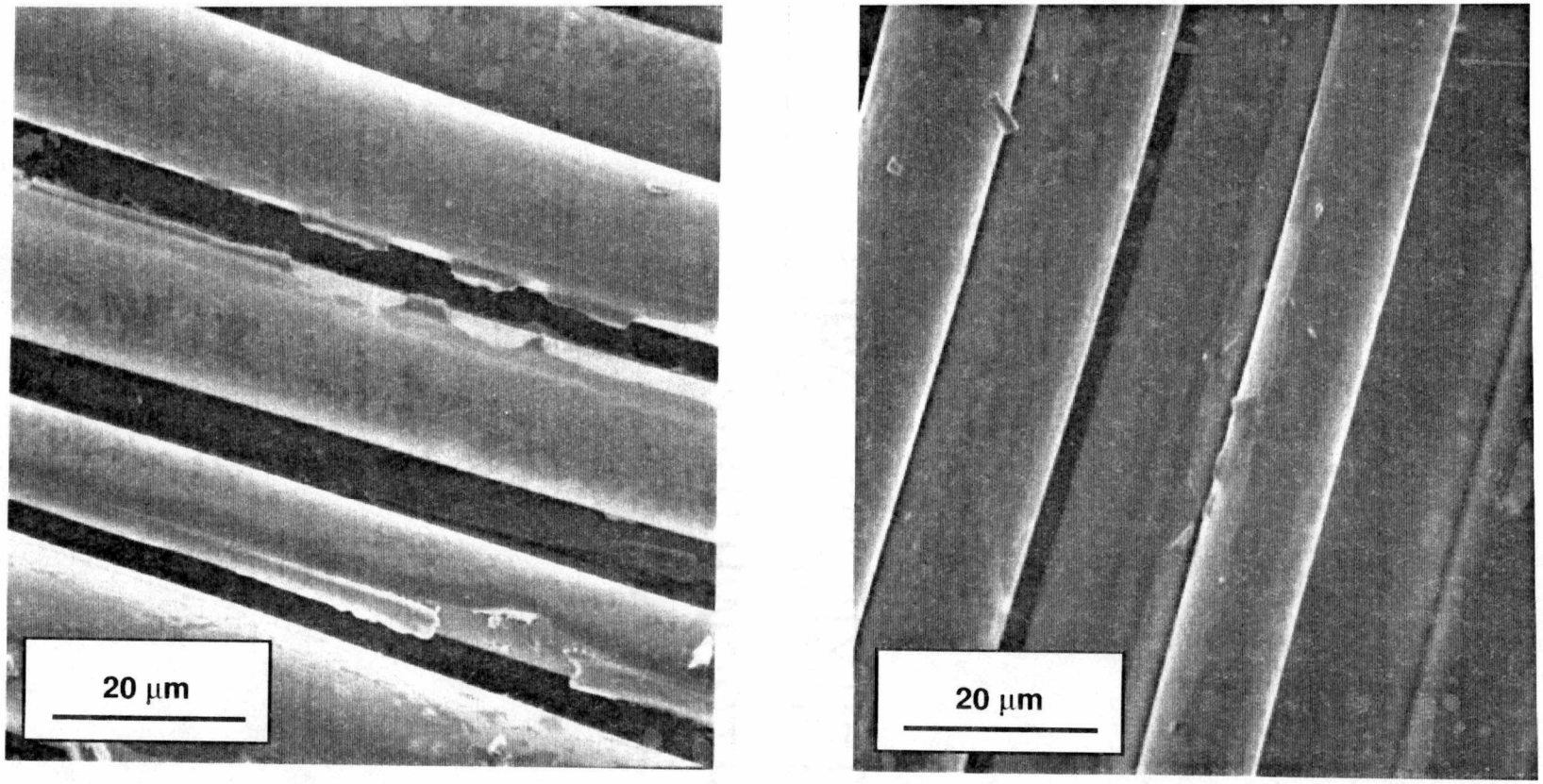

(a) (b)

Figure 6.2. SEM photographs of Nicalon fibers with thin (a) titania and (b) zirconia sol-gel derived coatings prior to carbon coating and densification.

densities. A control sample containing only a thin interfacial layer (~ 0.035 μm) of graphite was prepared by isothermal deposition prior to densification. Representative flexure stress versus displacement curves for the control and for samples with thick and thin sol-gel oxide interface coatings in the as-fabricated condition appear in Figure 6.3. Using maximum flexure fracture strength as a measure of effectiveness, composites with the thin coating out performed the thick coating in all three cases, with the control performing best of all. A summary of the average flexure fracture strengths and densities is found in Table 6.2., while the data for the individual bars appears in Appendix C. Increased fracture toughness vis-a-vis unreinforced SiC, which

Table 6.2. Mechanical properties for as-fabricated composites with sol-gel oxide and graphite interface coatings. Thickness measurements are based on weight gain.

COATING COMPOSITION	THICKNESS (μm)	FLEXURE STRENGTH (MPa)	DENSITY (g/cm^3)
Alumina	0.028	262 ± 42	2.61 ± 0.05
Alumina	0.031	182 ± 49	2.42 ± 0.03
Titania	0.015	198 ± 30	2.46 ± 0.05
Titania	0.020	186 ± 40	2.65 ± 0.02
Zirconia	0.019	68 ± 11	2.52 ± 0.05
Zirconia	0.023	30 ± 10	2.35 ± 0.04
Graphite	0.005	325 ± 20	2.60 ± 0.01

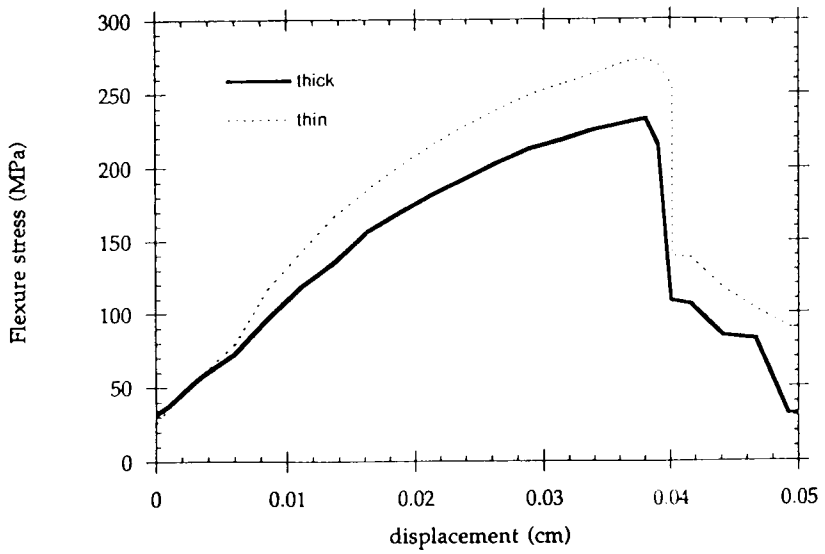

(a)

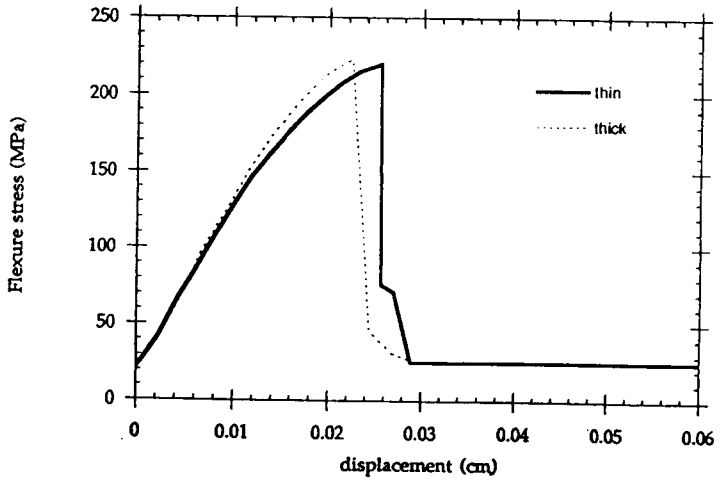

(b)

Figure 6.3. Representative stress deflection curves for as-fabricated composites with (a) alumina (samples thick-1 and thin-5), (b) titania (samples thick-1 and thin-4), (c) zirconia (samples thick-1 and thin-1) and (d) graphite (sample control-3) interfaces.

Figure 6.3 cont.

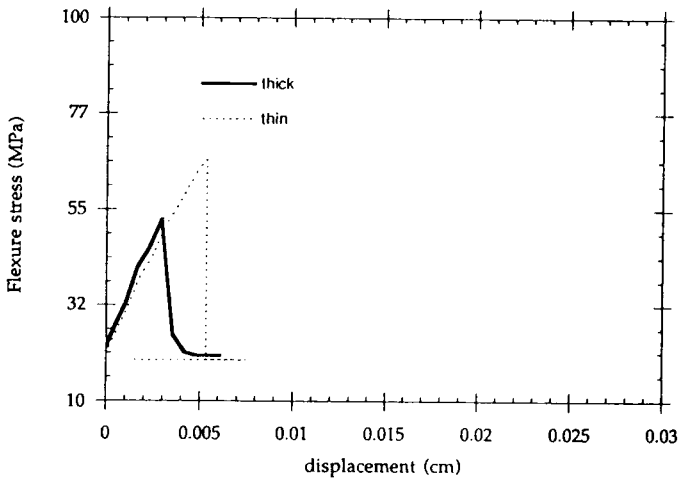

(c)

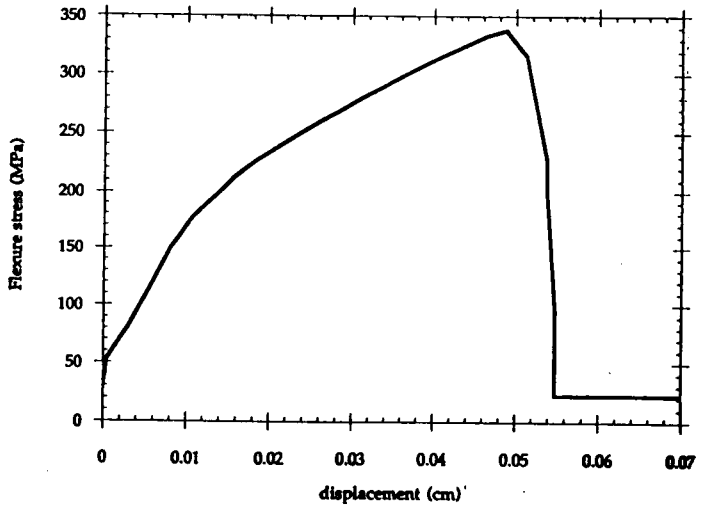

(d)

fails in brittle mode, was observed in the samples containing alumina, titania and graphite fiber coatings. These samples were characterized by a high degree of fiber pullout. The sample containing the zirconia coating was extremely weak, with very smooth fracture surfaces characteristic of brittle fracture.

6.3. Evaluation of High Temperature Behavior

A summary of flexure fracture strength test results, comparing samples exposed to air for 1000 h at 1273 K with and without seal coat with samples in the as-fabricated condition, appears in Table 6.3. Representative flexure stress versus displacement curves for sealed and unsealed samples are compared with the performance of as fabricated samples with alumina, titania and graphite interfaces in Figures 6.4-6.6. A measure of work of fracture was calculated from the area under the curves and is summarized in Table 6.4.

As previously described, SiC coatings were deposited on a number of flexure samples to prevent oxidation during exposure to high temperatures. These coatings ranged in thickness from 0.21-0.50 μm. Thicknesses were calculated based upon weight gain during deposition and surface area of the flexure bars. Flexure bars, with and without seal-coat, were placed in static air at 1273 K for 1000 hours. Samples with titania, zirconia and graphite interfacial layers

Table 6.3. Flexure strengths of Nicalon®/SiC composites after exposure to air for 1000 hours at 1273 K.

COATING	As Fabricated (MPa)	Heat treated (No seal) (MPa)	Heat treated (sealed) (MPa)
Al_2O_3-thin	262 ± 42	253 ± 41	275 ± 57
Al_2O_3-thick	182 ± 49	164 ± 21	217 ± 57
TiO_2-thin	198 ± 30	106 ± 18	212 ± 14
TiO_2-thick	186 ± 40	121 ± 40	188 ± 32
ZrO_2-thin	68 ± 11	---------	76 ± 15
ZrO_2-thick	30 ± 11	---------	34 ± 13
Graphite	325 ± 20	183 ± 12	335 ± 14

Table 6.4. Work of fracture of Nicalon®/SiC composites before and after exposure to air for 1000 hours at 1273 K. Values were calculated from the area under the flexure stress-displacement curves.

COATING	As Fabricated (kJ/m^2)	Heat treated (No seal) (kJ/m^2)	Heat treated (sealed) (kJ/m^2)
Al_2O_3-thin	70 ± 26	62 ± 35	53 ± 26
Al_2O_3-thick	48 ± 30	17 ± 8	50 ± 16
TiO_2-thin	36 ± 14	11 ± 2	32 ± 10
TiO_2-thick	27 ± 13	15 ± 5	15 ± 5
ZrO_2-thin	2.4 ± 1.1	---------	2.6 ± 1.3
ZrO_2-thick	1.2 ± 0.5	---------	1.2 ± 0.4
Graphite	125 ± 8	45 ± 5	125 ± 13

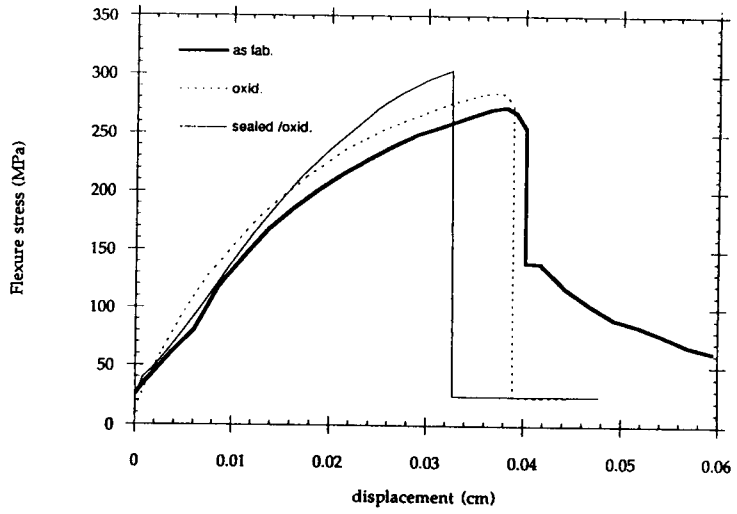

(a)

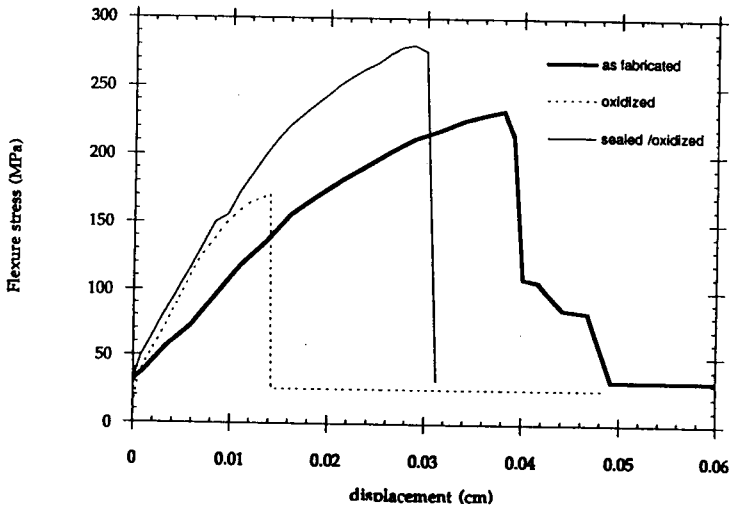

(b)

Figure 6.4. Representative flexure stress-deflection curves for composites with (a) thin (flexure samples 5,9 and 13) and (b) thick (flexure samples 1,6 and 10) alumina interface coatings upon exposure to air for 1000 h at 1273 K.

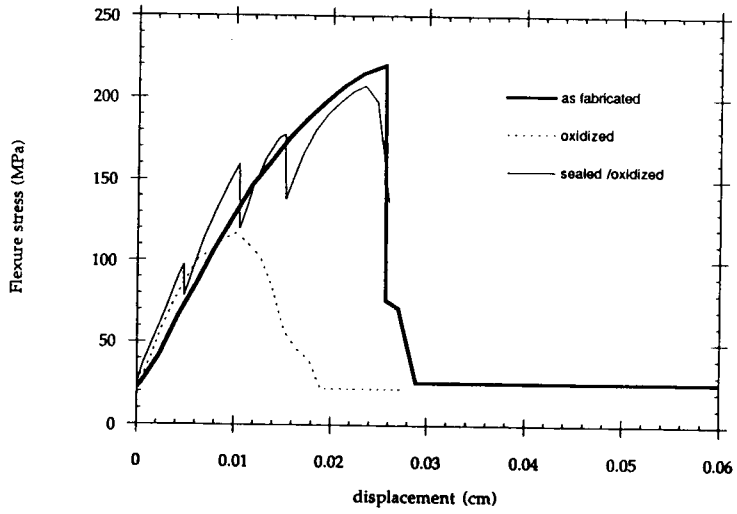

(a)

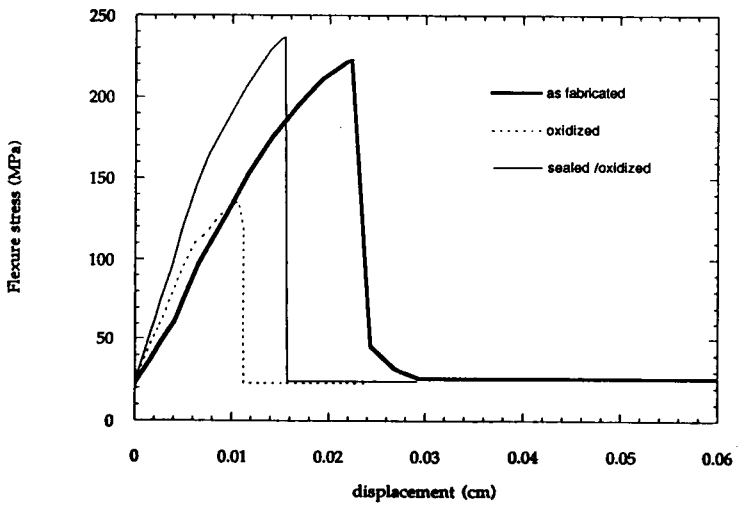

(b)

Figure 6.5. Representative flexure stress-deflection curves for composites with (a) thin (flexure samples 4,5 and 9) and (b) thick (flexure samples 1,5 and 12) titania interface coatings upon exposure to air for 1000 h at 1273 K.

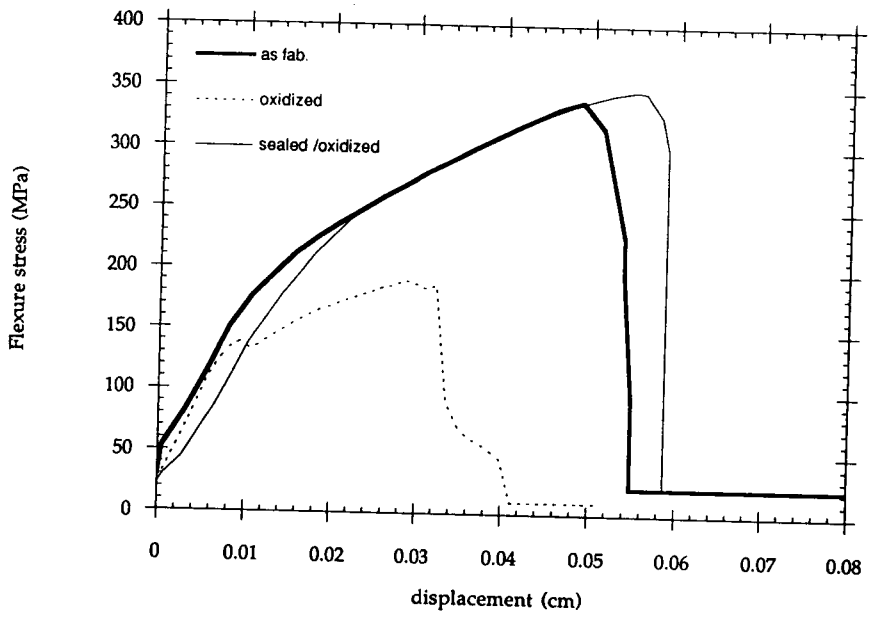

Figure 6.6. Representative flexure stress-deflection curves for composites with graphite (control flexure samples 3,6 and 11) interface coatings upon exposure to air for 1000 h at 1273 K.

displayed significant loss of strength and toughness when exposed to air at high temperatures without a protective layer of SiC. Samples containing a zirconia interface were often unable to withstand the weight of the fixture without undergoing fracture. It was impossible, therefore, to obtain an accurate measure of strength. While becoming significantly weaker upon exposure to air, the samples with titania and graphite interfaces still displayed a noticeable degree of composite behavior. Significant fiber pull-out occurred in these samples. Statistically, no loss of fracture toughness or flexure fracture strength was observed in the samples containing the thin alumina interface, where a substantial degree of fiber pull-out was observed. The specimens containing the thicker alumina interlayer suffered some reduction in strength and significant reduction of toughness.

The seal-coated samples were subsequently tested for flexure fracture strength. Samples with the seal-coat displayed strengths statistically identical with the as-fabricated samples (Table 6.3). Behavior with regard to fracture toughness was more varied. A large degree of fiber pull-out was seen in the samples with thin alumina, thin titania and graphite coatings. The specimens with the thin titania layer displayed stress-displacement behavior in which the stress level underwent repeated increases and decreases consistent with delamination between layers (Fig. 6.5a). While the loss of strength was insignificant, samples with

thicker alumina and titania interlayers failed at noticeably lower displacements, resulting in a reduction of fracture toughness. The bars containing zirconia coatings were again weak and brittle.

6.4. Microanalysis

6.4.1. Graphite interlayer (Control)

SEM analysis of the fracture surface of the composite containing a carbon interface displayed substantial fiber pull-out in the as-fabricated condition (Fig 6.7a). In the samples without the seal coat which were exposed to high temperature air, the regions closest to the external surface became embrittled while the center regions retained extensive fiber pull-out (Fig. 6.7b) The width of this embrittled region varied from 300-600 μm. The fracture surfaces of flexure specimens with the seal coat did not differ discernibly from those as-fabricated.

TEM analysis of the as-fabricated carbon interlayer revealed a continuous layer between the fiber and matrix approximately 0.04 μm in thickness (Fig. 6.8). Using high resolution TEM the carbon was identified to be graphite by its structure and atomic spacing. The spacing was measured to be 0.34 nm, the c-axis in graphite (Fig. 6.9). TEM analysis was conducted on the interface in the center region where fiber

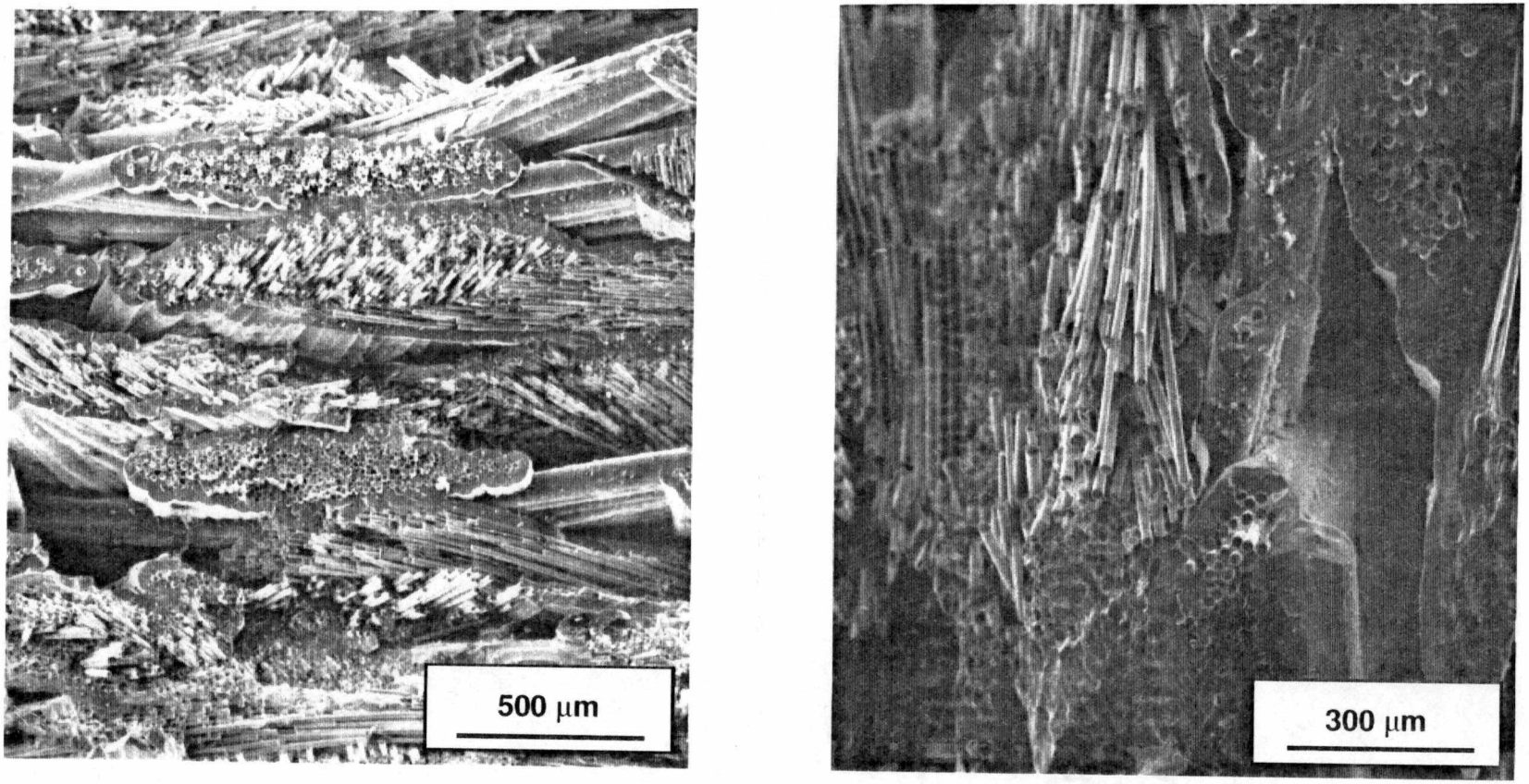

(a) (b)

Figure 6.7. SEM photographs of fracture surfaces of Nicalon®/SiC composite with graphite interlayer (a) as fabricated (control flexure 3) and (b) after exposure to air for 1000h at 1273 K (control flexure 6).

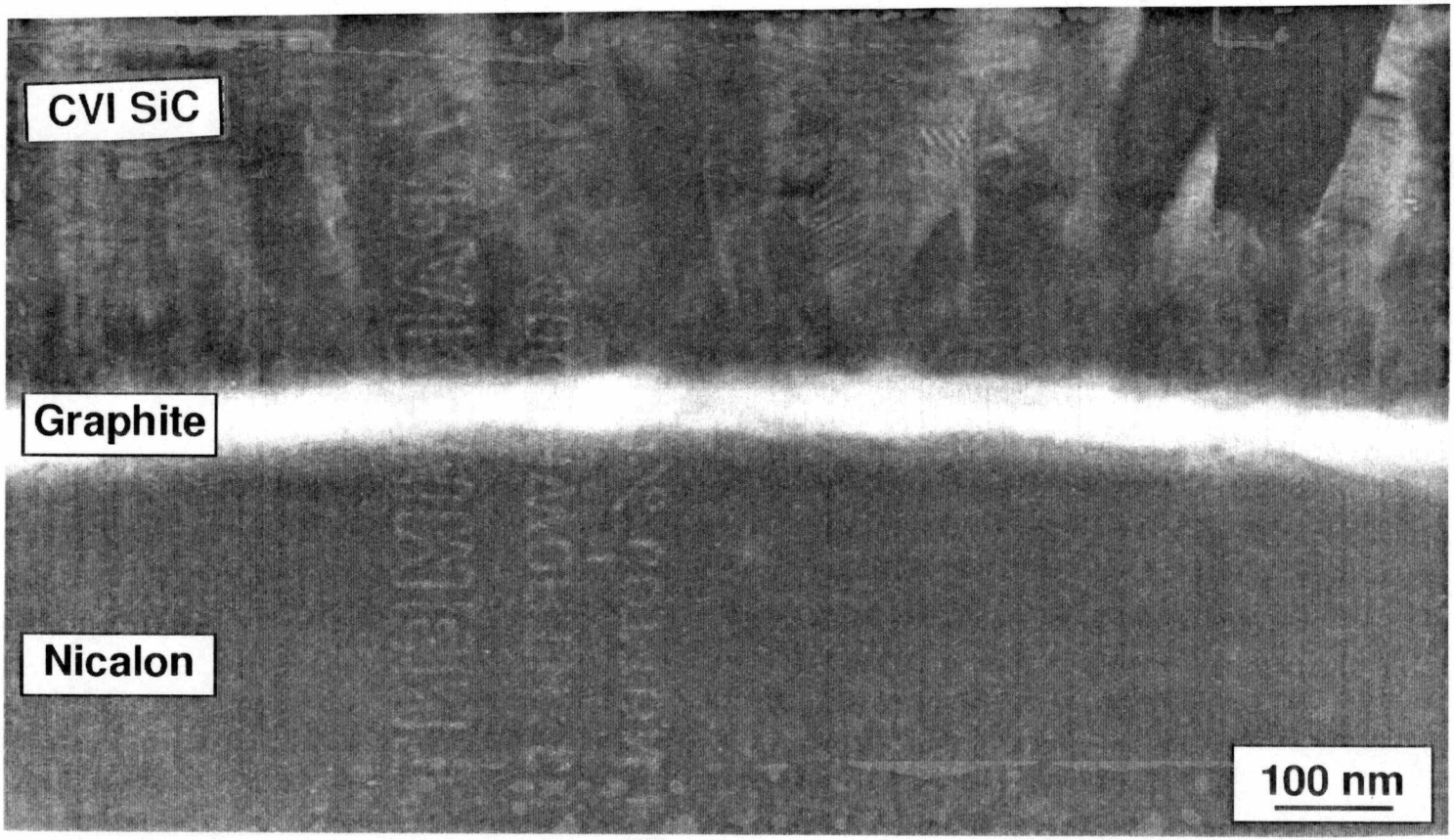

Figure 6.8. TEM micrograph of graphite interlayer in Nicalon®/SiC composite in as-fabricated condition (control flexure 3).

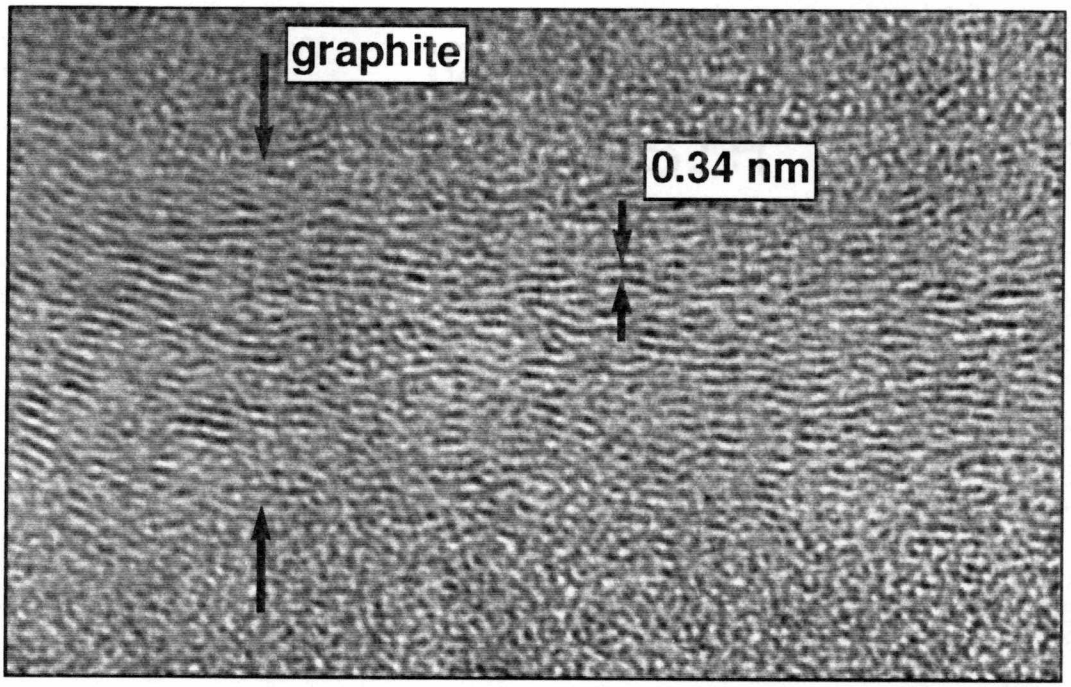

Figure 6.9. High resolution TEM photograph of graphite interlayer in Nicalon®/SiC composite (control flexure 3)

pull-out was retained in the uncoated samples which were exposed to air at 1000°C for 1000 h. No change was observed.

6.4.2. Alumina interlayer

SEM analysis of the fracture surfaces confirmed the abundance of fiber pull-out in the as-fabricated flexure samples containing thin alumina interlayers (Fig. 6.10). Use of energy dispersive X-ray (EDX) revealed the presence of aluminum at nearly all fiber-matrix interfaces. The aluminum peak was always quite weak in comparison to the silicon peak due to the great amount of silicon in both fiber and matrix. Use of EDX revealed trace amounts of aluminum on the matrix surfaces resulting from the pull-out of fibers (Fig. 6.11). SEM analysis of the thicker alumina coating likewise revealed a large degree of fiber pull-out with EDX analysis identical to that of the thinner coating.

The fracture surfaces of the flexure bars with the thin alumina layer subjected to oxidation conditions were likewise examined with no noticeable differences with the unexposed samples (Fig. 6.12). Fiber pull-out was retained throughout the composite, including the regions adjacent to the composite surface (Fig. 6.13). The fiber-matrix interfaces were subsequently examined using TEM analysis. Micrographs of the sample containing the thinner of the two alumina interfaces revealed a continuous layer, 0.04-0.08 μm in

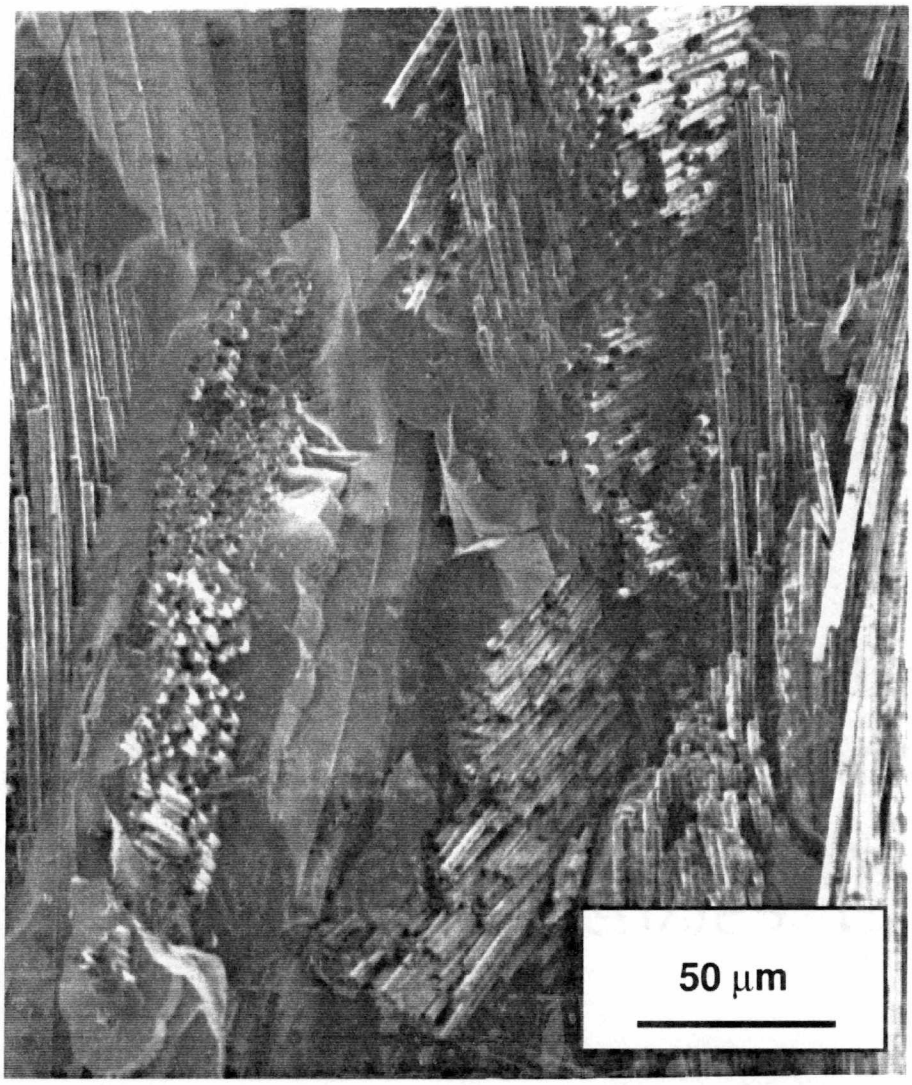

Figure 6.10. SEM photograph of fracture surface of flexure test bar of Nicalon®/SiC composite containing thin alumina interface (flexure sample 5) in as-fabricated condition.

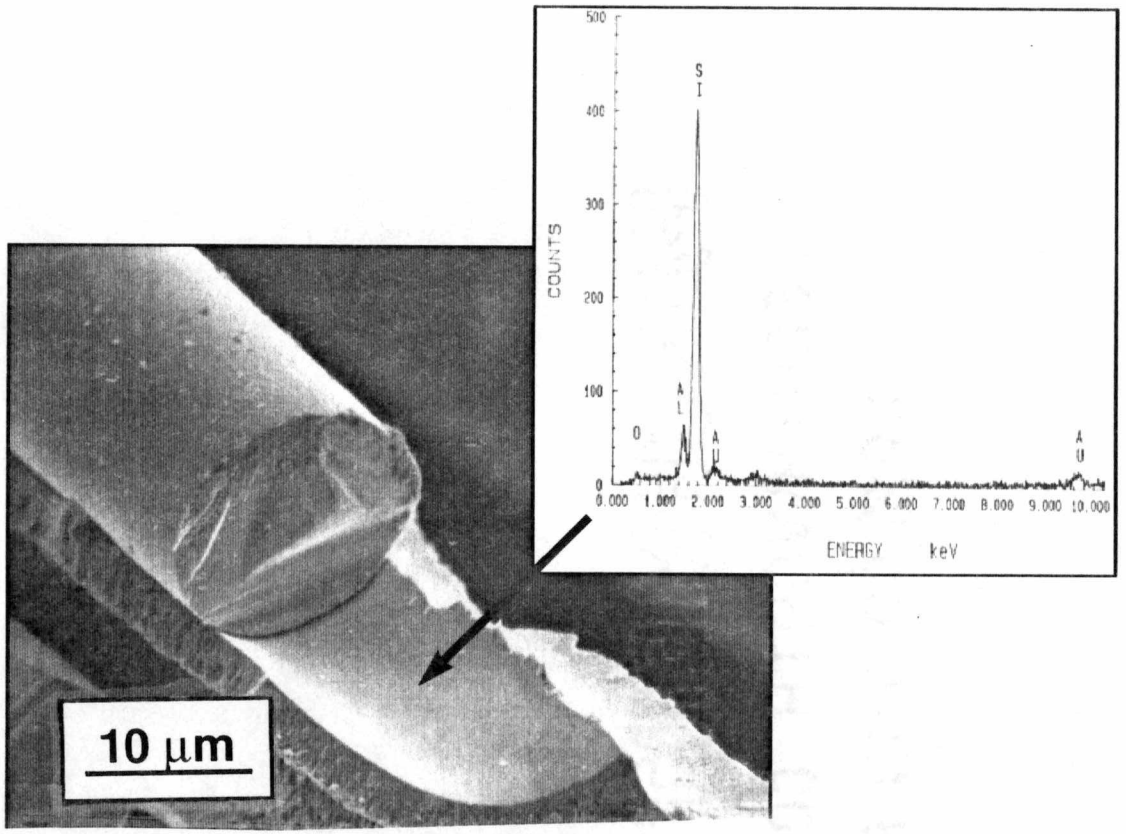

Figure 6.11. SEM photograph of SiC-matrix surface resulting from fiber pull-out in a composite with a thin alumina interlayer (flexure sample 4) and corresponding EDX spectrum.

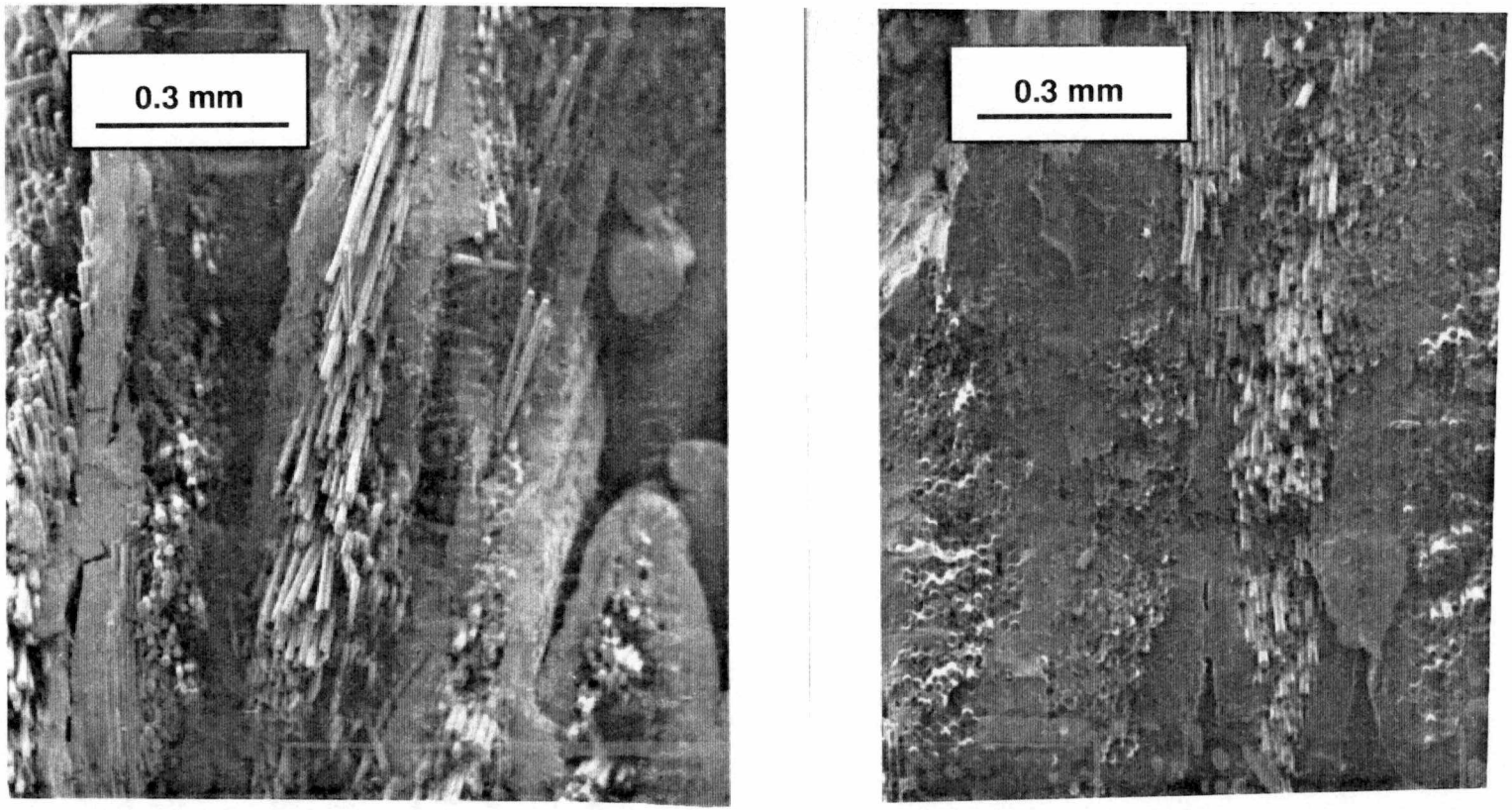

(a) (b)

Figure 6.12. SEM photographs of fracture surfaces of composites containing thin alumina interface after exposure to air at 1273 K for 1000 h (a) with (flexure sample 13) and (b) without (flexure sample 9) protective seal-coat.

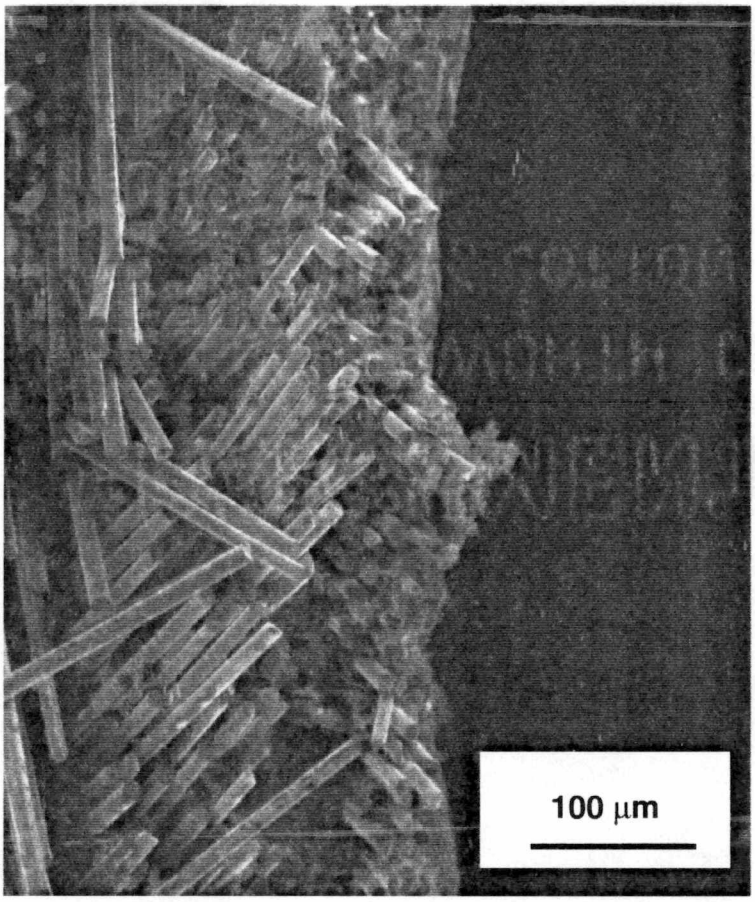

Figure 6.13. SEM photograph of region adjacent to the composite surface of Nicalon/SiC composite containing a thin alumina interlayer after exposure to air for 1000 h at 1273 K (thin-8).

thickness (Fig. 6.14). An elemental analysis, using EDX, was conducted on this layer and the neighboring fiber and matrix. Upon examination of the continuous layer, the resulting spectrum contained sharp peaks for aluminum and silicon, with the aluminum peak being nearly three times the intensity of that of silicon. Further analysis using a JEOL 4000EX high resolution transmission electron microscope revealed an ordered structure. Because of the extreme thinness of the coating, a clear electron diffraction pattern could not be obtained. An optical diffraction pattern was taken and a d-spacing of 3.37 Å was measured, which was then compared against values in the JCPDS card files.[63] Two possible matches were found; the 220 planes of both mullite ($Al_6Si_2O_{13}$) and Al_2SiO_5. The layer was identified as mullite based on the d-spacing and the apparent 3/1 aluminum/silicon ratio from EDX. EDX spectra on the fiber and matrix adjacent to the interlayer revealed no traces of aluminum. In addition, a discontinuous graphite layer, varying in thickness up to 5 atom layers (1.5 nm), was found between the coating and matrix (Fig. 6.15). Presumably this layer is a result of the preliminary deposition of graphite, conducted prior to densification. An equally thin graphite layer, identified by its distinct structure and interatomic spacing of 3.4 Å, was observed between the fiber and the mullite interlayer, possibly a product of Nicalon® fiber degradation.

This analysis was repeated on the thicker alumina

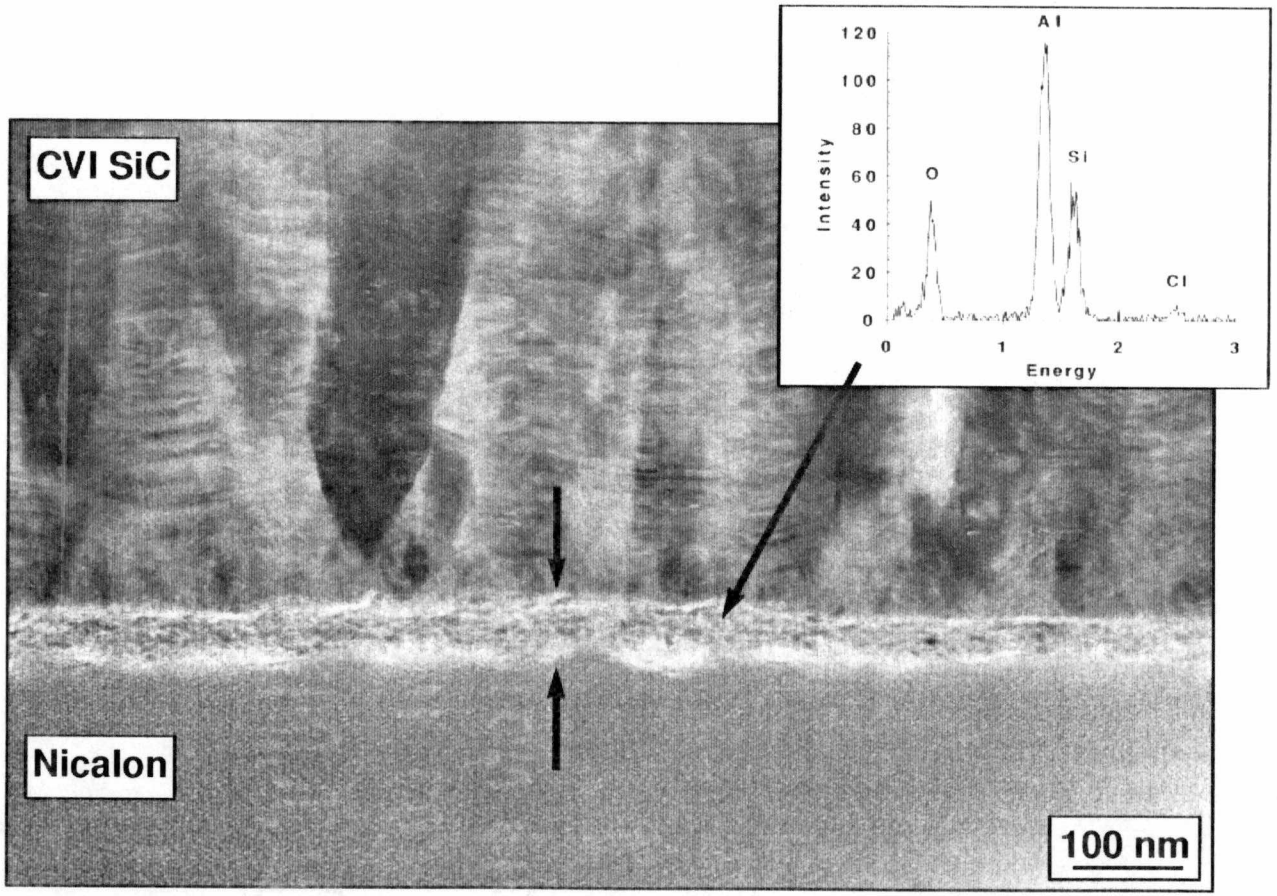

Figure 6.14. TEM micrograph of as-fabricated thin alumina (flexure sample 5) interface with corresponding EDX spectrum (arrows indicate the edges of the mullite layer).

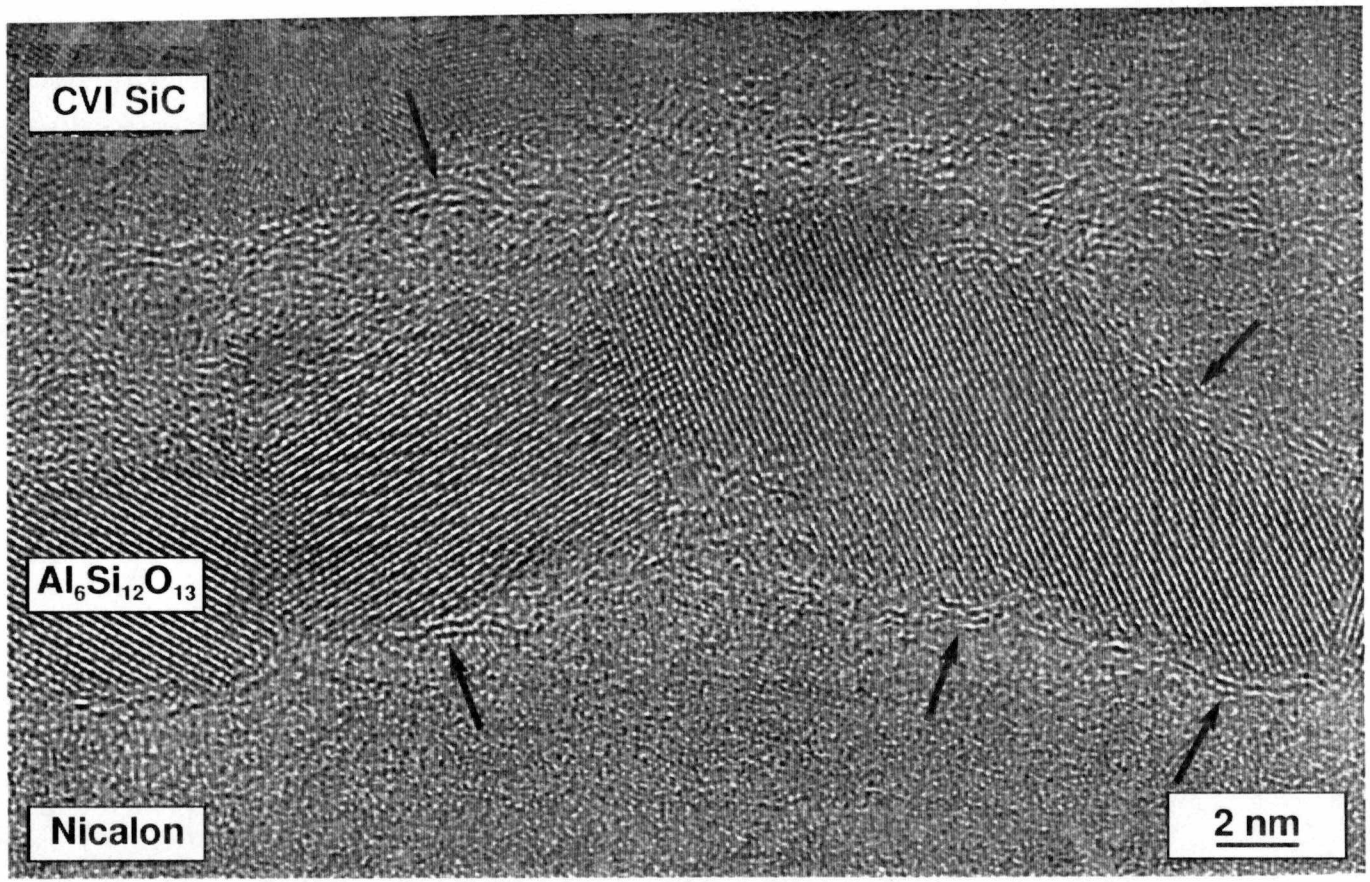

Figure 6.15. High resolution TEM micrograph of as-fabricated thin alumina (flexure sample 5) interfacial coating (arrows indicate graphitic carbon).

interface. SEM analysis of the fracture surface in the as-fabricated composite revealed a substantial amount of fiber pull-out (Fig. 6.16a), while a sample exposed to air at 1000°C displayed only limited fiber pull-out (Fig. 6.16b). TEM analysis of the interfacial oxide layer revealed the layer to be discontinuous. The interfacial material was often found in particles approximately 0.1 μm in thickness. The structure varied greatly from fiber to fiber with a total lack of alumina often observed (Fig. 6.17). Using electron diffraction, d-spacings were obtained and compared with the JCPDS card files[63] and the layer was found to consist of alumina. As in the sample containing the thinner alumina layer, an extremely thin layer (< 5 nm) layer of graphite was observed between the coating and matrix. No carbon layer, however, was observed between fiber and coating.

6.4.3. Titania interlayer

Analysis of the fracture surface of the as-fabricated titania-containing composite revealed a substantial amount of fiber pull-out which was uniform over the entire surface (Fig. 6.18a). Elemental analysis at the interface was attempted using EDX. In contrast with the case of the alumina-containing composite, titanium proved very elusive. EDX spectra consistently revealed peaks for silicon with no noticeable titanium peak. No difference was evident between

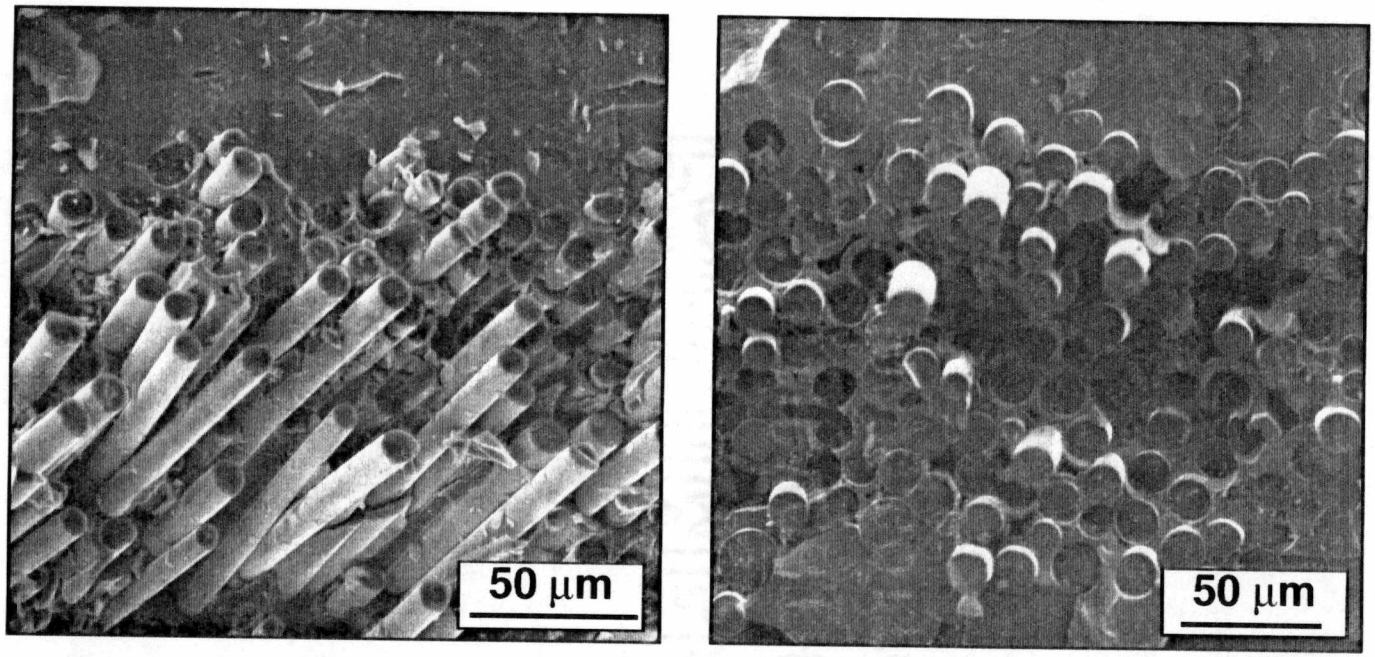

(a) (b)

Figure 6.16. SEM photographs of fracture surfaces of Nicalon®/SiC composites with thick alumina layer (a) as-fabricated (flexure sample 1) and (b) exposed to air at 1000°C for 1000 h (flexure sample 9).

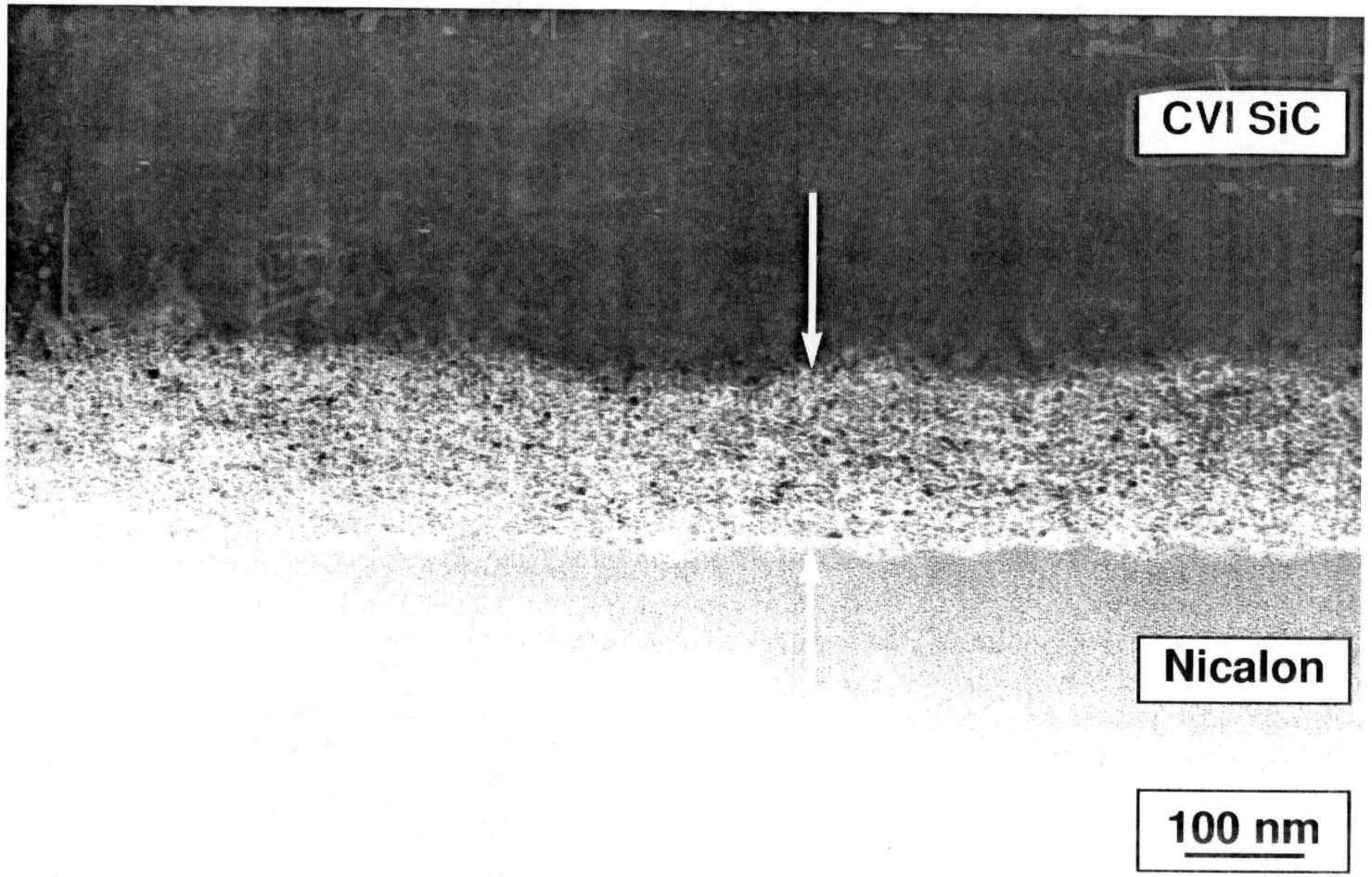

Figure 6.17. TEM micrograph of as-fabricated thick alumina (flexure sample 9) interface with arrows indicating coating edge.

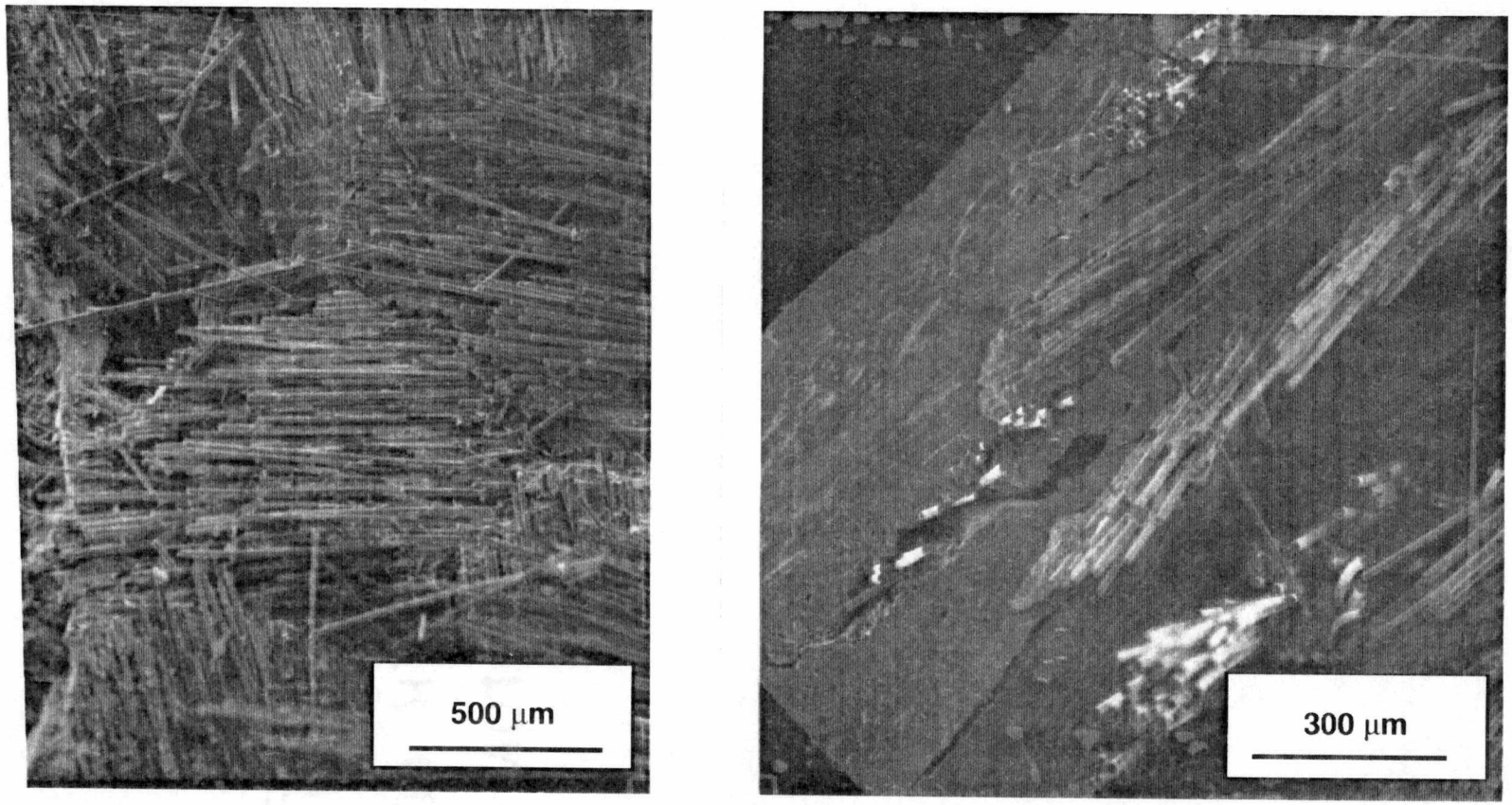

(a) (b)

Figure 6.18. SEM photographs of composite with thin titania interface (a) before (flexure sample 1) and, (b) after exposure to air at 1273 K for 1000 hours without seal-coat (flexure sample 8).

the thin and thick coatings with both samples demonstrating fiber pull-out.

The fracture surfaces of the titania-containing samples exposed to air at 1273 K for 1000 h were subsequently examined by SEM, with large differences in behavior very apparent in the samples without the protective seal-coat. As in the case of the control sample, significant fiber pull-out was seen in the center regions of the sample, while those areas adjacent to the edges were strongly bonded at the fiber-matrix interface, where the sample fractured in a brittle manner (Fig. 6.18b-19). The width of the embrittled region varied from 250 to 600 μm. Those samples with the protective seal-coat displayed fiber pull-out throughout the fracture surface as in the as-fabricated case. In all cases, no difference was discernible between thin and thick coatings.

TEM analysis of the titania interfacial layer in as-fabricated Nicalon®/SiC revealed a heterogenous layer consisting of several distinct regions (Fig. 6.20). The total thickness and structure of all components of the layer did not differ in any significant manner between thick and thin coatings. EDX analysis of the interface region revealed that titanium and was present only in small (0.2-0.8 μm in diameter), spherical inclusions, which were dispersed along the interface. These inclusions were identified as TiC by electron diffraction. The pattern was typical of a cubic structure and the d-spacings of 2.39, 2.00 and 1.42 Å were

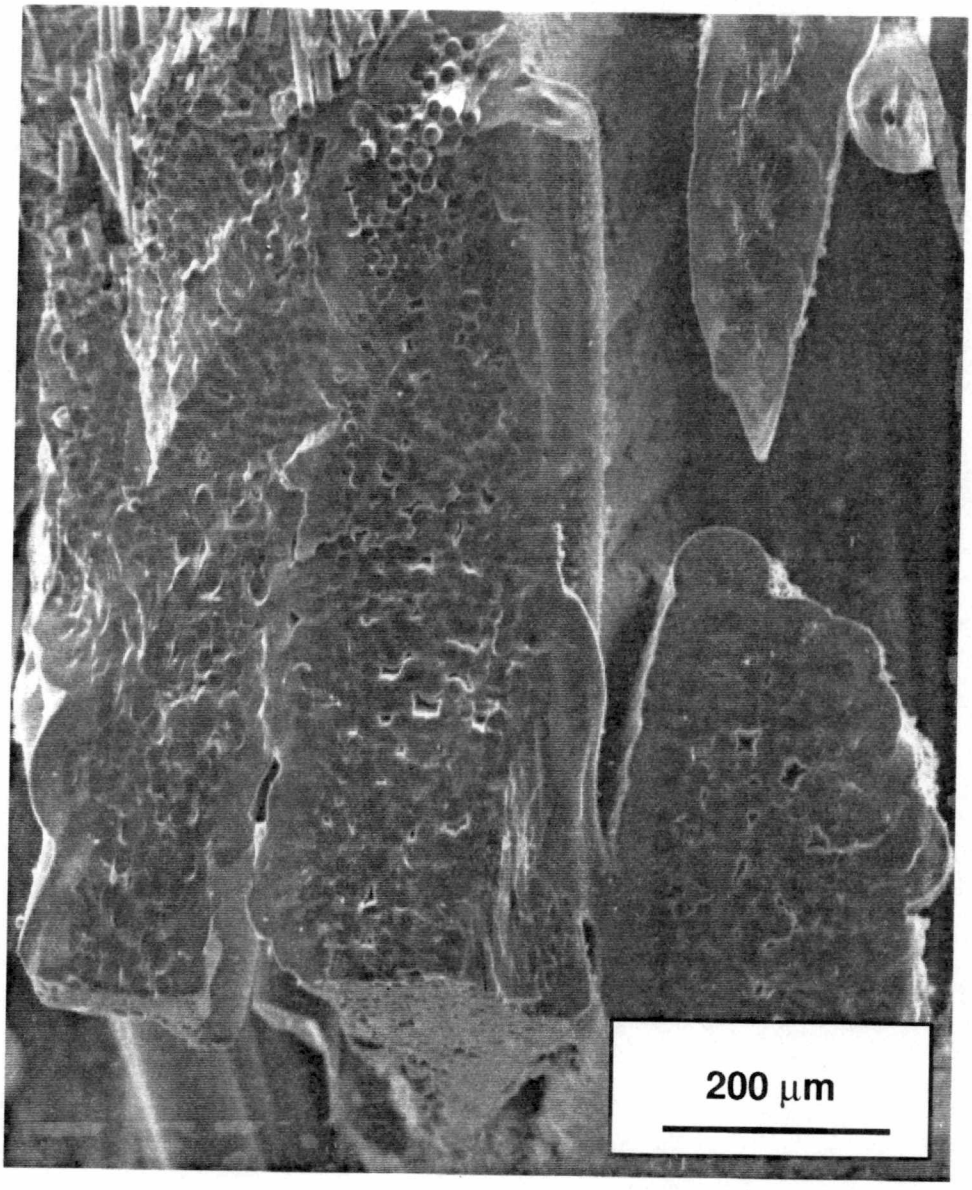

Figure 6.19. Oxidized region near the surface of unsealed composite with thin titania interface (flexure sample 8) after exposure to air for 1000 h at 1273 K.

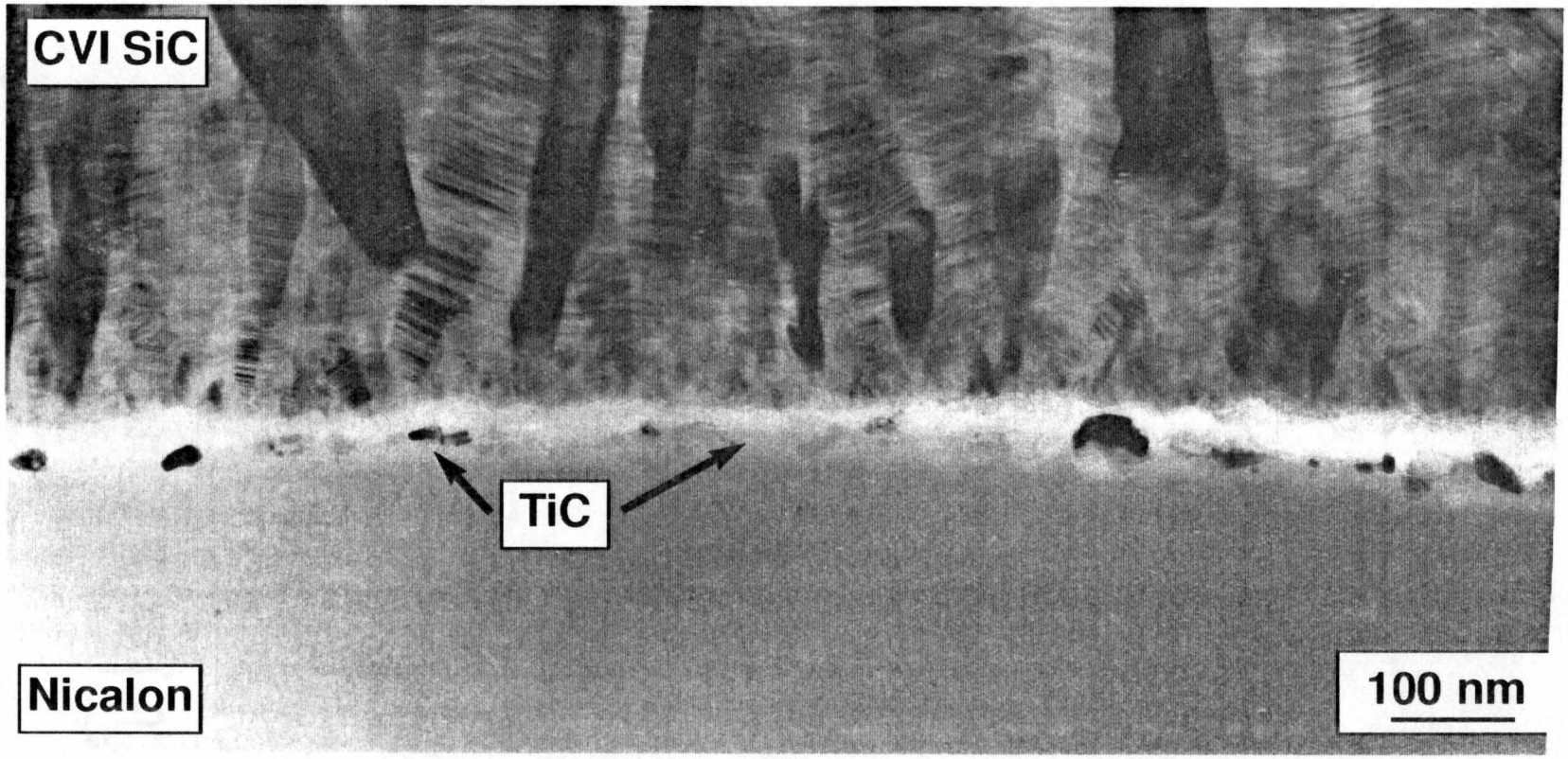

Figure 6.20. TEM micrograph of as-fabricated thin titania (flexure sample 1) interlayer in Nicalon®/SiC composite.

consistent with the 111, 200 and 311 planes, respectively, of TiC[63] (Fig. 6.21). Between the TiC inclusions was an amorphous region, 0.2-0.7 μm in thickness, devoid of titanium. Unlike the thin alumina layer samples, graphite was not detected between the fiber and coating. Graphite (0.03-0.04 μm in thickness) was detected in a continuous layer at the coating/matrix interface, presumably deposited as previously described.

The interfaces were also examined after exposure to air for 1000 h at 1273 K for samples with and without the protective seal-coat. As previously noted, samples exposed to air without the seal coat possessed regions with varying behavior. TEM analysis of the interface was conducted on the embrittled region adjacent to the surface of the sample, as well as on the interface in the center region which exhibited substantial fiber pull-out (Fig.6.22). The interface in the center region was identical to that of the as-fabricated sample. In the embrittled region, the graphite layer was absent, replaced by voids and a new distinct layer, approximately 0.080 μm in thickness. EDX analysis revealed this layer to be devoid of titanium. TEM analysis in previous studies of the oxidation behavior of Nicalon®/SiC composites with graphite interlayers showed a similar layer after the composite was to exposed air (Fig. 2.6)[19-20]. Lowden showed this layer to be composed of silica. Given the absence of Ti in this layer along with its similarity to the layer observed

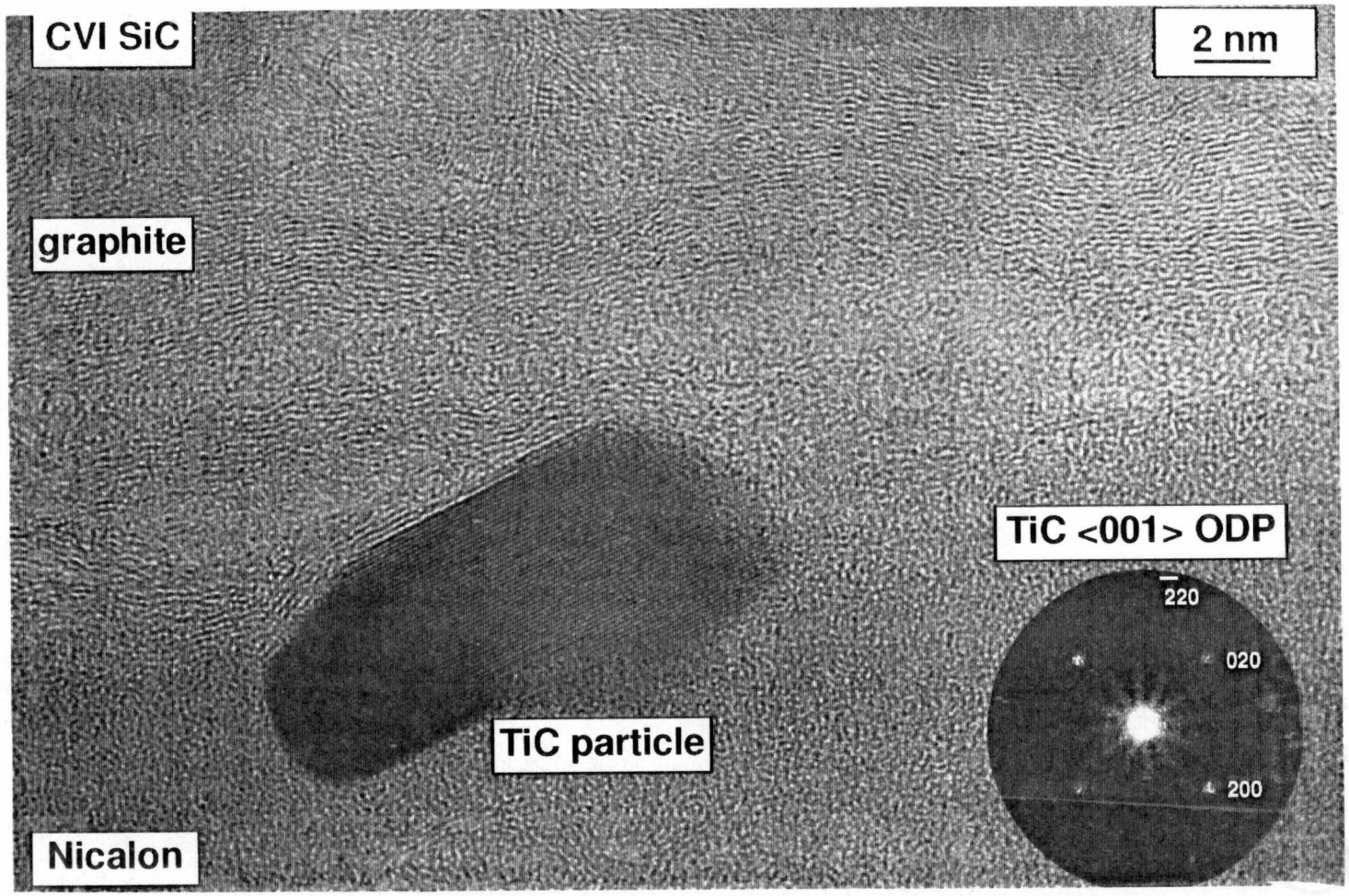

Figure 6.21. High resolution TEM micrograph of as-fabricated thin titania interlayer (flexure sample 1) with an electron diffraction pattern of the TiC particle.

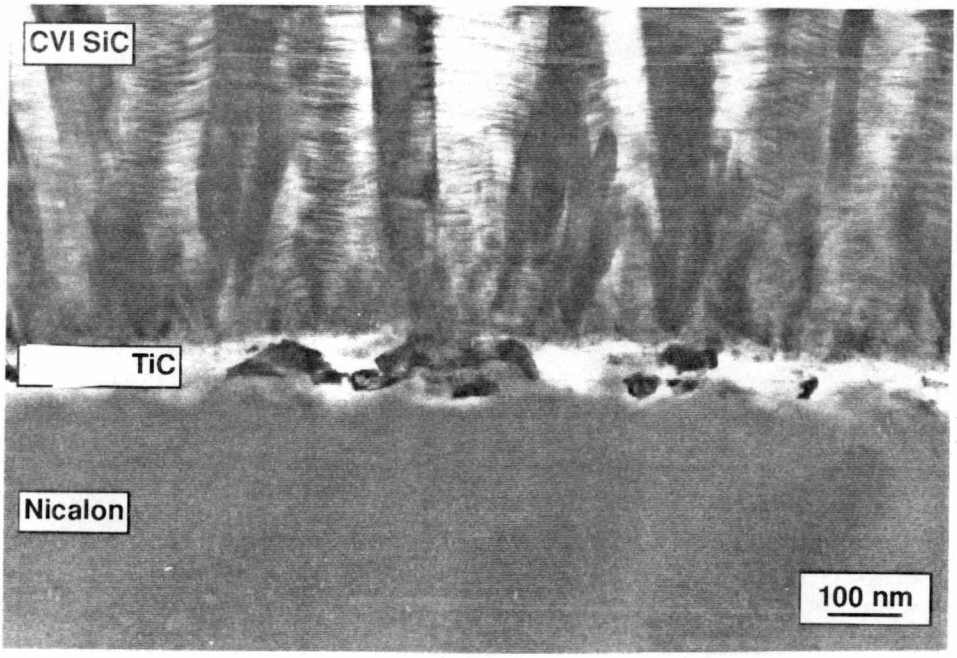

(a)

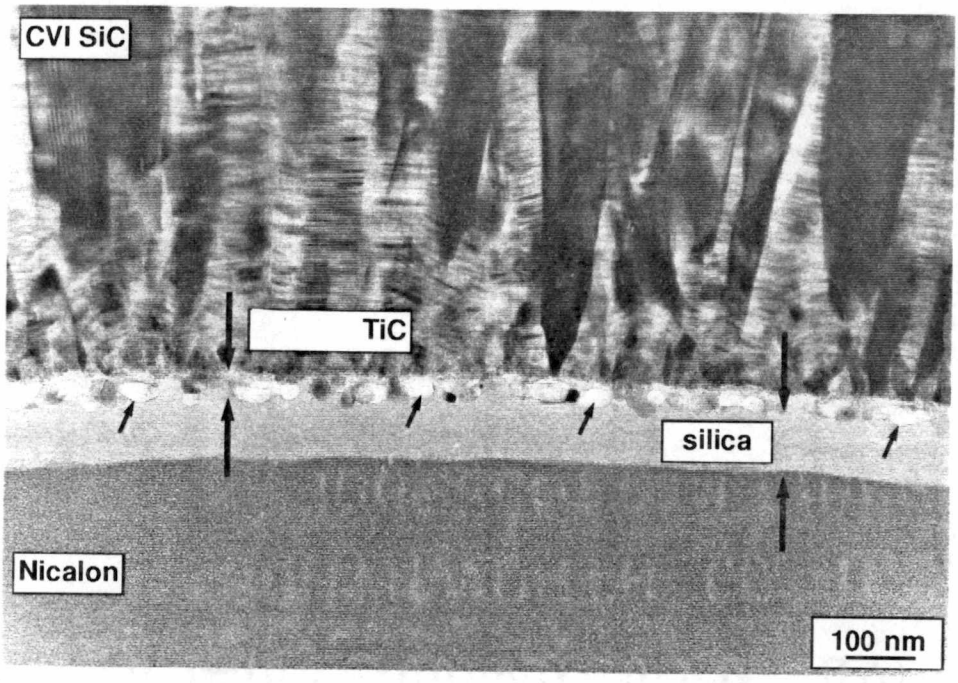

(b)

Figure 6.22. TEM micrographs of thin titania interlayer (flexure sample 8) in a Nicalon®/SiC composite after oxidation; (a) at the center and (b) near the surface without seal-coat.

by Lowden, this layer is assumed to be silica. TiC was stable and appeared unchanged and was again identified with electron diffraction. In the samples with the seal coat, the interface was unchanged from the as-fabricated condition.

6.4.4. Zirconia interlayer

As seen in Figure 6.23, samples containing the zirconia interlayer fractured in a very brittle manner. The fracture surface demonstrates no crack deflection or fiber pull-out. as expected based on the flexure tests. As in the case of the titania interlayer, EDX analysis with the SEM rarely revealed the presence of zirconia. Samples with both thick and thin interfacial coatings were found to be identical.

As in the case of the titania interface, TEM analysis revealed a heterogeneous interface with no discernible difference between thick and thin coatings. EDX analysis revealed zirconium present only in inclusions, varying in size up to 0.1 μm in diameter (Fig. 6.24). Employing optical diffraction and high resolution TEM, the inclusions were shown to have a d-spacing of 2.95 Å. This value was compared against the JCPDS card files[63] and was found to be consistent with several forms of ZrO_2. The d-spacing value was not consistent with any value for zircon ($ZrSiO_4$). Without any other data, it is impossible to eliminate any of the possible forms of zirconia and identify the structure precisely. A

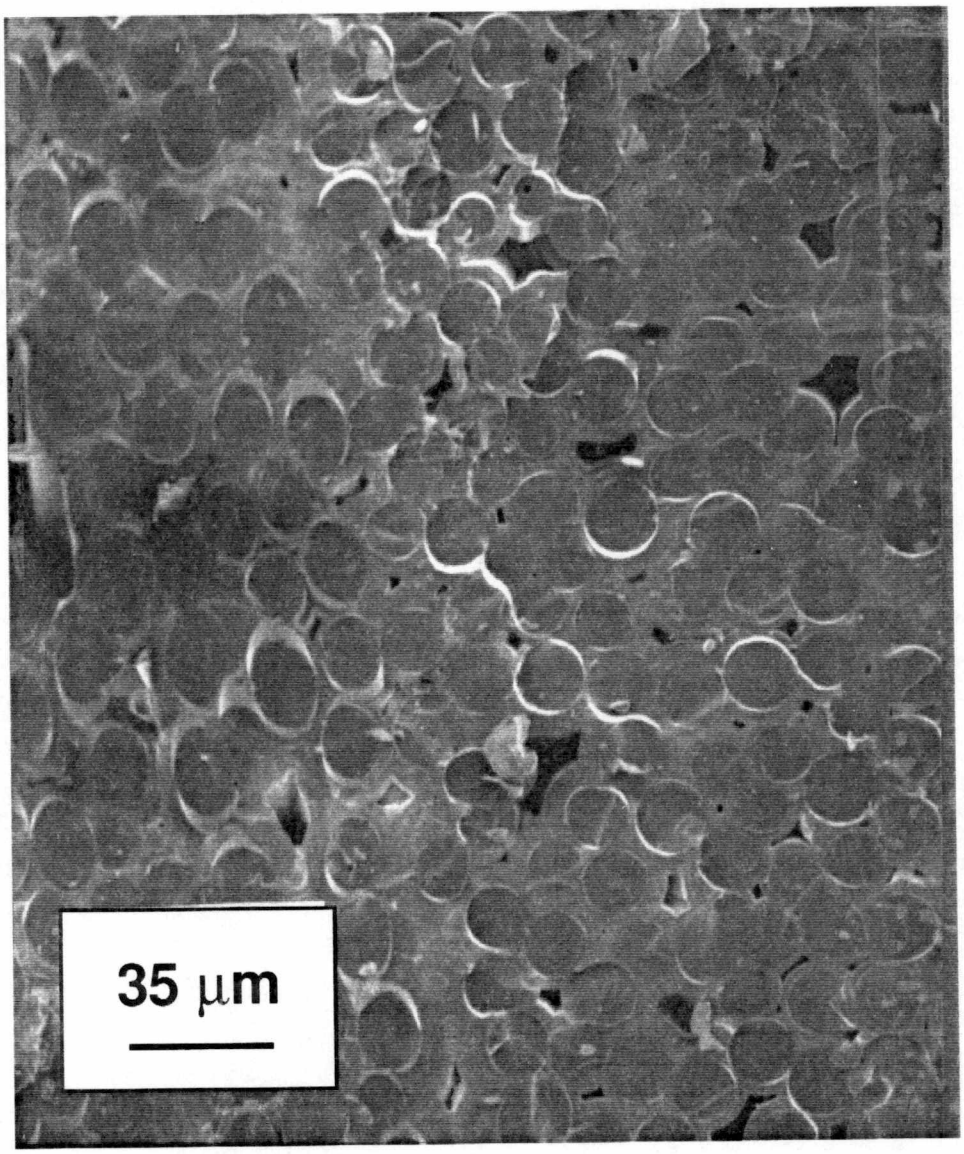

Figure 6.23. SEM photograph of fracture surface of composite with as-fabricated thin zirconia (flexure sample 2) interlayer.

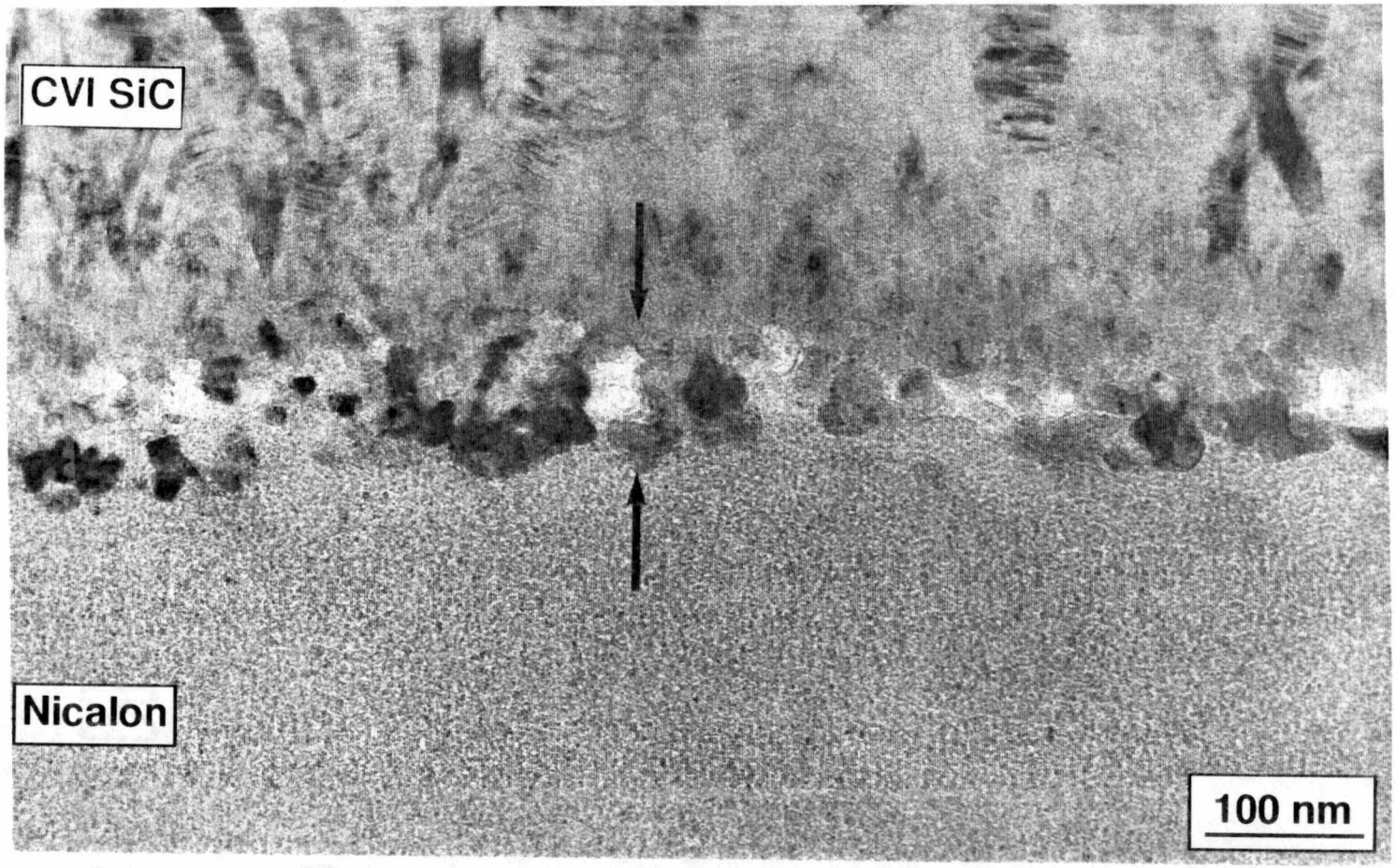

Figure 6.24. TEM micrograph of as-fabricated thin zirconia (flexure sample 2) interlayer.

thin layer of graphite (5-6 nm) was present between the coating and matrix, while no graphite was detected between fiber and coating.

7. DISCUSSION

The thin nature of the deposited oxide and carbon interface layers afforded little reduction in the residual, clamping stress based on the thermomechanical calculations. At coating thickness < 0.05 μm, none of the proposed coatings reduces clamping stress at either fiber-coating or coating-matrix interface to any significant degree. The presence of a poorly bonded, continuous interface layer, however, does require less energy for the initiation of fiber pull-out.

During room temperature flexure testing, the control composite material possessing a graphite interlayer demonstrated significant flexure strength (325 ± 8 MPa). This value is in close agreement with the work of Lowden[18], who recorded room-temperature flexure strengths of 320-340 MPa in Nicalon®/SiC composites with graphitic interlayers, 0.03 μm in thickness. Again, the fracture surface was characterized by large degree of fiber pull-out.

The most serious deficiency of graphite as an interfacial material is its lack of oxidation resistance. The oxidation of carbon interlayers and subsequent formation of silica to bond fiber and matrix is well documented.[11,18,20,32] As graphite is oxidized, cavities form at the fiber-matrix interface which facilitate oxygen diffusion into the composite. Oxygen initiates the decomposition of the fiber, resulting in the formation of graphite and silica. Silica

layers grow on both fiber and matrix surfaces until the layers grow together and fuse. The interface thus becomes tightly bonded resulting in brittle fracture behavior.

Some retention of strength and fracture toughness has also been observed by Pluvinage in Nicalon®/SiC composites with a thin (< 0.1 μm) graphite fiber coating.[64] A mechanism was proposed suggesting the growth of silica films on Nicalon® and SiC at the surface of the composite, which proceeded until the films grow together to close the interface. Silica then serves to prevent further oxygen diffusion at the interface, protecting the central regions of the composite. Other studies of the oxidation of carbon interlayers were usually concerned with layers which were significantly thicker (> 0.1 μm) than in this study.[19-20] No retention of fiber pull-out after 1000 h exposure to air at 1000°C had been observed as the samples failed in a brittle manner throughout the composites.

In this work, flexure strength in Nicalon®/SiC composites with a graphitic interlayer was reduced ~40% after exposure to air for 1000 h at 1000°C. However, unlike the work of Lowden, only the outer regions adjacent to the surface of the composite sample were embrittled. Some fiber pull-out was observed in the center of the composite. The embrittlement of the outer edges, which varied in width from 0.3 to 0.5 mm, served to decrease the effective fiber volume fraction and lower the elastic modulus of the composite after matrix

cracking, decreasing the ultimate strength. For a flexure sample with dimensions 3 mm x 4 mm, embrittlement of the outside surface to a depth of 0.5 mm would result in an effective cross section of 2 mm x 3 mm, a reduction of 50%. Recalling equation 6 (Sec. 2),

$$\sigma_{cu} = V_f \sigma_{fu}$$

where σ_{cu}, V_f and σ_{fu} are composite ultimate strength, fiber volume fraction and ultimate strength of the fiber, respectively, it is clear that a 50% drop in effective fiber volume would result in a 50% drop in maximum strength.

The alumina interface samples demonstrated abundant fiber pull-out but the strength and fracture toughness were reduced by 20% and 44%, respectively, as compared to the graphite interface composite. This may be due to fiber-oxide interactions which affect, the structural integrity of the fiber. A reduction in strength of Nicalon® fibers has been previously observed due to high temperature coating-fiber interactions occurring during processing.[65] Nicalon® fibers coated with alumina by plasma CVD suffered a 30-40% reduction in tensile strength when compared to fibers coated with carbon by the same method. Damage to the fibers could be a result of either chemical reaction or mechanical damage resulting from thermal expansion mismatch between fiber and coating, or a combination of both. Such a reduction in strength of alumina-

coated fibers could cause the loss of composite strength.

In this study alumina reacted during composite densification with silica in the fiber to form mullite. A thin layer of graphite also formed between the mullite and Nicalon®. This phase formation agrees with the thermodynamic equilibria which were calculated in Sec. 4. Mullite and graphite formation is predicted on the low alumina concentration side of the phase diagram, where the thinness of the coating would cause the system to fall into that region.

The resulting mullite coating was observed to be very thin, not affording significant reduction of the clamping stresses at the interface. The observed retention of moderate strength and fracture toughness may have thus resulted from limited chemical bonding between the various components. The thin graphite layers (< 6 nm) observed at the fiber-coating and coating-matrix interfaces may have prevented significant adhesion and thus allowed some toughening of the material.

Unlike the case of the graphite interface, which proved susceptible to attack by oxygen, post-oxidation flexure testing of bars containing the thin alumina coating revealed flexure strength and toughness values unchanged by the exposure to high temperature air. The mullite layer was bordered at both fiber-coating and coating-matrix interfaces by extremely thin (~ 5 atom layers) graphite layers, unlike the thicker graphite layer in the control sample. Based on the model proposed by Pluvinage[64], these layers would suffer

only minor oxidation attack because of their extreme thinness. Growth of a silica layer on the exposed composite surface would quickly seal the surface and prevent oxidation. Diffusion of oxygen into the composite through the mullite layer would proceed much slower than through the open annular space in the case where voids are created, as in the cases involving thicker graphite layers. Eventually the mullite exposed at the composite surface could become covered with a protective layer of silica, preventing large scale oxygen diffusion into the composite. Long-term damage to the fiber-matrix interface by oxygen diffusion at high temperatures would thus be limited.

Like the alumina interlayer the titania interlayer was not stable during densification. The post-infiltration interface consisted of TiC particles in an amorphous region depleted of all titanium. Another product of this reaction was carbon, which is seen in the form of a graphite layer (~ 0.05 μm thick) between the TiC and SiC matrix. As in the case of the alumina interlayer, the formation of these phases agrees with the thermodynamic calculations in Sec. 4. Under room temperature flexure testing, these samples displayed considerable fiber pull-out but moderately low strength (~185 MPa). This composite behavior would suggest weakened interfacial bonding, most likely due to the graphite. The reduction in strength suggests that the fibers were damaged during densification.

The oxidation behavior of the titania interlayer reinforces the hypothesis that the fiber pull-out was due to the graphite layer present between the TiC particles and matrix. After densification, this graphitic layer is similar in thickness to the control. In comparison with the carbon layer deposited on the alumina coated fibers under the same conditions, the carbon layer deposited on the titania coated fibers was relatively thick (0.04 μm versus 0.005 μm). The relative thickness of this layer is possibly the result of more extensive fiber degradation, which would cause a greater reduction in strength. As in the case of the control, fiber-matrix bonding occurred only in the regions adjacent to the composite surface and flexure strength was again reduced ~40% upon exposure to air for 1000 hours at 1000°C.

The zirconia interlayer was the only oxide layer which was stable during densification, even though the thermodynamic equilibria calculations indicated that zircon would form. The sample nonetheless performed poorly. Debonding did not occur at the interface. The zirconia layer differed from the alumina/mullite layer in that no carbon was present after densification. It is possible that the presence of a thin carbon layer allows for decreased chemical bonding. The absence of this layer in the case of the zirconia coated fibers may allow for strong chemical bonding between coating and fiber.

8. CONCLUSIONS

Sol-gel derived oxides displayed mixed results when used as interfacial coatings in Nicalon®/SiC composites. With the sol-gel method, it is difficult to deposit thick coatings with a large degree of uniformity. Coating of the areas at the intersections of and within the fiber bundles is complicated by viscosity effects. In addition, the oxide coatings displayed limited stability with respect to Nicalon® fiber. In accordance with thermochemical calculations, the alumina and titania fibers reacted with the fibers to form mullite and TiC, respectively.

Coating morphology played a vital role in the toughening of the SiC composites produced in this study. Abundant fiber pull-out was observed in those samples with even, uniform layers at the fiber-matrix. The mullite and control layers were very uniform. TEM analysis of the titania coatings showed them to be composed of particles which varied greatly in size. These particles, however, were covered by a carbon layer, 0.03-0.04 μm thick, which resulted in a smooth carbon-matrix interface. In contrast, there was only a very thin carbon layer ($<$ 0.01 μm) between coating and matrix in the composite containing zirconia coated fibers. The resulting interface was not smooth, possibly a source of increased bonding.

The resulting mullite layer functioned moderately well as

an interfacial layer. An increase in fracture toughness, as characterized by fiber pull-out, was observed in composites with the mullite interface. Most importantly, these composites displayed no significant loss in strength and fracture toughness when exposed to air at 1000°C for 1000 hours. Further research into the behavior of other oxide coatings, particularly mullite, may be of interest.

REFERENCES

REFERENCES

1. Wei, George C. and Paul F.Becher, "Developmnet of SiC-Whisker-Reinforced Ceramics," *Am. Ceram. Soc. Bull.* **64**(2), pp.298-304 (1985).

2. Phillips, D.C., "The Fracture Energy of Carbon-Reinforced Glass," *J. Mater. Sci.* **7**, pp.1175-91 (1972).

3. Phillips, D.C., "Interfacial Bonding and the Toughness of Carbon Fibre Reinforced Glass and Glass-Ceramics," *J. Mater. Sci.* **9**, pp.1847-54 (1974).

4. Prewo, Karl M. et al., "High-strength silicon carbide fibre-reinforced glass-matrix composites," *J. Mater. Sci.* **15**, pp.463-8 (1980).

5. Prewo, Karl M. and John J. Brennan, "High-strength silicon carbide fibre-reinforced glass-matrix composites," *Ceram. Bull.* **65**(2), pp.305-22 (1986).

6. Besmann, T.M. et al., "Vapor-Phase Fabrication and Properties of Continuous-Filament Ceramic Composites," *Science* **253**, pp.1104-09 (1991).

7. Caputo, A.J. et al., "Fiber-Reinforced SiC Composites with Improved Properties," *Am. Ceram. Soc. Bull.* **66**(2), pp.368-72 (1987).

8. Lowden, R.A. et al., "Properties of Ceramic-Ceramic Composites Fabricated by Forced Chemical Vapor Infiltration," pp.774-88 in the Proceedings of the 5th Technical Meeting of the American Society of Composites, East Lansing, Michigan June 11-13, 1990.

9. Budiansky, B. et al., "Matrix Fracture in Fiber Reinforced Ceramics," *J. Mech. Phys. Solids* **34**(2), pp.167-89 (1986).

10. Marshall, D.B. and A.G. Evans, "Failure Mechanisms in Ceramic-Fiber/Ceramic-Matrix Composites," *J. Amer. Ceram. Soc.* **68**(5), pp.225-31 (1985).

11. Evans, Anthony G. and David B. Marshall, "Mechanical Behavior of Ceramic Matrix Composites," pp.1-39 in Fiber Reinforced Ceramic Composites: Materials, Processing and Technology, ed. by K.S. Mazdiyasni, Noyes Publications, Park Ridge, New Jersey, (1990).

12. Thouless, Michael D. et al., "Effect of Interface Mechanical Properties on Pullout in a SiC-Fiber-Reinforced Lithium Aluminum Silicate Glass-Ceramic," *J. Am. Ceram. Soc.* **72**(4), pp.525-32 (1989).

13. Aveston, J. et al., "Single Multiple Fracture: The Properties of Fiber Composites," *National Physics Lab Conference Proceedings*, pp.15-26 Nov 1971.

14. Aveston, J. and A. Kelly, "Theory of Multiple Fracture of Fibrous Composites," *J. Mater. Sci.* **8**, pp.352-62 (1973).

15. Lowden, R.A. and D.P. Stinton, "Interface Modification in Nicalon®/SiC Composites," *Ceram. Eng. Sci. Proc.* **9**(7-8), pp. 705-22 (1988).

16. Lowden, R.A., *Characterization and Control of the Fiber-Matrix Interface in Ceramic Matrix Composites*, ORNL/TM-11039, Oak Ridge National Laboratory, Oak Ridge, Tenn., March 1989.

17. Lowden, Richard A. and Karren L. More, "The Effect of Fiber Coatings on Interfacial Shear Strength and the Mechanical Behavior Of Ceramic Composites," pp. 205-14 in MRS Symposium Proceedings, Vol. 170: Interfaces in Composites, Materials Research Society, Pittsburgh, Pennsylvania (1990).

18. Lowden, R.A., "Fiber Coatings and the Mechanical Properties of a Fiber-Reinforced Ceramic Composite," pp.619-30 in Ceramic Transactions, Vol. 19: Advanced Composite Materials, ed. by Michael D. Sacks, The American Ceramic Society, Westerville, Ohio (1991).

19. James, R.D. et al., "The Effects of Oxidation and Combustion Environments on the Properties of Nicalon®/SiC Composites," pp.925-35 in Ceramic Transactions, Vol. 19: Advanced Composite Materials, ed. by Michael D. Sacks, The American Ceramic Society, Westerville, Ohio (1991).

20. Lowden, R.A. and R.D. James, *High Temperature Corrosion of Nicalon®/SiC Composites*, ORNL/TM-11893, Oak Ridge National Laboratories, Oak Ridge, Tenn., August 1991.

21. Partlow, D.P. and Bulent E. Yoldas, "Colloidal versus Polymer Gels and Monolithic Transformation in Glass-Forming Systems," *Jour. Non-Cryst. Sol.* **46**, pp.135-61 (1981).

22. Yoldas, Bulent E., "Alumina Sol Preparation from Alkoxides," *Ceram. Bull.* **54**(3), pp.289-90 (1975).

23. Yoldas, Bulent E., "Alumina gels that form porous transparent Al_2O_3," *J. Mater. Sci.* **10**, pp.1856-60 (1975).

24. Holiday, L., Composite Materials, Elsevier Publishing Company, New York, 1966.

25. Jones, Robert M., Mechanics of Composite Materials, Hemisphere Publishing Corp., Washington (1975).

26. Donald, I.W. and P.W. McMillan, "Review of Ceramic-Matrix Composites," *J. Mater. Sci.* **11**, pp. 949-972 (1976).

27. Phillips, D.C., "Long-Fibre Reinforced Ceramics," pp. 167-98 in Ceramic Matrix Composites, ed. by R. Warren, Chapman and Hall, New York (1992).

28. Piggott, M.R., Load Bearing Fibre Composites, Pergamon Press, Oxford, England (1980).

29. Coyle, T.W. et al., "Mechanical Behavior of a Microcracked Ceramic Composite," *Ceram. Eng. Sci. Proc.* **8**(7-8), pp.947-57 (1987).

30. Khaund, A.K. et al., "Influence of elastic and thermal mismatch on the local crack-driving force in brittle composites," *J. Mater. Sci.* **12**, pp.2269-73 (1977).

31. Rice, R.W. et al., "The Effect of Ceramic Fiber Coatings on the Room Temperature Mechanical Behavior of Ceramic-Fiber Composites," *Ceramic Eng. Sci. Proc.* **5**(7-8), pp.614-24 (1984).

32. Bender, B.A. et al., "Electron Microscopy of Ceramic Fiber-Ceramic Matrix Composites-Comparison with Processing and Behavior," *Ceramic Eng. Sci Proc.* **5**(7-8), pp.513-29 (1984).

33. Bender, Barry et al., "The Effect of Fiber Coatings and Composite Processing on Properties of Zirconia-Based Matrix SiC Fiber Composites," *Am. Ceram. Soc. Bull.* **65**(2), pp.363-69 (1986).

34. Naslain, Roger, "CVI Composites," pp. 199-244 in Ceramic Matrix Composites, ed. by R. Warren, Chapman and Hall, New York (1992).

35. Prewo, Karl M. et al., "Fiber Reinforced Glasses and Glass-Ceramics for High performance Applications," *Ceram. Bull.* **65**(2), pp.305-22 (1986).

36. Jones, Russell H. et al., "Interfacial Chemistry and Structure in Ceramic Composites," pp. 157-89 in Structure & Property Relationships for Interfaces, ed. by John L. Walter et al., ASM International (1991).

37. Yajima, Seishi et al., "Synthesis of Continuous SiC Fibers with High Tensile Strength," *J. Am. Ceram. Soc.* **59**(7-8), pp.324-27 (1976).

38. Johnson, S.M. et al, "Degradation Mechanisms of Silicon Carbide Fibers," *J. Am. Ceram. Soc.* **71**(3), pp. C132-35 (1988).

39. Bibbo, G.S. et al., "Effect of carbon monoxide partial pressure on the high-temperature decomposition of Nicalon fibre," *J. Mater. Sci.* **26**, pp.5075-80 (1991).

40. Cooper, R.F. and K. Chyung, "Structure and Chemistry of Fibre-Matrix Interfaces in Silicon Carbide Fibre-Reinforced Glass-Ceramic Composites", *J. Mater. Sci.*, **22**, pp.3148-60 (1987).

41. Fischbach, D.B. and P.M. Lemoine, "Influence of a CVD Carbon Coating on the Mechanical Property Stability of Nicalon SiC Fiber," pp. 55-61 in Composites Science and Technology, Elsevier Science Publishers, London (1989).

42. Hsueh, Chun-Hway et al., "Effects of Interfacial Films on Thermal Stresses in Whisker-Reinforced Ceramics," *J. Am. Ceram. Soc.* **71**(11), pp.929-33 (1988).

43. Tredway, William K, and Karl M. Prewo, "Improved Performance in Monofilament Fiber Reinforced Glass Matrix Composites through the Use of Fiber Coatings,"pp.215-21 in MRS Symposium Proceedings, Vol. 170: Interfaces in Composites, Materials Research Society, Pittsburgh, Pennsylvania (1990).

44. Singh, Raj N., "Influence of Interfacial Shear Stress on First-Matrix Cracking Strerss in Ceramic-Matrix Composites," *J. Am. Ceram. Soc.* **73**(10), pp.2930-37 (1990).

45. Dugne, O. et al., "AES, APS and TEM Characterization of Boron Nitride Deposited Under Chemical Vapor Infiltration Conditions," *J. de Physique*, **50**(5) pp.333-41 (1989).

46. Naslain, Roger et al., "Boron Nitride Interphase in Ceramic-Matrix Composites," *J. Am. Ceram. Soc.*, **74**(10), pp.2482-88 (1991).

47. Lynch, Charles T. ed., Practical Handbook of Materials Science, CRC Press Inc., Boca Raton, Florida (1989).

48. Engineering Property Data on Selected Ceramics Volume III, Single Oxides, Metals and Ceramics Information Center, Columbus, Ohio, July 1981.

49. Eriksson, G.,"Thermodynamic Studies of High Temperature Equilibria XII. Solgasmix," *Chem. Scri.* (Sweden) **8**(3), pp. 100-03 (1975).

50. Besmann, T.M., "SOLGASMIX-PV, a Computer Program to Calculate Equilibrium Relationships on Complex Chemical System," ORNL/TM-5775, Oak Ridge National Laboratory, Oak Ridge, Tenn., April,1977.

51. Eriksson, G.and K. Hack, "CHEMSAGE-A Computer Program for the Calculation of Complex Chemical Equilibria," *Metall. Trans.* **21**(B), pp.1013-23 (1990).

52. Chase, M.W. et al., JANAF Thermochemical Tables, Journal of Physical and Chemical Reference Data, **16** (1977).

53. The SGTE Solution and Pure Substances Database was supplied by the developers of the CHEMSAGE program: GTT Gesellschaft fur Technische, Thermochemie und -Physik mbH, Kaiserstrasse 100, 5120 Herzogenrath 3.

54. Barin, Ihsan, Thermochemical Data of Pure Substances, VCH, Weinheim, Germany (1989).

55. Touanen, M. et al., "Theoretical Approach to the Chemical Vapour Deposition in the Atomic System Ti-SiC-Cl-H," *J. Mater. Sci. Let.* **8**, pp. 98-101 (1989).

56. Bunsell, A.R., "Ceramic Fibres," pp. 427-78 in Composite Materials Series: Fibre Reinforcements for Composite Materials; Vol. 2, ed. by A.R. Bunsell, Elsevier, New York, (1988).

57. Yoldas, Bulent E., "Hydrolysis of Aluminium Alkoxides and Bayerite Conversion," *J. appl. Chem. Biotechnol.* **23**, pp.803-9 (1973).

58. Yi, Guanghua and Michael Sayer, "Sol-Gel Processing of Complex Oxide Films," *Ceram. Bull.* **70**(7), pp.1173-9 (1991).

59. ORNL Instrumentation and Controls Division, Metrology Research and Development Laboratory Procedure no. MRDL-017, Oak Ridge National Laboratories, Oak Ridge, Tenn., August 31, 1992.

60. Cartwright, B.S. and P. Popper, "The Deposition of Pyrolytic Silicon Carbide from Methyltrichlorosilane," pp.473-99 in Science of Ceramics: Vol. 5, ed. by C Brosset and E. Knopp, The Swedish Institute for Silicate Research, Gothenburg, Sweden (1970).

61. Fischman, Gary S. and W.T. Petuskey, "Thermodynamic Analysis and Kinetic Implications of Chemical Vapor Deposition of SiC from Si-C-Cl-H Gas Systems," *J. Am. Ceram. Soc.* **68**(4), pp.185-190 (1985).

62. ASTM TEST STANDARD D790-81, American Society for the Testing of Metals, 1916 Race St., Philadelphia, PA 19103.

63. Powder Diffraction Files; Sets 1-42, International Centre for Diffraction Data, Swarthmore, PA 19801-2589.

64. Pluvinage, P. et al., "Mechanical Behavior and Oxidation Resistance of a Unidirectional SiC/SiC fibrous Composite," pp.937-44 in Ceramic Transactions, Vol. 19: Advanced Composite Materials, ed. by Michael D. Sacks, The American Ceramic Society, Westerville, Ohio (1991).

65. Langley, Neal R. et al., "Coatings for Ceramic Fiber Thermal Stability," pp.157-167 in NASA Publication 2482, Metal Matrix, Carbon, and Ceramic Matrix Composites, ed. by J.D. Buckley, 1987.

APPENDICES

APPENDIX A

The equations derived by Hsueh[42] for the calculation of interfacial stresses induced by post-processing cool down are presented here. The stress at the coating-fiber interface (σ_{cf}) is given by the expression:

$$\sigma_{cf} = \{(1+\nu_c)(\alpha_m-\alpha_c) + [[a^2+b^2(1-2\nu_c)/2b^2(1-\nu_c)] + (b^2-a^2)/a^2 \times (1+\nu_m)/2(1-\nu_c^2)(E_c/E_m)] \times [(1+\nu_c)\alpha_c + (\nu_f-\nu_c)\alpha_m - (1+\nu_c)\alpha_c]\}\Delta T / \{[-2a^2(1-\nu_c^2)/(b^2-a^2)E_c] + [a^2+b^2(1-2\nu)/2b^2(1-\nu_c) + ((b^2-a^2)/b^2) \times ((1+\nu_m)E_c/2(1-\nu_c^2)E_m)] [(1+\nu_f)(1-2\nu_f)/E_f + [a^2(1-2\nu_c)+b^2](1+\nu_{c)}/(b^2-a^2)E_c]\},$$

while the stress at the matrix-coating interface (σ_{mc}) is given by:

$$\sigma_{mc} = \{(1+\nu_c)\alpha_c + (\nu_f-\nu_c)\alpha_m - (1+\nu_c)\alpha_c + [(b^2-a^2)/2a^2] \times (E_c(\alpha_m-\alpha_c)/(1-\nu_c)[(1+\nu_f)(1-2\nu_f)/E_f + (a^2(1-2\nu_c) + b^2)(1+\nu_c)/E_c(b^2-a^2)])\}\Delta T / \{-2b^2(1-\nu_c^2)/(b^2-a^2)E_c) + [(a^2+b^2(1-2\nu_c)/2b^2(1-\nu_c)) - ((b^2-a^2)/a^2) \times (1+\nu_m)/2(1-\nu_c^2)(E_c/E_m)] [(1+\nu_f)(1-2\nu_f)/E_f + [a^2(1-2\nu_c)+b^2](1+\nu_{c)}/(b^2-a^2)E_c]\},$$

where the subscripts c, f and m denote coating, fiber and matrix, respectively, and E is elastic modulus, ν is the Poisson's ratio and α is the coefficient of thermal expansion of the elements of the composite.

APPENDIX B- Species considered for thermodynamic calculations.

Gaseous Phases

Al	AlC	AlCl	$AlCl_2$
$AlCl_3$	AlH	AlO	AlOCl
AlOH	AlO_2	AlO_2H	Al_2
Al_2Cl	Al_2O	Al_2O_2	Ar
C	CCl	CCl_2	CCl_3
CCl_4	CH	CH_2	CH_2O
CH_2O_2	CH_2OH	CH_3	CH_3Cl
CH_3O	CH_3OH	CH_4	CO
COCl	$COCl_2$	CO_2	C_2
C_2Cl_2	C_2H	C_2H_2	C_2H_3
C_2H_4	$C_2H_4O_2$	$C_2H_4H_4$	C_2H_5
C_2H_6	C_2H_5OH	$(CH_3)_2O$	C_2O
C_3	C_3H_6O	$n\text{-}C_3H_7$	$i\text{-}C_3H_7$
C_3H_8	C_3H_7OH	C_3O_2	C_4
$C_4H_8O_4$	$n\text{-}C_4H_{10}$	$i\text{-}C_4H_{10}$	C_5
C_6H_5	C_6H_5O	C_6H_6	C_6H_5OH
C_7H_8	C_8H_{16}	$n\text{-}C_8H_{18}$	$i\text{-}C_8H_{18}$
$C_{12}H_9$	Cl	ClO	ClO_2
Cl_2	Cl_2O	H	HAlO
HCO	HCl	HOCl	HO_2
H_2	H_2O	H_2O_2	O
OH	O_2	O_3	Si
SiC	SiC_4H_{12}	SiC_2	SiCl
$SiCl_2$	$SiCl_3$	$SiCl_4$	SiH
$SiHCl_3$	SiH_2Cl_2	SiH_3Cl	SiH_4
SiO	SiO_2	Si_2	Si_2C
Si_3	$SiCH_6$	SiC_3H_9Cl	$SiCH_3Cl_3$
SiC_2H_6Cl	Ti	TiCl	$TiCl_2$
$TiCl_3$	$TiCl_4$	TiO	TiO_2
TiOCl	$TiOCl_2$	Zr	ZrCl
$ZrCl_2$	ZrClH	$ZrCl_3$	$ZrCl_4$
ZrO	ZrO_2	ZrClH	

Condensed Phases-(all phases solid unless designated by "l"-[liquid])

Al	Al(l)	$AlCl_3$
$AlCl_3$(l)	$Al_2O_3(\alpha)$	Al_2O_3(delta)
Al_2O_3(kappa)	Al_2SiO_5	Al_2SiO_5(kyanite)
$Al_2Si_2O_7$	$Al_6Si_2O_{13}$	Al_4C_3
$AlCl_3$	$AlCl_3$(l)	C(graphite)
C_7H_8(l)	C_8H_{18}(l)	Si
Si(l)	$SiC(\beta)$	SiO_2(low quartz)
SiO_2(high quartz)	SiO_2(crist.)	SiO_2(l)

Ti(α)	Ti(β)	Ti(l)
TiC	TiC(l)	$TiCl_2$
$TiCl_3$	$TiCl_4$(l)	TiO(α)
TiO(β)	TiO(l)	TiO_2(ru)
TiO_2(an)	TiO_2(l)	Ti_2O_3(a)
Ti_2O_3(b)	Ti_2O_3(l)	Ti_3O_5
Ti_3O_5(l)	Ti_4O_7	Ti_4O_7(l)
SiTi	Si_2Ti	Si_3Ti_5
TiH_2	Ti_3SiC_2	Zr(a)
Zr(b)	Zr(l)	ZrO_2(a)
ZrO_2(b)	ZrO_2(l)	$ZrSiO_4$
SiZr	$SiZr_2$	Si_2Zr
Si_3Zr_5	ZrC	

Table C.1. Load, flexure strength and dimensions of individual flexure bars with graphitic interlayer. Flexure samples 1-4 were tested as fabricated. Samples 5-8 tested after exposure to air at 1000°C for 1000 h without seal coat and 9-13 were tested after exposure with seal coat.

SAMPLE	LOAD (kg)	LENGTH (cm)	THICKNESS (cm)	WIDTH (cm)	WEIGHT (g)	DENSITY (g/cc)	FLEXURE STRENGTH (MPa)
CONTROL1	45.8	5.01	0.31	0.38	1.58	2.60	337.2
CONTROL2	46.6	5.01	0.32	0.38	1.59	2.60	337.4
CONTROL3	48.4	4.98	0.32	0.39	1.63	2.61	335.2
CONTROL4	43.7	4.98	0.33	0.39	1.64	2.57	290.9
CONTROL5	26.0	4.98	0.33	0.39	1.62	2.54	171.9
CONTROL6	26.0	5.01	0.32	0.38	1.59	2.61	188.4
CONTROL7	25.2	4.97	0.33	0.39	1.61	2.58	172.9
CONTROL8	28.2	5.01	0.32	0.38	1.61	2.63	200.7
CONTROL9	48.2	5.00	0.32	0.38	1.59	2.60	345.7
CONTROL10	43.6	5.01	0.31	0.36	1.49	2.63	341.1
CONTROL11	50.1	4.98	0.33	0.38	1.63	2.59	335.3
CONTROL12	45.5	4.97	0.33	0.39	1.65	2.61	308.1
CONTROL13	48.3	4.97	0.32	0.39	1.55	2.55	347.6

Table C.2. Load, flexure strength and dimensions of individual flexure bars with alumina interlayer. Flexure samples 1-5 were tested as fabricated. Samples 6-10 tested after exposure to air at 1000°C for 1000 h without seal coat and 10-13 were tested after exposure with seal coat.

SAMPLE	LOAD (kg)	LENGTH (cm)	THICKNESS ∫cm)	WIDTH (cm)	WEIGHT (g)	DENSITY (g/cc)	FLEXURE STRENGTH (MPa)
THIN.1	30.08	5.00	0.31	0.37	1.471	2.60	239.6
THIN.2	24.72	5.00	0.31	0.37	1.538	2.66	192.9
THIN.3	38.07	5.00	0.31	0.37	1.543	2.67	297.2
THIN.4	39.89	4.99	0.31	0.38	1.487	2.56	309.2
THIN.5	36.94	5.00	0.31	0.38	1.545	2.56	271.7
THIN.6	27.76	5.00	0.31	0.38	1.534	2.63	215.2
THIN.7	28.53	5.00	0.32	0.38	1.552	2.58	209.3
THIN.8	41.34	4.99	0.32	0.38	1.544	2.57	303.3
THIN.9	38.76	5.00	0.32	0.38	1.538	2.56	284.3
THIN.10	46.80	5.00	0.31	0.38	1.546	2.59	348.8
THIN.11	33.76	5.00	0.31	0.38	1.539	2.59	254.0
THIN.12	25.99	5.00	0.31	0.38	1.544	2.59	193.7
THIN.13	40.16	5.00	0.31	0.38	1.553	2.63	304.3
THICK.1	22.99	5.02	0.27	0.38	1.258	2.40	227.1
THICK.2	24.85	5.02	0.27	0.39	1.276	2.41	242.3
THICK.3	13.95	5.02	0.31	0.39	1.452	2.42	105.3
THICK.4	15.04	5.02	0.27	0.37	1.187	2.40	158.7
THICK.5	22.90	5.01	0.31	0.38	1.481	2.49	174.0
THICK.6	21.76	5.02	0.31	0.38	1.437	2.46	170.4
THICK.7	20.54	5.01	0.27	0.40	1.287	2.37	195.1
THICK.8	19.90	5.02	0.31	0.41	1.496	2.34	140.9
THICK.9	21.26	5.01	0.31	0.41	1.472	2.31	150.0
THICK.10	28.62	5.02	0.27	0.38	1.232	2.41	292.0
THICK.11	23.76	5.02	0.31	0.39	1.515	2.50	178.2
THICK.12	20.58	5.02	0.27	0.39	1.253	2.36	200.6
THICK.13	18.36	5.03	0.27	0.39	1.266	2.38	178.9

Table C.3. Load, flexure strength and dimensions of individual flexure bars with titania interlayer. Flexure samples 1-4 were tested as fabricated. Samples 5-8 tested after exposure to air at 1000°C for 1000 h without seal coat and 9-12 were tested after exposure with seal coat.

SAMPLE	LOAD (kg)	LENGTH (cm)	THICKNESS (cm)	WIDTH (cm)	WEIGHT (g)	DENSITY (g/cc)	FLEXURE STRENGTH (MPa)
THIN.1	31.71	5.01	0.32	0.37	1.43	2.42	235.3
THIN.2	22.94	5.00	0.32	0.36	1.49	2.53	169.9
THIN.3	23.26	5.01	0.33	0.36	1.44	2.41	166.9
THIN.4	29.90	5.00	0.32	0.37	1.45	2.45	219.8
THIN.5	17.45	5.01	0.33	0.38	1.45	2.32	117.3
THIN.6	12.90	5.01	0.34	0.38	1.44	2.28	85.4
THIN.7	14.13	5.01	0.34	0.37	1.43	2.27	94.2
THIN.8	17.76	5.01	0.33	0.37	1.47	2.43	126.8
THIN.9	26.26	5.00	0.33	0.37	1.42	2.36	187.1
THIN.10	31.99	5.01	0.32	0.36	1.38	2.38	240.2
THIN.11	27.62	5.01	0.33	0.34	1.35	2.38	206.8
THIN.12	30.03	5.01	0.33	0.37	1.43	2.39	215.9
THICK.1	29.58	5.00	0.33	0.35	1.54	2.68	219.9
THICK.2	18.99	5.00	0.32	0.37	1.53	2.62	141.9
THICK.3	19.90	5.00	0.32	0.37	1.54	2.66	151.0
THICK.4	31.39	5.00	0.32	0.37	1.57	2.66	232.9
THICK.5	19.17	5.00	0.33	0.37	1.58	2.61	135.7
THICK.6	19.04	5.00	0.32	0.36	1.51	2.63	145.2
THICK.7	8.27	5.00	0.32	0.37	1.51	2.52	60.0
THICK.8	19.90	5.00	0.33	0.37	1.56	2.61	143.0
THICK.9	22.26	5.00	0.32	0.37	1.53	2.55	161.4
THICK.10	21.22	5.01	0.32	0.37	1.53	2.61	158.5
THICK.11	31.89	5.01	0.32	0.37	1.54	2.60	236.6
THICK.12	26.94	5.00	0.33	0.37	1.56	2.59	193.7

Table C.4. Load, flexure strength and dimensions of individual flexure bars with zirconia interlayer. Flexure samples 1-4 were tested as fabricated. Samples 5-8 tested after exposure to air at 1000°C for 1000 h without seal coat and 9-12 were tested after exposure with seal coat.

SAMPLE	LOAD (kg)	LENGTH (cm)	THICKNESS (cm)	WIDTH (cm)	WEIGHT (g)	DENSITY (g/cc)	FLEXURE STRENGTH (MPa)
THIN.1	11.68	5.01	0.33	0.37	1.41	2.30	80.1
THIN.2	10.50	5.00	0.33	0.36	1.39	2.33	75.3
THIN.3	7.18	5.01	0.33	0.37	1.45	2.38	49.6
THIN.4	11.40	5.00	0.33	0.37	1.41	2.35	81.3
THIN.5	0.00	4.99	0.33	0.38	1.45	2.32	0.0
THIN.6	0.00	4.99	0.34	0.38	1.46	2.32	0.0
THIN.7	0.00	4.99	0.34	0.37	1.38	2.21	0.0
THIN.8	0.00	5.01	0.33	0.37	1.41	2.33	0.0
THIN.9	26.26	5.00	0.33	0.37	1.43	2.39	187.1
THIN.10	31.99	5.01	0.32	0.36	1.42	2.45	240.2
THIN.11	27.62	5.01	0.33	0.36	1.38	2.35	199.4
THIN.12	30.03	5.01	0.33	0.37	1.44	2.40	215.9
THICK.1	3.41	5.00	0.33	0.36	1.51	2.57	24.8
THICK.2	4.86	5.00	0.32	0.37	1.44	2.46	36.3
THICK.3	6.13	5.00	0.32	0.37	1.47	2.53	46.6
THICK.4	2.91	5.00	0.32	0.37	1.49	2.53	21.6
THICK.5	0.00	5.00	0.33	0.37	1.38	2.28	0.0
THICK.6	0.00	5.00	0.32	0.36	1.37	2.41	0.0
THICK.7	0.00	5.00	0.32	0.37	1.41	2.36	0.0
THICK.8	0.00	5.00	0.33	0.37	1.45	2.42	0.0
THICK.9	3.41	5.00	0.32	0.36	1.41	2.42	25.4
THICK.10	5.68	5.01	0.32	0.37	1.38	2.35	42.4
THICK.11	3.68	5.01	0.32	0.37	1.43	2.42	27.3
THICK.12	6.13	5.00	0.33	0.37	1.39	2.32	44.1

VITA

Donald Matthew Walukas was born on July 7th, 1965 in Pittsburgh, Pennsylvania. He entered the University of Tennessee in 1984 and graduated in 1988 with a Bachelor of Arts Degree with a major in Chemistry. After working in Finland for two years, he returned to Tennessee, enrolling the Master of Science program in Materials Science and Engineering. He presently resides in Ann Arbor, Michigan.